SRNL-STI-2011-00652
Revision 0

Impacts of Antifoam Additions and Argon Bubbling on Defense Waste Processing Facility (DWPF) REDuction/OXidation (REDOX)

C. M. Jantzen
F. C. Johnson

June 2012

Savannah River National Laboratory
Savannah River Nuclear Solutions, LLC
Aiken, SC 29808

Prepared for the U.S. Department of Energy under
contract number DE-AC09-08SR22470.

SRNL
SAVANNAH RIVER NATIONAL LABORATORY

DISCLAIMER

Printed in the United States of America

Prepared for
U.S. Department of Energy

SRNL-STI-2011-00652
Revision 0

Keywords: *antifoam, reduction, oxidation, HLW, vitrification*

Retention:

Impacts of Antifoam Additions and Argon Bubbling on Defense Waste Processing Facility (DWPF) REDuction/OXidation (REDOX)

C. M. Jantzen
F. C. Johnson

June 2012

Savannah River National Laboratory
Savannah River Nuclear Solutions, LLC
Aiken, SC 29808

Prepared for the U.S. Department of Energy under contract number DE-AC09-08SR22470.

REVIEWS AND APPROVALS

AUTHORS:

Carol M. Jantzen, Process Technology Programs Date

Fabienne C. Johnson, Process Technology Programs Date

TECHNICAL REVIEWERS:

Michael E. Stone, Process Technology Programs Date

Alexander S. Choi, Engineering Process Development Date

APPROVERS

Connie C. Herman, Manager, Process Technology Programs Date

Sharon L. Marra, Manager, Date
Environmental & Chemical Process Technology Research Programs

John E. Occhipinti, Manager, Date
Waste Solidification Engineering

EXECUTIVE SUMMARY

Control of the REDuction/OXidation (REDOX) state of glass in High Level Waste (HLW) melters, such as the Defense Waste Processing Facility (DWPF), is critical in order to eliminate the formation of metallic species from overly reduced melts while minimizing foaming from overly oxidized melts. The REDOX control is normally a balance of the oxidants and reductants from the feed and from processing additives. However, after reflux in the Sludge Receipt and Adjustment Tank (SRAT) and the Slurry Mix Evaporator (SME), the balance between the oxidizing salts vs. reducing salts can be altered once the mixture is fed to the melter if the melt pool is bubbled with gaseous species that either oxidize or sparge the melt of oxygen. Hence, for a bubbled melt pool, the REDOX of the melt pool must be targeted based on the balance of the oxidizing and reducing salts from the feed and from the processing additives, as well as, accounting for the effects of any gas being bubbled through the melt to improve convection and mixing while also increasing melt rate. For example, one would not set a REDOX target of $Fe^{2+}/\Sigma Fe$ of 0.20 based on chemical balancing and then bubble pure air through the melter as pure air would oxidize the melt pool to an $Fe^{2+}/\Sigma Fe \sim 0$. Some gases, such as argon, are inert but act as chemical sparging agents or "degassing[‡] agents" that can sparge out oxygen from the melt and cause the glass to become more reducing.

This study examines DWPF flowsheets at various concentrations of antifoam (a reducing processing additive) in the absence of melt pool bubbling (crucible and production data) and in the presence of melt pool bubbling with argon (crucible and production data), a known sparging/degassing agent. In order to de-convolute the impacts of antifoam on the melt pool REDOX from the impacts of melt pool bubbling, crucible studies were performed with (1) varying antifoam concentrations without bubbling, and (2) minimal antifoam with Ar bubbling. This allowed an antifoam term to be added to the REDOX model and suggested that (1) more oxidizing $Fe^{+2}/\Sigma Fe$ ratios could be targeted which would create more oxidizing species in the cold cap to offset the effects of Ar-sparging or (2) Ar-air gas mixtures could be blended with a mixing valve to control the melt pool REDOX at the same $Fe^{2+}/\Sigma Fe$ ratios (same $-\log fO_2$) as chosen for the chemical REDOX balancing.

The 2006 EE REDOX model is an electron equivalents (EE) model that balances the electrons lost during oxidation of a reductant against the electrons gained during the reduction of an oxidant. The EE terms for the formates, nitrates, and oxalates in the REDOX model are based on the formated salts like NaCOOH, the nitrated salts like $NaNO_3$, and the oxalated salts like NaC_2O_4 that have higher decomposition temperatures than their acidic counterparts which flash off. Thus it is the higher decomposition salts that participate in the establishing the melt REDOX during their interactions in the melter cold cap.

For the antifoam feed additive, which is an organic chain structure composed of methyltrisiloxane (MTS) end groups and a center polymer chain of varying length (8 to 12 polyethyleneoxide or PEO groups), such salts do not form and so an EE term must be based on the number of carbons in each part of the organic group and their relative EE term. This is the same strategy used to fit a carbon term for coal in the EE model but the antifoam molecule contains carbons of different oxidation states so it is more complex.

The MTS end groups of the antifoam molecule have 7-8 carbons of -4 charge and the 8 chain PEO groups have 16 carbons of -1 charge while the 12 chain polymers have 24 carbons of -1 charge. Since the ratio of the 8:12 polymer chains is 90%:10%, there are 16.8 carbons of -1 charge in the weighted polymer

‡ Assuming that one wants to rid a solution of oxygen and/or carbon dioxide, bubbling with an inert gas substitutes the dissolved harmful, reactive gases such as oxygen and carbon dioxide. Nitrogen, argon, helium, and other inert gases are commonly used. To complete the substitution, the solution should be stirred vigorously and bubbled for a long time (from www.wikipedia.org/wiki/Degasification).

chain and 8 carbons in the MTS if the MTS groups are assumed to be octa-MTS instead of hepta-MTS for a total of 24.8 carbons in the antifoam organic molecule (sum of 0.9*16 + 0.1*24). The -1 carbons of the PEO exchange 5EE's per carbon to oxidize to CO_2 in the melter. The -4 carbons of the octa-MTS exchange 8EE's per carbon to oxidize to CO_2 in the melter. Experimentation and modeling have shown that the MTS cleave off the antifoam during processing and do not participate in reduction of the melt pool. Therefore, the EE of the PEO are 16.8/24.8 carbons * 5 EE per carbon for a total EE transfer term of +3.39 per mole/kg of carbon once the following conversions are made

mg/kg of antifoam→mg/kg of total carbon in antifoam→mol/kg of total carbon in antifoam.

This method of conversion from antifoam to mol/kg of carbon was chosen because the DWPF data available was in mg/kg of antifoam calculated from how many gallons of antifoam had been measured per SME batch and sealed crucible studies that had been performed after known amounts of antifoam had been added were available in mg./kg of antifoam. The DWPF data was also available as the measured Total Organic Carbon (TOC) in mg/kg of carbon. The mg/kg of carbon from the antifoam was determined by subtracting the carbon contribution from formic acid, oxalate/oxalic acid, and coal. Modeling was performed using mol/kg carbon derived from gallons of antifoam used and from TOC measurements.

Experimentation and modeling has shown that the antifoam PEO's are 80-100% effective in melt pool reduction. The modeling performed for the REDOX model for antifoam suggests that the efficiency is 85%. Therefore, 85% of +3.39 EE yields an overall EE transfer of +2.88 per mol/kg of carbon from antifoam compared to +2 for formic acid and +4 for oxalate and coal. Having an antifoam term in the DWPF REDOX model may allow antifoam to be used as a reductant source while also controlling feed foaming.

There is an additive impact on the melt pool REDOX from the argon bubbling. Argon (Ar) degasses or sparges the oxygen from the melt. Thus, REDOX is a function of both the oxidants and reductants in the melt pool and the Ar sparging. While Ar is an inert gas, Ar replaces the free oxygen in a glass. This process also occurs when inert gasses are used to sparge the oxygen or other gasses out of solutions, molten metals, or glasses. The REDOX equilibrium in a glass melt can be represented by

$$Fe^{3+}_{melt} + \frac{n}{2} O^{2-}_{melt} \leftrightarrow Fe^{2+}_{melt} + \frac{n}{4} O_{2\,melt}$$

where n = the number of electrons transferred
O^{2-} = the oxygen ion activity or basicity of the melt
O_2 is the physically dissolved oxygen in the holes of the network structure.

The REDOX-oxygen balance equation is written as reversible as going from the right hand side (RHS) to the left hand side (LHS) is the reduction of ferric to ferrous iron and going from LHS to RHS is the oxidation of ferrous to ferric iron. Since the DWPF melt pool reductants shift the equilibrium to the RHS where dissolved oxygen exists in the glass, it is the dissolved oxygen on the RHS of this equation that is being displaced by the Ar in the melt pool. This is because the free oxygen on the RHS of the equation is being sparged out and the equilibrium between the RHS and the LHS no longer exists, driving the equilibrium to the RHS. Therefore, O_2 must be provided by either (1) additional melt pool oxidants (the theory of targeting a more oxidizing REDOX target to compensate for the Ar sparging) or (2) using a mixing valve to admix small amounts of air into the argon while sparging. This study provides the calculations of Ar-air mixtures that would be acceptable if the latter route is desired.

Measurement of the REDOX of DWPF pour stream (PS) samples (with and without Ar bubbling) and measurement of a simulated SB6 feed that was Ar bubbled during the feed-to-glass transformation in a sealed crucible inside an Ar bubbled oven demonstrated that the argon bubbling impact is a linear constant of $Fe^{+2}/\Sigma Fe$ of ~0.1. Therefore, it is recommended that targeting a chemical REDOX of 0.1 should yield a realized $Fe^{+2}/\Sigma Fe$ of ~0.2. While there is no EE term that can be developed for Ar sparging, "effective offset" term has been added to the REDOX model to account for Ar degassing. Since the Savannah River National Laboratory (SRNL) has developed a sealed bubbled REDOX crucible procedure with Ar bubbling that agrees with the data from the pour stream samples any additional testing of the "effective offset" term can be performed using this crucible methodology.

The DWPF REDOX model then takes the form

$$\frac{Fe^{2+}}{\Sigma Fe} = f\left[\left(2[F]+4[C]+4[O_T]+3.39*eff[C_A]-5[N]-5[Mn]\right)\frac{45}{T}\right] = f[\xi_A]$$

where f = indicates a function
[F] = formate (mol/kg feed)
[C] = coal (carbon) (mol/kg feed)
$[O_T]$ = $oxalate_{Total}$ (soluble and insoluble) (mol/kg feed)
$[C_A)$ =carbon from antifoam (mol/kg feed)
eff = effective antifoam impact = 0.85
[N] = nitrate + nitrite (mol/kg feed)
[Mn] = manganese (mol/kg feed)
T = total solids (wt%)

$$\xi_A = \left[\left(2[F]+4[C]+4[O_T]+3.39*eff[C_A]-5[N]-5[Mn]\right)\frac{45}{T}\right]$$

When the REDOX data generated were fit as a linear function of ξ_A they fell within the confidence bands of the 2006 EE model and so the slope and intercept were not refit. This gives the form of the DWPF REDOX model with an antifoam term as:

$$\frac{Fe^{2+}}{\Sigma Fe} = 0.2358 + 0.1999\xi_A$$

The impact of Ar sparging on REDOX was quantified and the Ar adjusted DWPF model takes on the form:

$$\frac{Fe^{2+}}{\Sigma Fe} = 0.2358 + 0.1999\xi_A + 0.1_{Ar}$$

The DWPF REDOX is currently in control. The equations derived in this study will restore the ability to accurately predict the REDOX even though the melt pool is bubbled and increased antifoam concentrations have recently been necessary.

TABLE OF CONTENTS

LIST OF TABLES

LIST OF FIGURES

LIST OF ABBREVIATIONS

AMFT	Additive Mix Feed Tank
ARP	Actinide Removal Process
CSSX	Caustic Side Solvent Extraction
DWPF	Defense Waste Processing Facility
EE	Electron Equivalent
EMF	Electro-Motive Force
HHW	High Heat Waste
HLW	High Level Waste
IIT	Illinois Institute of Technology
LHS	Left Hand Side
LHW	Low Heat Waste
MCU	Modular CSSX Unit
MFT	Melter Feed Tank
MSDS	Material Safety Data Sheet
MTS	MethylTriSiloxane
NBO	Non-Bridging Oxygen
OLS	Ordinary Least Square
PCCS	Product Composition Control System
PEO	Poly-ethylene oxide
PISA	Potential Inadequacy of Safety Analysis
POM	Poly-oxy-methylene
PNNL	Pacific Northwest National Laboratory
PS	Pour Stream
PSAL	Process Science Analytic Laboratory
REDOX	REDuction/OXidation
RHS	Right Hand Side
RMSE	Root Mean Square Error
SB	Sludge Batch
SCF	Shielded Cell Facility
SME	Slurry Mix Evaporator
SMECT	Slurry Mix Evaporator Condensate Tank
SMRF	Slurry Melt Rate Furnace
SPC	Statistical Process Control
SQC	Statistical Quality Control
SRAT	Sludge Receipt and Adjustment Tank
SRNL	Savannah River National Laboratory
TAR	Technical Assistance Request
TOC	Total Organic Carbon
TSR	Technical Safety Requirement
TTR	Technical Task Request
WVNS	West Valley Nuclear Services

1.0 INTRODUCTION

During melting of HLW glass, the REDOX of the melt pool cannot be measured. Therefore, the $Fe^{+2}/\Sigma Fe$ ratio in the glass poured from the melter must be related to melter feed organic and oxidant concentrations to ensure production of a high quality glass without impacting production rate (e.g., foaming) or melter life (e.g., metal formation and accumulation).

A production facility such as the Defense Waste Processing Facility (DWPF) cannot wait until the melt or waste glass has been made to assess its acceptability, since by then no further changes to the glass composition and acceptability are possible. Therefore, the acceptability decision is made on the upstream process, rather than on the downstream *melt* or glass product. That is, it is based on "feed forward" statistical *process* control (SPC)[†] rather than statistical *quality* control (SQC).[††] In SPC, the feed composition to the melter is controlled *prior* to vitrification. Use of the DWPF REDOX model has controlled the balance of feed reductants and oxidants in the Sludge Receipt and Adjustment Tank (SRAT) (see Figure 1). Once the alkali/alkaline earth salts (both reduced and oxidized) are formed during reflux in the SRAT, the REDOX can only change if (1) additional reductants or oxidants are added to the SRAT, the Slurry Mix Evaporator (SME), or the Melter Feed Tank (MFT) or (2) if the melt pool is bubbled with an oxidizing gas or sparging gas that imposes a different REDOX target than the chemical balance set during reflux in the SRAT.

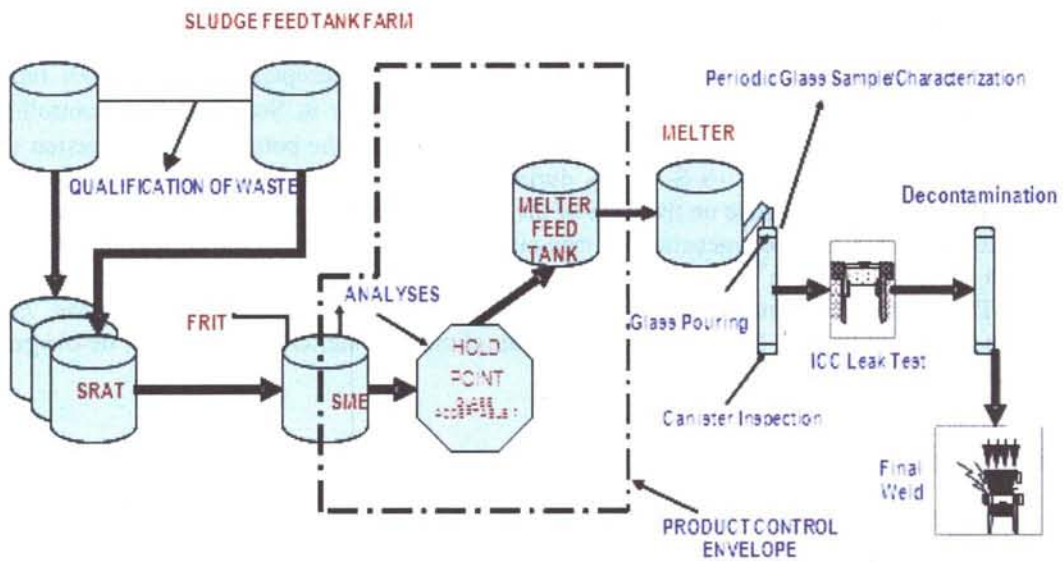

Figure 1. DWPF flowsheet showing sludge receipt from the tank farm into the SRAT followed by frit addition in the SME and qualification of the SME product (sludge and frit) via analyses and processing through the Product Composition Control System (PCCS) before the acceptable feed can be transferred to the MFT and onto the melter.

In the DWPF SRAT, acids are added to the waste sludge [1] for the following reasons:

[†] This controls the Slurry Feed to the Melter *prior* to vitrification.
[††] Which would adjudicate product release by sampling the glass *after* it's been made.

- control potential foaming by gaseous species in the melter by:
  - converting NO_3 (entering as nitrate species in the feed or as nitric acid) to nitrated salts such as $NaNO_3$ and $NaNO_2$,
  - destroying nitrites
  - converting carbonates in the feed to CO_2 which vaporizes in the SRAT off-gas and
  - converting >66% of the oxidized Mn^{+4} or Mn^{+3} present as MnO_2, Mn_2O_3, Mn_3O_4, or $NaMn^{+7}O_4$ and/or hydrous complexes in the feed to $Mn^{+2}O$ or $Mn^{+2}(COOH)_2$, liberating O_2 to the SRAT off-gas. Note that 66% is the goal based on studies of foaming but >66% may not always be achieved (this is discussed in more detail in Section 2.2.2);
- reduce and steam strip mercury for subsequent removal, $HgO \rightarrow Hg°$; and
- improve slurry rheology by neutralizing excess hydroxide (OH^-) in the feed by converting species such as NaOH to NaCOOH (sodium formate) salt.

The NaCOOH and $NaNO_3$ salts represent the refluxed species that react in the melter cold cap at elevated temperatures as HCOOH and HNO_3 would just flash off in the melter at ~90°C if not refluxed during SRAT processing.

The SRAT product is then fed to the DWPF SME, where a borosilicate glass frit slurry is added to produce the melter feed slurry. The melter feed slurry is nominally concentrated to 40-50 wt% total solids in the SME and then fed to the MFT which is just a holding tank for transfer of the melter feed into the DWPF Joule-heated melter where it is fused into glass (vitrified) at 1150°C.

Based upon the development of an electromotive force (EMF) series for DWPF glasses and melter experience at Pacific Northwest National Laboratory (PNNL), an acceptable iron REDOX ratio was defined for DWPF melts as $0.09 \leq Fe^{2+}/\Sigma Fe \leq 0.33$ (see discussion in Section 2.1). Controlling the DWPF melter at a REDOX equilibrium of $Fe^{+2}/\Sigma Fe \leq 0.33$ prevents the potential for conversion of NiO $\rightarrow$ Ni°, $RuO_2 \rightarrow$ Ru°, and $2SO_4^{=} \rightarrow S_2 + 4O_2$ during vitrification; such that metallic and sulfide rich species do not form and accumulate on the floor of the melter where they can interfere with Joule heating. Control of foaming due to de-oxygenation of manganic species is achieved by having 66-100% of the oxidized Mn species (Mn^{7+}, Mn^{4+}, Mn^{3+}) converted to Mn^{2+} (as oxides, hydroxides, formates, or oxalates) during SRAT processing. At the lower REDOX limit of $Fe^{+2}/\Sigma Fe \sim 0.09$ about 99% of the Mn^{+4}/Mn^{+3} is converted to Mn^{+2}. Therefore, the lower REDOX limit eliminates melter foaming from de-oxygenation of Mn in the melt pool.

1.1 Sludge Batch 1

During DWPF Sludge Batch 1 (SB1), the REDOX model only included terms for nitrate, nitrite, and formates, i.e. an overly oxidized flowsheet was being implemented as REDOX was calculated by balancing one mole of nitrate/nitrite against one mole of formate in the feed.[2] Off-gas surges were experienced in the melter during processing of SB1 when these nitric acid rich feeds were being processed. The surges were studied by neural net modeling of thirty-nine DWPF melter parameters. This modeling indicated that melter feed flow and melter level (which includes any contributions from foam generation) had a direct impact on the melter pour surges.[3]

1.2 Sludge Batch 2

Off-gas surges were more noticeable during processing of DWPF Sludge Batch 2 (SB2) even after the implementation of a more reducing REDOX correlation [4] that balanced one mole of nitrate against three moles of formate in the feed. DWPF SB2 contained higher noble metal content than SB1 feeds [5]

and it is known that higher noble metal content can catalyze formic acid decomposition [6] and liberate excess gases especially H_2 during feed preparation.

1.3 Sludge Batch 3

DWPF Sludge Batch 3 (SB3) was purported to contain high concentrations of reductants that were not in the simple formate vs. nitrate REDOX correlations used for SB1 and SB2: species such as oxalate and coal. An Electron Equivalents REDOX model was developed with terms for the additional reductants [7,8]. In addition, a manganese term was added to the EE model to account for potential differences in the oxidation state of Mn in the feed (+4) and in the glass (+2). When coal and oxalate were absent, the EE model reverted to an [F]-2.5[N] stoichiometry plus the term for manganese. At the time the EE model was developed for SB3, further investigation into the role of oxidized Mn species (+4, +5, +6, and +7) in the feed was suggested. The EE model has been validated against DWPF samples (SME 224) taken during SB2 operations, numerous SRNL pilot scale melters, REDOX data from West Valley Nuclear Services (WVNS), and data from PNNL's quartz crucible tests and pilot scale tests.

1.4 Sludge Batch 4

For Sludge Batch 4 (SB4), an investigation of the EE parameter for manganese was initiated because non-radioactive melt rate testing of the manganese rich SB4 feeds produced glasses that were overly oxidized. These overly oxidized feeds foamed and the copious amounts of foam adversely impacted melt rate [9]. It was determined that the reduced manganese from the SRAT could be re-oxidized in high nitrate feeds by transient molten salt phases that form in the cold cap [10] and could be present as Mn^{+7} instead of Mn^{+4}. In order to account for molten salt re-oxidation of manganese to +7, the EE term was adjusted from -2 to -5 (as a transfer of Mn^{+4} to Mn^{+2} is -2 EE's, but a transfer of Mn^{+7} to Mn^{+2} is a 5EE transfer). This is discussed in more detail in Section 2.2.2.

The EE model was validated during SB2 (SME 224) and SB4 (SME 434) operations when the only reductants and oxidizers were those included in the 2006 EE REDOX model, e.g. nitrates, formates, oxalates, manganese, and coal. Since the amount of antifoam added to SB1-SB4 laboratory studies were in the range of 800-1000 ppm or mg/kg, the antifoam had a negligible effect on the melt pool REDOX and hence a term for antifoam was not included in the 2006 EE REDOX model.

During SB4 processing more antifoam was required for SRAT and SME processing. This was due to the increase in time required to steam strip mercury and to accommodate the dilute Actinide Removal Process (ARP) and Modular Caustic Side Solvent -Extraction (CSSX) Unit (MCU) streams. The organics from MCU have been reported to have little to no impact on melt REDOX [11,12].

While antifoam has always been added to DWPF feeds, the antifoam additions in the DWPF facility are driven procedurally and are time dependent based on the antifoam effectiveness. Prior to the declaration of the Potential Inadequacy in Safety Analysis (PISA) for the impact of antifoam on melter off-gas flammability, longer cycle times resulted in the more antifoam being added. The amount of antifoam added in the facility can be driven by several factors. These include the following:

- SRNL observations during the SB qualification runs,
- The amount of time required to steam strip the Hg° during the SRAT cycle,
- The amount of time spent boiling off the water contained in the ARP and MCU streams,
- The amount of time spent boiling the decontamination canister water additions to the SME (for each can blasted ~1000 gallons of water is added to the SME).

Since the resolution of the PISA, DWPF has minimized the amount of antifoam added during the SRAT and SME process.

1.5 Sludge Batch 5 and 6

For SB5 and SB6, the Hg concentrations were the highest ever seen in the DWPF facility to date, thus there were some very long SRAT cycles and increased amounts of antifoam were added to the SRAT and SME from SB4 and forward. During SB5 (SME 520), antifoam concentrations were higher than previous sludge batches but argon bubbling had not been initiated.

During SB6 from SME batch 540 and forward, argon bubbling was implemented. For SME 549, 550, 551, and 558 antifoam concentrations were higher than previous sludge batches but the melter was simultaneously bubbled with argon to improve melt rate [13]. The increased antifoam additions and ARP/MCU contributions continued into SB6 processing with argon melt pool bubbling. Concerns about the excess organics and potential flammability [14] curtailed the usage of IIT-747 antifoam and initiated several studies to examine the impact of antifoam IIT-747 on DWPF glass REDOX.

1.6 The Current Study

The results of the studies of antifoam IIT-747 on DWPF glass REDOX are summarized in this study and used to develop an IIT-747 antifoam term for the EE REDOX model (HLW-SDWPF-TTR-2011-0017-May 2011). Impacts of Ar melt pool bubbling are also discussed and address HLW-DWPF-TAR-2010-0022 (September 2010) and HLW-DWPF-TAR-2011-0002 (February 2011). The antifoam term is developed theoretically and fitted to sealed crucible data, then applied to DWPF melter pour stream (PS) data and DWPF radioactive feed tested in sealed crucibles.

For SB6 REDOX modeling the data from bubbled vs. non-bubbled crucibles is compared to the results of the MFT melt in a static crucible and the corresponding pour stream sample from the bubbled melt pool to quantify the impact of Ar on melt pool REDOX. This allowed a methodology by which excess oxidizers can be added to the SRAT to offset the impacts of Ar sparging. Lastly, argon-air ($0.78N_2$-$0.21O_2$) gas mixtures are calculated that could be used to introduce more oxygen into the melt pool by a gaseous route rather than by a chemical route. Note that air is chosen and not pure O_2 to minimize any safety issues. Since the air contains 78% N_2 this would sparge the melt pool in a similar manner to the Ar.

2.0 BACKGROUND

2.1 The DWPF REDOX Limits

The REDOX equilibrium in a HLW melter must be controlled to prevent the following [2,16]:

- liberation of oxygen which can cause foaming from decomposition of Mn^{+7}, Mn^{+4} or Mn^{+3} because the $MnO_2 \rightarrow MnO + \frac{1}{2} O_2$ or $2NaMnO_4 \rightarrow 2MnO + Na_2O + 2.5O_2$ reactions liberate oxygen at the melt temperature
- liberation of NO_x and oxygen caused by decomposition of nitrate species via reactions such as $NO_3 \rightarrow NO + O_2$ or $2NO_3 \rightarrow N_2 + 3O_2$
- retardation of melt rate due to foaming from nitrates and manganic species
- reduction of metallic species such as $NiO \rightarrow Ni^\circ + \frac{1}{2} O_2$ and $RuO_2 \rightarrow Ru^\circ + O_2$ which can fall to the melter floor and cause shorting of electrical pathways in the melt and accumulations which may hinder glass pouring

- reduction of sulfate ($SO_4^{=}$) to sulfide ($S^{=}$) which can complex with Ni° and/or Fe° to form metal sulfides which can fall to the melter floor and cause shorting of electrical pathways and/or hinder glass pouring
- overly reduced glasses which can be less durable than their oxidized equivalents when the $Fe^{+2}/\Sigma Fe$ exceeds 0.33 [15].

Controlling the HLW melters at a REDuction/OXidation (REDOX) equilibrium of $Fe^{+2}/\Sigma Fe \leq 0.33$ [16, 17] prevents the potential for conversion of $NiO \rightarrow Ni° + ½\ O_2$, $RuO_2 \rightarrow Ru° + O_2$, and $2SO_4^{=} \rightarrow S^{=} + 4O_2$ during vitrification. Control of foaming due to deoxygenation of manganic species is achieved by having 66-100% of the MnO_2 or Mn_2O_3 or any other oxidized Mn species converted to MnO [18] during pretreatment in the SRAT. At the lower REDOX limit of $Fe^{+2}/\Sigma Fe \sim 0.09$ about 99% of the manganic species are converted to Mn^{+2} [16, 17]. Therefore, the lower REDOX limit eliminates melter foaming from deoxygenation of manganic oxides.

The REDOX equilibria for DWPF borosilicate glasses were initially investigated by Schreiber [16,19,20,21]. Schreiber developed an electromotive force (EMF) series for DWPF glasses that correlates a given oxygen fugacity to the ratio of the reduced to oxidized species in a glass for all REDOX sensitive multi-valent species such as Mn, Fe, Ni Cr, Cu, U, S, etc. (Figure 2). The EMF series was determined in small furnaces where the oxygen fugacity (f_{O_2}) of the vapor in equilibrium with a melt was controlled by varying gas mixtures at a constant melt temperature of 1150°C. Therefore, the EMF series is independent of melter feed additives, e.g. oxidizers and/or reductants.

The EMF series allows the estimation of the REDOX state of all REDOX pairs present based on the measurement of only one REDOX ratio in DWPF glass, e.g. $Fe^{+2}/\sum(Fe^{+2}+Fe^{+3})$. Schreiber measured the $Fe^{+2}/\sum(Fe^{+2}+Fe^{+3})$ couple at 1% Fe, 5% Fe, and 10% Fe in a borosilicate frit and found that the total Fe concentration moved the $Fe^{+2}/\sum(Fe^{+2}+Fe^{+3})$ couple slightly. Since DWPF glasses contain between 8 -14 wt% Fe_2O_3[§] or 5.6 - 9.8 wt% Fe_{total}, the region between the 5 wt% and 10 wt% Fe correlation (nominally the V^{+4}/V^{+5} couple) determined by Schreiber is normally used. In other words, the measurement of the $Fe^{+2}/\sum(Fe^{+2}+Fe^{+3})$ ratio allows one to determine the oxygen fugacity f_{O_2} of the DWPF melt and the oxidation states of all the other REDOX pairs. For example, in Figure 2 when the $Fe^{+2}/\sum(Fe^{+2}+Fe^{+3})$ is 0.09 (9% of all the Fe present is reduced to Fe^{+2}), the log f_{O_2} is -3.5 and 98% of all the Mn^{+3} present is reduced to Mn^{+2}.

Schreiber's experimental data indicated that the oxygen fugacities in DWPF waste glass melters at 1150°C should be maintained between f_{O_2} values of 10^{-2} and 10^{-7} atm to simultaneously avoid foaming due to deoxygenation of transition metal species and metal precipitation [16]. This was based on bounding cases of 1 wt% Fe and 10 wt% Fe. Goldman's 1986 data, in support of the WVNS melter, recommended that the oxygen fugacity be controlled between f_{O_2} values of 10^{-4} to 10^{-7} atm. [22] Schreiber's publication specifically stated that "a melter must be operated at oxygen fugacities lower

---

§ The historic glass data on which the {[F]-[N]}, and the {[F]-[3N]} models were developed had Fe_2O_3 concentrations in the range of 10.6-13.8 wt% while the EE model included both the historic data and SB3 glasses made at waste loadings of 25, 30, 35, and 40 wt%. For the one hundred sixty five SB3 glasses, only 22 had Fe_2O_3 concentrations lower than 10 wt %, while the range of values varied from 8.33-29.02 wt% Fe_2O_3. The SB4 crucible samples added to the REDOX database had Fe_2O_3 values ranging from 8.35-12.29 wt%. The SB5 crucible samples added to the REDOX database had Fe_2O_3 values ranging from 10.53-11.03 wt%. The SB6 crucible samples added to the REDOX database had Fe_2O_3 values ranging from 7.55-9.03 wt%. The SB7a crucible samples added to the REDOX database had Fe_2O_3 values ranging from 8.70-9.37 wt% and SB7b was 8.8-9.71 wt%. The AFA glasses which are SB6 simulated feeds doped with varying amounts of antifoam (discussed later in this document) have a Fe_2O_3 content of ~10.01 wt%.

(more reduced) than f_{O_2} =10^{-2} atm in order to eliminate the oxidized states of manganese, cerium, and chromium as the cause of melter foaming" but his final oxidized waste processing limit was recommended at 10^{-4} atm to be conservative [16].

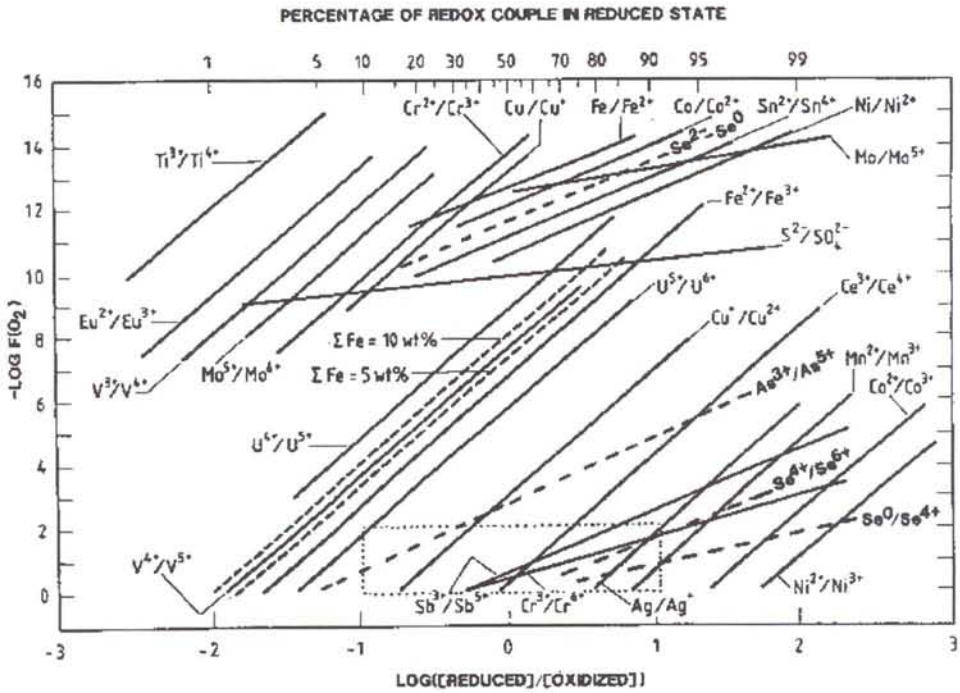

Figure 2. Electromotive Force (EMF) series developed for DWPF glasses at 1150°C [16].

Schreiber recommended routine measurement of the Fe^{+2}/Fe^{+3} or $Fe^{+2}/\sum Fe$ of a glass as the most accurate methodology by which the oxygen fugacity in a melt could be evaluated [21]. Glass REDOX measurement was shown to be more accurate than f_{O_2} measurement based on the use of oxygen probes in the melt or melt plenum.

Based on Schreiber's correlation of iron REDOX with oxygen fugacity, a glass with an iron REDOX ratio ($Fe^{+2}/\sum Fe$) between 0.09 (at 10% Fe) and 0.33 (at 10% Fe) provides the bounding f_{O_2} range between 10^{-4} and 10^{-7} atm. in the melter plenum and, hence, the optimum operating range to prevent foaming and metal precipitation. These conditions keep 98% of the Mn present as Mn^{+2}, >97% of the Cr present as Cr^{+3}, ≈100% of the Ni present as Ni^{+2}, 70-95% of the Cu present as Cu^{+}, 90-97% of the Ce present at Ce^{+3}, 25-65% of the U^{+6} present as U^{+5}, and 5-25% of the U^{+5} present as U^{+4}.

Jantzen and Plodinec [17] compared the recommendations of Schreiber [16], Goldman [22], Hrma [18], and others [25] and recommended that the DWPF REDOX ratio based on $Fe^{+2}/\Sigma Fe$ be controlled between 0.09 and 0.33 (i.e., the corresponding oxygen fugacity range of 10^{-4} to 10^{-7} atm at ~10 wt% Fe). Additional calculations by P. Kent Smith [23] in 1981 at SRNL had shown that an optimum range of oxygen fugacity for the DWPF was 10^{-5} to 10^{-8} atmospheres.

Confirmation of the impact of REDOX on DWPF melt rate was made by Michael E. Smith and others in 2004-2005 [9,24]. A specially designed melt rate furnace (MRF) was used to show a direct correlation between REDOX, foaming, and melt rate. At a $Fe^{+2}/\Sigma Fe$ of 0.1 and above the melt rate was maximized while the melt rate decreased significantly (≥25%) at $Fe^{+2}/\Sigma Fe$ of ≤0.1 thus verifying the lower REDOX limit of 0.09.

It should also be noted that [25] foaming and reboil were determined to be a strong function of oxygen fugacity in the melts of simple two component glasses (Na_2O-SiO_2) that contain no REDOX active species such as Mn and Fe. Foaming and reboil both decreased in this simple two component glass as the oxygen fugacity decreased, i.e. became more reduced than 10^{-2} atm. In these experiments, the oxygen partial pressures ranged from 10^{-2} to 10^{-12} atmospheres and were controlled by varying gas mixtures. Bubble stability and foaming were shown to be minimized at oxygen fugacities more reduced than 10^{-12} atmospheres, while DWPF operates more oxidizing (10^{-4} to 10^{-7}) than 10^{-12} but more reducing than 10^{-2} atm.

The REDOX range of $0.09>Fe^{+2}/\Sigma Fe<0.33$ has remained the DWPF REDOX limit since it was defined in the mid 1980's. Additional testing with Cu enriched feeds and during REDOX modeling (described in the next section) versus feed composition has been confirmatory of these limits and there has not been any data to indicate that the limits should be changed, e.g. above a $Fe^{+2}/\Sigma Fe$ of 0.33 metallic species and/or metallic sulfide species will form.

2.2 REDOX Modeling

The first REDOX model developed at SRNL balanced formic acid [F] and nitric acid [N] with a 1:1 stoichiometry [2,26,27,28] which implied that the oxidizing power of nitric acid was equivalent to the reducing power of formic acid on a molar basis. The equation developed is shown below.

Equation 1 $$Fe^{2+}/\Sigma Fe = -0.8 + 0.87\{[F]-[N]\},\ R^2 = 0.80$$

During the initial study, which was primarily a crucible study in which formated feeds were doped with different reductants and oxidants, it was shown that $\{[F]-[N]\}<0.9$ corresponded to an $Fe^{2+}/\Sigma Fe$ ratio of <0.05. In this region the absolute concentrations of formate and nitrate in the melter feed had no appreciable effect on glass REDOX since the feeds were oxidizer-rich and reductant-poor such that there was no impact on the REDOX ratio. No appreciable impact on glass REDOX causes a plateau to form at $Fe^{2+}/\Sigma Fe$ of ~0 (Figure 3). For overly reduced glasses ($Fe^{2+}/\Sigma Fe \geq 0.6$ and $\{[F]-[N]\}>1.7$), the absolute concentrations of formate and nitrate were shown to have no appreciable effect on glass REDOX. In this overly reduced regime, excess reductant reduced >60% of the ferric iron to ferrous and then began conversion of $NiO \rightarrow Ni°$ and $1.5SO_4^{=} \rightarrow 1.5S^{2-} + 3O_2$ causing Ni_3S_2 and/or Ni° to form (Figure 3). This causes a second plateau at a $Fe^{2+}/\Sigma Fe$ of ~0.65 (Figure 3). In the range between $Fe^{2+}/\Sigma Fe$~0.05-0.6 or an $\{[F]-[N]\}$ between 0.9 and 1.7, the $Fe^{2+}/\Sigma Fe$ response is linear with respect to $\{[F]-[N]\}$ and Equation 1 was fit to the data (Figure 3).

In 1997, the data used to develop the $\{[F]-[N]\}$ relationship was revisited because inclusion of any data from the two plateau regions shown in Figure 3 can highly leverage the Ordinary Least Squares (OLS) fit to the data. Hence, glass quality and REDOX measurement criteria were developed to screen the data used for modeling. This redefined the population of glasses by excluding those below one half the $Fe^{+2}/\Sigma Fe$ measurement detection limit of 0.03 or 0.015 and those that precipitated metallic and/or sulfide

species. Averaging of formate, nitrate and measured REDOX ratios was used to minimize model error. The OLS fit of the redefined "Model Data" over the {[F]-[N]} range between zero and 2.5 (Equation 2) demonstrated that the {[F]-[N]} parameter was a less accurate (R^2= 0.68 and a Root Mean Square Error (RMSE) = 0.109) predictor of waste glass REDOX [4] than had previously been calculated (see Figure 4). The large RMS value indicates that at a given {[F]-[N]} there is an associated large scatter in the REDOX response and this can be seen in Figure 3 and Figure 4.

Equation 2 $$Fe^{2+}/\Sigma Fe = -0.0257 + 0.31667\{[F]-[N]\}, R^2=0.68$$

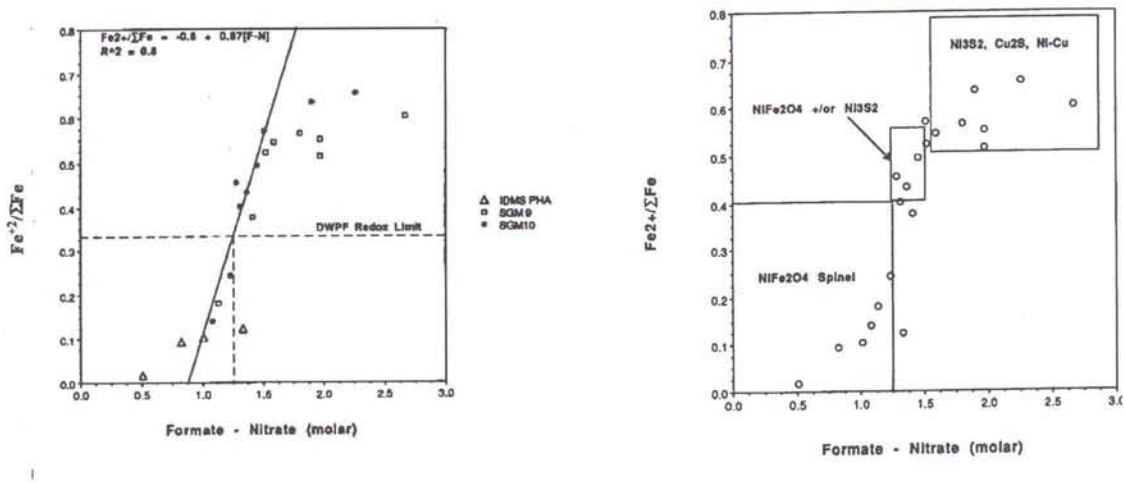

Figure 3. REDOX ratio relationship to {[F]-[N]} showing the "S" shaped curvature of the response. Equation 1 and Equation 2 hold only for the linear portion of the relationship between $Fe^{2+}/\Sigma Fe$~0.05-0.6. Note that the $Fe^{2+}/\Sigma Fe$ limits of 0.09 and 0.33 are not derived from this figure but from scale melter experience and References 16,19,20,21 as discussed in Section 2.1.

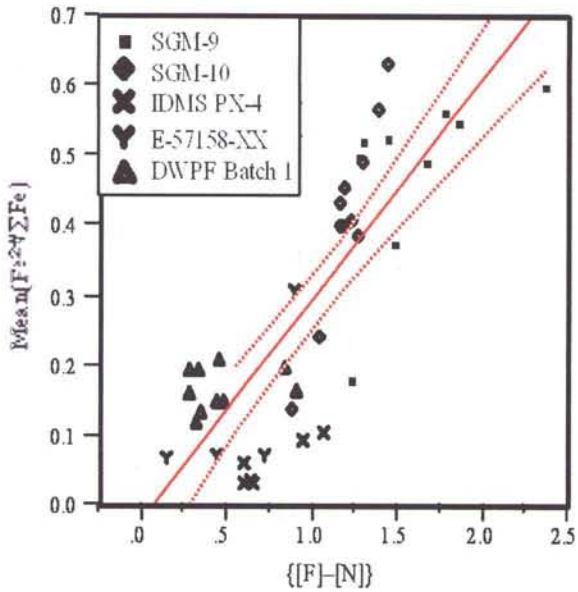

Linear Fit

Fe2+/∑Fe = -0.0257 + 0.31667 {[F]–[N]}

Summary of Fit

RSquare	0.687754
RSquare Adj	0.679537
Root Mean Square Error	0.108973
Mean of Response	0.286587
Observations (or Sum Wgts)	40

Analysis of Variance

Source	DF	Sum of Squares	Mean Square	F Ratio
Model	1	0.9939372	0.993937	83.6988
Error	38	0.4512562	0.011875	**Prob>F**
C Total	39	1.4451934		<.0001

Parameter Estimates

Term	Estimate	Std Error	t Ratio	Prob>|t|
Intercept	-0.025664	0.038233	-0.67	0.5061
{[F]–[N]}	0.3167722	0.034625	9.15	<.0001

Figure 4. Relationship between the $Fe^{2+}/\Sigma Fe$ ratio and the difference of mean molar formate [F] and nitrate [N] concentrations as re-determined in the 1997 study [4].

In addition, there was no known mechanistic impetus for using the molar difference between the reductants and oxidants for REDOX prediction. This artificially set the relative oxidation/reduction potentials of nitrate and formate to be equivalent when it was well known that nitric acid is a strong oxidizer and formic acid is a weak reductant.

Regression of the redefined data demonstrated that the {[F]-[N]} parameter was a less accurate predictor (R^2=0.68) of waste glass REDOX than had previously been reported (R^2=0.80).

The regression of the redefined data showed that there was an {[F]-3[N]} relationship between the feed reductants, oxidants, and the glass REDOX ratio

Equation 3 $Fe^{2+}/\Sigma Fe = 0.217 + \{0.253[F]-0.739[N]\}$, R^2=0.89

where the F and N concentrations are normalized to a feed that is 45 wt% solids. Both the {[F]-[N]} and the {[F]-3[N]} REDOX models assumed that the melter feeds were properly formated to the formate salts during reflux in the SRAT to ensure that 66-100% of the oxidized Mn^{3+} and Mn^{4+} were converted to Mn^{+2} as $Mn(COOH)_2$ during preprocessing, e.g., before the melter feed entered the melter.

In 2003, sludges with additional reductants (coal and oxalate) from Tank 7 were being incorporated into SB3 feeds, and in 2006 oxidizers (manganese) from Tank 11 Purex high heat waste (HHW) were being incorporated into SB4 feeds. [29] This required a mechanistic REDOX model that could account for all oxidizers (nitrates, nitrites, soluble and insoluble manganic species) and reductants (formates, sugar, coal, oxalate). In addition the model needed to be able to account for the relative oxidizing and reducing power

of each species. At this point, an EE model was developed based on the REDOX reactions that were known to occur in the melter cold cap.

2.2.1 THE COLD CAP REDOX REACTIONS (IN THE ABSENCE OF ARGON BUBBLING)

During feed-to-glass conversion, the REDOX reactions occur primarily in the cold cap along with feed decomposition and calcination. In the melt pool, further degassing and homogenization occur primarily by additional REDOX reactions. The gaseous products from the cold cap and the volatile feed components further react with air in the melter vapor space. In order to represent the gradual nature of the feed-to-glass conversion, a 4-stage cold cap model was developed by Choi [30] which approximates the melting of feed solids as a continuous, 4-stage counter-current process [31]. In Stage 1 formate salts formed in the SRAT, such as NaCOOH[f], are decomposed to CO, CO_2 and H_2 or steam. The Na forms oxides or otherwise interacts with any silicate, borate, or aluminate species available in the cold cap. The CO subsequently gets oxidized by the air diffusing into the cold cap from the top and by the oxygen being liberated during the Stage 2 denitration reactions (at further depth in the cold cap). Thus the overall decomposition and calcination reactions occurring in Stages 1 and 2 can be represented by the combined equation:

Equation 4

$$\underbrace{2NaCOOH + 2NaNO_3}_{melter\ feed} \rightarrow \underbrace{CO\uparrow + CO_2\uparrow + H_2\uparrow}_{Stage\ 1} + \underbrace{N_2O\uparrow + 2O_2\uparrow}_{Stage\ 2} + \underbrace{2Na_2O}_{Stage\ 1\ and\ 2} \rightarrow$$

$$\underbrace{2CO_2\uparrow + H_2O\uparrow + N_2\uparrow + 1.5O_2\uparrow}_{plenum} + \underbrace{2Na_2O}_{glass}$$

Multiple oxides begin to form during Stage 3. These oxides are assumed to form solid solutions such as spinels which coexist with the REDOX species in the same phase. Stage 4 represents the final fusion where the oxides formed in Stage 3 form aluminate, borate, or silicate groups in the melt, e.g., Fe_2SiO_4 and Na_2SiO_3. In order to represent all four stages of cold cap reaction simultaneously and include terms for reduced and oxidized iron and silica one can assume a generalized form of the reactions as follows:

Equation 5 $$Fe_2O_3 + 5SiO_2 + 6NaCOOH + 2NaNO_3 \rightarrow Fe_2SiO_4 + 6CO_2\uparrow + N_2\uparrow + 4Na_2SiO_3 + 3H_2O\uparrow$$

Equation 5 assumes that Fe^{3+} enters the melter as Fe_2O_3 and that the reductant $COOH^-$ and the oxidizer NO_3^- enter as sodium formate and sodium nitrate, respectively. The formated and nitrated salts react with glass formers such as SiO_2 to form Fe^{+2} and Na_2SiO_3 components in the glass and liberate CO_2, N_2O and H_2O vapors to the melter plenum (Equation 4 and Equation 5).

---

f While the example equations are written as the sodium salts, i.e. NaCOOH, it should be noted that such species as $Ca(COOH)_2$, $Ni(COOH)_2$, $Mn(COOH)_2$ form and undergo similar reaction.

2.2.2 ELECTRON EQUIVALENTS MODEL [7,8,10]

For simplicity and consistency in prediction, a mechanistic REDOX model was developed using the generalized form of the cold cap reactions (Equation 5). This equation can be rewritten in terms of Fe^{2+} and Fe^{3+} instead of the iron oxides, and the SiO_2 term can be omitted as it is not involved in the REDOX reactions, e.g. it does not change oxidation state. In addition, the vapor species generated in Stage 1 and Stage 2 of the cold cap, where these reactions occur, are used as the product phases rather than the vapor species measured in the plenum (see Equation 5) as these are the gases that diffuse upward though the cold cap and provide the oxygen for the oxidation of organics to CO_2. This generates Equation 6 below as one of the controlling REDOX reactions, the one between reducing formate salts and oxidizing nitrated salts, in the cold cap:

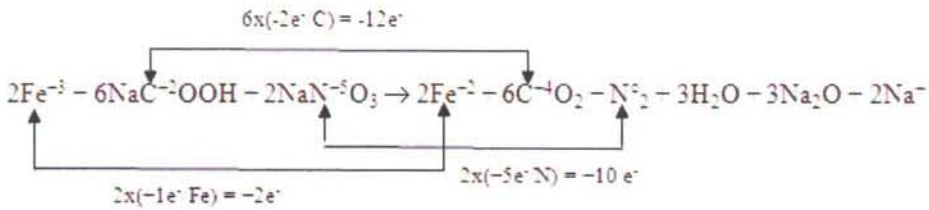

Equation 6

The oxidation/reduction equilibrium shown in the Equation 6 between nitrate and formate indicates that one mole of nitrate gains 5 electrons when it is reduced to N_2 while one mole of carbon in formate loses 2 electrons during oxidation to CO_2. This is an oxidant:reductant ratio of 5:2 which indicates that nitrate is approximately 2½ times as effective an oxidizing agent as formate is a reducing agent (when nitrogen gas is the reaction product).

The oxidation/reduction equilibrium shown in Equation 7 between coal and the oxidized nitrated salts indicates that one mole of nitrate gains 5 electrons when it is reduced to N_2 while one mole of carbon in coal loses 4 electrons during oxidation to CO_2. This is an oxidant:reductant ratio of 5:4 which indicates that nitrate is only 1¼ times as effective an oxidizing agent as coal is a reducing agent (when nitrogen gas is the reaction product).

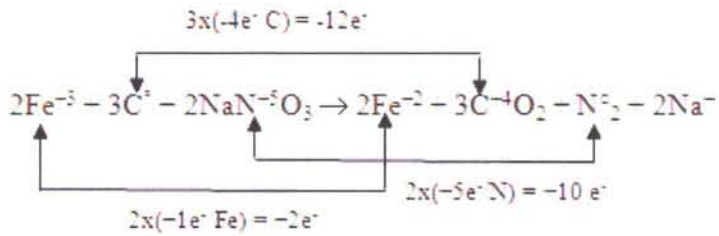

Equation 7

The oxidation/reduction equilibrium between the oxalate and nitrate salts is given in Equation 8.

Equation 8

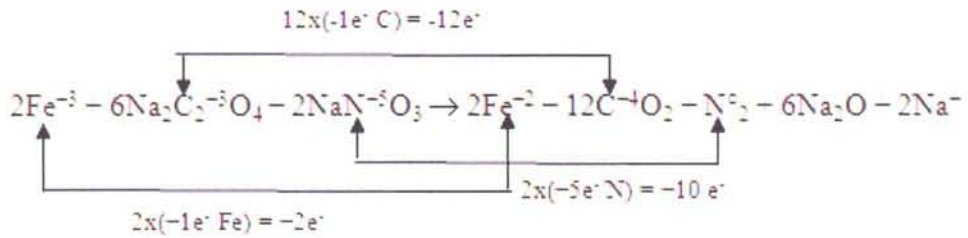

One mole of nitrate should gain 5 electrons when it is reduced to N_2 and one mole of carbon in oxalate should lose 1 electron during oxidation to CO_2. This is an oxidant:reductant ratio of 5:1 which indicates that nitrate is 5 times as effective an oxidizing agent as the carbon in oxalate is a reducing agent (when nitrogen gas is the reaction product).

However, the REDOX modeling data indicated that oxalate was twice as strong a reductant as would be indicated by a 5:1 ratio. During further investigation of the apparent increase in the reducing power of oxalate, data became available that demonstrated that oxalate salts convert to oxalic acid, which then disproportionates to formic acid and CO_2 during SB3 SRAT processing [32] via Equation 9:

Equation 9

$$6HC_2^{+3}O_4^- \rightarrow 12HC^{+2}O_2^- + 12C^{+4}O_2 \uparrow$$

The formic acid is converted to sodium formate, and therefore is stable until it reacts in the melter cold cap oxidation/reduction reactions. The carbon in the newly formed sodium formate is twice as strong a reductant as the initial carbon in the oxalate, and exchanges 2e⁻ per carbon (see Equation 6). Stated another way, half of the carbon in one mole of oxalate is providing the same number of electrons as a mole of formate, i.e. oxalate is twice as reducing as initially expected and the associated REDOX EE factor is 4 instead of 2. This can be expressed as shown in Equation 10 below:

Equation 10

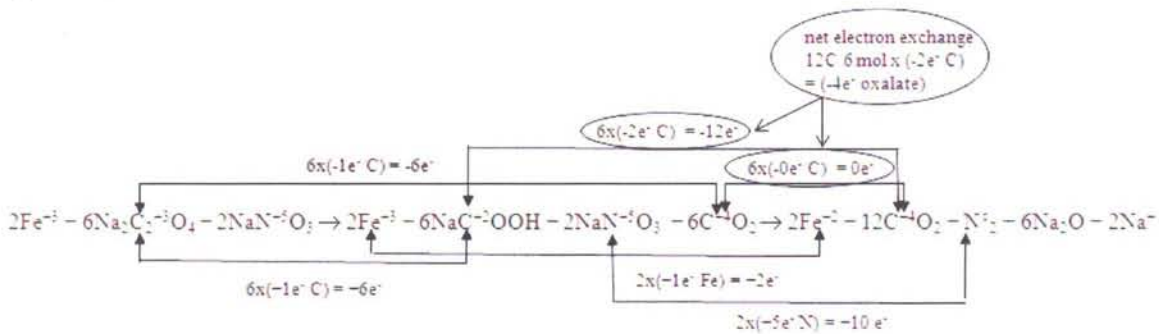

In Equation 10 the electron exchanges that are shaded cancel each other out as 6 carbons are oxidized and 6 carbons are reduced in the disproportionation reaction. Experimentally, it was found that between 8-37% of the oxalate present in the SRAT was determined to disproportionate during processing into

HCOOH and CO_2 gas [32]. Therefore, it was assumed that additional disproportionation occurs in the SME or cold cap when the liquid slurry impacts the melt pool surface.

While antifoam has been added to all SB3-SB7b SRAT and SME campaigns with simulants the antifoam additions have all been small and all followed the following protocol:

- 200 ppm prior to nitric acid
- 100 ppm prior to formic (this addition not added to all runs)
- 500 ppm prior to SRAT boiling
- 100 ppm prior to SME processing

Therefore, a generic 800 ppm antifoam concentration has been added to each SB3, SB4, SB5, SB6, and SB7a/b sample in the REDOX database used for this study.

An EE equation can be written for the reduction of manganese by any carbon containing species and its re-oxidation by nitrated salts in the cold cap [10], for example

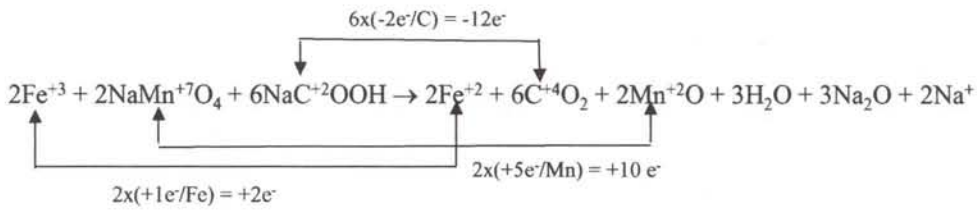

Equation 11

If the left hand side (LHS) of the equation had Mn^{+4} reducing to Mn^{+2}, then the EE term would be $-2e^-$ per mole of Mn instead of $-5e^-$ per mole of Mn. However, since the DWPF cannot ensure that >66% of the manganese in the SRAT is +2 (presumably as $Mn(COOH)_2$) it is more conservative to assume that more oxidized species of manganese such as Mn^{+4} or Mn^{+7} are present. In addition, re-oxidation of Mn in the cold cap by molten salts was proven [10] for SB4, and so the more conservative EE term for Mn (to prevent foaming) was applied which is -5.

Equation 6, Equation 7, Equation 8, and Equation 11 demonstrate that the relative factors for the electrons exchanged upon oxidation and reduction are the following:

- +4 EE/mole of coal
- +2 EE/mole of formate
- +4 EE/mole of oxalate
- -5 EE/mole of nitrate
- -5 EE/mole of manganese.

Since the model is {reductants – oxidants} or {R-O}, the signs for the oxidants are negative and the signs for reductants are positive.

The effectiveness of the oxidants and reductants depends on their concentrations relative to the other slurry components. Therefore, the molar EE term must be multiplied by the factor 45/T, where T is the

total solids (wt%) content of the slurry. This factor puts all concentrations on a consistent basis of 45 wt% total solids. The normalized molar Electron Equivalents, ξ are then:

$$\xi\left(\begin{matrix} mol/kg\ feed \\ @45\ wt\%\ solids \end{matrix}\right) = (2[F] + 4[C] + 4[O_T] - 5[N] - 5[Mn])\frac{45}{T}$$

Equation 12

where the concentrations of the reductants and oxidants are expressed in mol/kg of feed. Therefore, the basis for the relation of REDOX to electron equivalent transfers,ξ is

$$\frac{Fe^{2+}}{\Sigma Fe} = f\left[(2[F] + 4[C] + 4[O_T] - 5[N] - 5[Mn])\frac{45}{T}\right] = f[\xi]$$

where f = indicates a function
[F] = formate (mol/kg feed)
[C] = coal (carbon) (mol/kg feed)
$[O_T]$ = $oxalate_{Total}$ (soluble and insoluble) (mol/kg feed)
[N] = nitrate + nitrite (mol/kg feed)
[Mn] = manganese (mol/kg feed)
T = total solids (wt%)

$$\xi = (2[F] + 4[C] + 4[O_T] - 5[N] - 5[Mn])\frac{45}{T}$$

When the REDOX data generated in References 10, 7, 8 and the data from the 1997-8 study [4] were fit as a linear function of ξ:

$$\frac{Fe^{2+}}{\Sigma Fe} = 0.2358 + 0.1999\xi$$

Equation 13

which is the DWPF Electron Equivalents REDOX model with an adjusted R^2 of 0.81 and a Root Mean Square Error of 0.0704 for 139 data observations (67 data points[‡] from the historic data study [4], 53 data points from the 2003 SB3 study [7, 8], and 19 data points from the 2006 SB4 study [10]). The model ranges for REDOX values, reductant concentrations, and oxidant concentrations will be discussed in Section 2.2.4 followed by validation of the EE model in Section 2.2.5. However, the minimization of error in the REDOX measurement is discussed in Section 2.2.3.

‡ During the 2003 REDOX modeling a decision was made to use the 67 data values from the 1997 REDOX study rather than the 40 averaged mean values used in the 1997 study. This decision was made because the formate, nitrate and REDOX values in Appendix A of the 1997 study were comprised of 123 individual analyses that were averaged for the modeling. During the current REDOX modeling the 1997 individual values given in Appendices B, C, and D of the 1997 report were used since the SB3 data was comprised of individual analyses. Of the 123 values from 1997, only 72 measurements had $Fe^{+2}/\Sigma Fe$ ratios greater than the detection limit. Of the 72 values, two were missing formate concentrations, one was missing a nitrate concentration, and two were missing Mn values. This left an "historic" data pool of 67 samples.

2.2.3 REPORTING OF THE REDOX MEASUREMENT TO MINIMIZE ERROR

The historical REDOX samples used in the 1997 model were determined based on one sample replicate from each SME crucible batch. The $Fe^{+2}/\Sigma Fe$ analysis was performed by the Baumann method [33] which is the method also used by the SRNL Process Science Analytic Laboratory (PSAL) [34] and in the SRNL Shielded Cell Facility (SCF). These analyses were used to develop the {[F]-[N]} and the {[F]-3[N]} DWPF REDOX models [2,4] as well as the EE REDOX model [7,8,10]. In this method, a single dissolution is performed and two absorbances representing the REDOX state in a given glass are measured: (1) one for Fe^{2+} and (2) one for the total Fe (or ΣFe) after all Fe^{3+} was forcibly reduced to Fe^{2+}. The iron REDOX ratio appropriate for control–the fraction of iron present in the reduced state or $Fe^{2+}/\Sigma Fe$ is computed from these two measured absorbances. The best estimate of the REDOX ratio for a glass from n measurements is the average of the n computed ratios (from the n pairs of measured absorbances):

$$\frac{Fe^{2+}}{\Sigma Fe} = \frac{1}{n}\sum_{i=1}^{n}\left(\frac{Fe_i^{2+}}{\Sigma Fe_i}\right) = \overline{\left(\frac{Fe^{2+}}{\Sigma Fe}\right)}$$

Equation 14

The glasses used for REDOX modeling are often measured in duplicate or triplicate. Even for glasses in which only one REDOX ratio is measured, two absorbance measurements representing the REDOX state in the glass are made: 1) one for Fe^{2+} and 2) one for the total Fe (or $\sum Fe$) after all Fe^{3+} is forcibly reduced to Fe^{2+}.[33,34] Thus the iron REDOX ratio appropriate for control–the fraction of iron present in the reduced state, or $Fe^{2+}/\sum Fe$, is computed from these two measured values.[35] However, since both of these measurements contain error, the best manner in which to compute the REDOX ratio for a glass from multiple REDOX measurements is:

$$\frac{Fe^{2+}}{\Sigma Fe} = \frac{\frac{1}{n}\sum_{i=1}^{n} Fe_i^{2+}}{\frac{1}{n}\sum_{i=1}^{n} \Sigma Fe_i} = \frac{\overline{Fe^{2+}}}{\overline{\Sigma Fe}}$$

Equation 15

or the ratio of the mean reduced and mean total iron from the n measurements.

In other words, the n pairs of measured absorbances from each sample were averaged and then the REDOX ratio was calculated. These averages are tabulated in Reference 4. The DWPF Environmental Assessment (EA) glass [36], with a known REDOX, was always analyzed in tandem as a standard.

There are errors associated with each measurement in the REDOX model, e.g. measurement of the iron absorbances, the nitrate, nitrite, manganese, coal, oxalate, and formate. Since the iron absorbances, nitrate concentrations, and formate concentrations are still the dominant sources of error in both the {[F]-3[N]} and the EE model, Table 1 is provided below from Reference 4.

Table 1. Random Effects Model Summary for the SRNL Model Crucible Data

	All Data				Model Data Only			
	N	Variance	Std. Dev.	Std. Error	N	Variance	Std. Dev.	Std. Error
Formate (M)	151	0.01856	0.1362	0.07866[a]	119	0.019551	0.1398	0.08073[a]
Nitrate (M)	151	0.000948	0.0308	0.01778[a]	119	0.000958	0.03095	0.01787[a]
$Fe^{2+}/\Sigma Fe$	111	0.003004	0.0548	0.03876[b]	85	0.002163	0.04651	0.03289[b]

(a) Assuming three samples are available for the formate and nitrate concentration measurements. Note also that these errors underestimate those for these parameters since the total weight percent solids measurements which should be used to normalize these values to a 45% total solids basis (and thus add error) are unavailable for these data.
(b) Assuming duplicate samples are available for REDOX ratio measurements.

It should also be noted that once metallic species start to precipitate at concentrations of $Fe^{+2}/\Sigma Fe$ 0.33, it becomes more difficult to measure the $Fe^{+2}/\Sigma Fe$ ratio exactly. This occurs because the precipitation of the metallic species chemically alters the REDOX of the surrounding glass due to electron transfers between the iron species and the metallic species and sulfides and the precipitates physically make the glass inhomogeneous. Therefore, more replicates are necessary to get an accurate or average $Fe^{+2}/\Sigma Fe$ measurement.

2.2.4 MODEL RANGES

The 2006 EE model was developed with data from the 1997 historic model and with REDOX data from SB3 and SB4. It was the high nitrate in SB4 that demonstrated that the manganese term should be a -5 instead of a -2. However, before one can validate the 2006 EE model for SB5, SB6, SB7a, SB7b and the antifoam glasses (designated as AFA) one must determine if the model ranges for the newer sludge batches and the AFA glasses are within the original model ranges.

In 1997 the {[F]-3[N]} was fitted over the independent variables used in the regression analyses that possessed the following ranges:

$$0.03 \leq Fe^{+2}/\Sigma Fe \leq 0.64$$
$$0.31 \leq \text{Formate (M)} \leq 2.66$$
$$0.11 \leq \text{Nitrate (M)} \leq 0.76.$$

However, the formate and nitrate concentrations from the 1997 study were divided by the slurry weight percent solids to enable the comparison to be made on a consistent basis independent of whether a given slurry was more dilute or less dilute, e.g. mol/kg feed was normalized to 45% solids. This normalization was also used in development of the subsequent 2003 and 2006 EE models where Mn was -2 in 2003 and went to -5 in 2006 to account for Mn^{+7} species.

The independent variables used in the historic 1997 regression analyses possess the following ranges in mol/kg slurry, the units used to define ξ (see Equation 12): $0.23 \leq$ formate (mol/kg) ≤ 1.87; and $0.06 \leq$ nitrate (mol/kg) ≤ 0.59. The independent variables used in the 2003 EE model (53 data points) cover narrower ranges: $0.24 \leq$ formate (mol/kg) ≤ 0.68; and $0.14 \leq$ nitrate (mol/kg) ≤ 0.38.

The 2006 EE model used the historic data set (1997), the SB3 and the SB4 datasets. The following individual species feed composition ranges are covered:

$0.03 \leq Fe^{+2}/\Sigma Fe \leq 0.71$
$0.25 \leq$ Formate (mol/kg slurry) ≤ 1.63
$0.09 \leq$ Nitrate (mol/kg slurry) ≤ 0.65
$0.00 \leq$ Oxalate (mol/kg slurry) ≤ 0.53
$0.00 \leq$ Coal (mol/kg slurry) ≤ 0.10
$0.00 \leq$ Manganese (mol/kg slurry) ≤ 0.15

Because the individual species concentrations vary widely it is more appropriate to look at the range of ξ in the various studies. The 1997 {[F]-3[N]} model had a range of $-1.14 \leq \xi \leq 1.768$. The 2003 and 2006 EE models had a range of Xi (ξ) that fell within the 1997 so that the pooled variance of the historic, 2003 (SB3), and 2006 (SB4) EE model is still $-1.14 \leq \xi \leq 1.768$.

The comparisons of the ranges of the individual components are shown in Figure 5 in what are known as quantile plots. The plots show the individual points and the midline in the box represents the sample median value. The top of the box is the 75th quantile and the bottom of the box is the 25% quantile. The difference between the 25% and 75% quantiles is known as the "interquantile" and the whisker values represent 1.5 times the interquantile box. This allows comparisons of the median values of all the SB glasses to the historic glasses, SB3 glasses, and SB4 glasses that were used to develop the 2006 EE model and to DWPF operational glasses and the AFA glasses discussed later in this study. It also allows each SBs studied after the 2006 EE model was developed to be assessed as to whether the feeds were in the range of the model or not.

Figure 5a shows the ranges of nitrate in mol/kg and demonstrates that the maximum nitrate in SB3 crucible feeds were higher than the maximum nitrate in the SB4 crucible feeds but the median value of the SB4 crucible feeds was higher in nitrate than the SB3 crucible feeds. The high nitrate in the SB4 crucible feeds were the driver for the re-evaluation of the Mn term from -2 to -5 as the Mn was shown to re-oxidize in the cold cap from the formation of molten salt to the +7 state and/or the nitrate was so high that >66% of the manganese had not been reduced to the +2 state. Due to these uncertainties in the manganese state entering the melter or in the cold cap, it is conservative to use the -5 term for the EE model as the median nitrate values for SB5, SB6, and SB7a/b are all higher than the median value of the historic data and the median value of the SB3 data while not as high as the median value of the SB4 data. Figure 5a also demonstrates that the AFA glasses (first antifoam study) have higher nitrate than many of the other crucible feeds, including the second antifoam study (Antifoam-II), but the AFA glasses are still within the maximum range of nitrate values on which the 2006 EE model is based.

Figure 5b shows the ranges of formate in mol/kg and demonstrates that the median formate in SB3 crucible feeds was lower than the historic or SB4 crucible feeds. The median value for SB5 formate is higher than all the other feeds tested except for the AFA feeds. All the feeds for all the crucible studies and all the DWPF campaigns fall well within the model maximum and minimum.

Figure 5c shows the ranges of oxalate tested in mol/kg. This figure demonstrates that the SB3 feeds had the widest variation in oxalate and that all the other sludge batches and DWPF campaigns had much lower median values of oxalate. The diagram for coal (which is not shown) is almost identical to that of oxalate as both those terms were added to the EE model in 2003 based on the SB3 testing.

Figure 5d shows the ranges of manganese tested in mol/kg. This figure demonstrates that the SB4 feeds had the highest manganese median of the three data sets used to develop the 2006 EE model. SB4 had the highest median nitrate (Figure 5a) coupled with the highest manganese (Figure 5d) and that was the basis for being able to understand the interactions between high manganese content feeds in the presence of

high nitrate feeds and the role of molten salts in reoxidizing the manganese after it leaves SRAT/SME processing. Since the median value of manganese in DWPF feeds is high and the DWPF SRAT/SME/MFT batches have gotten enriched in manganese as the DWPF transitioned from feeding SB3 to SB4,5,6. The role of Mn is especially important because SB4 contained HM waste from Tank 11 and HM HHW is simultaneously high in Al and Mn (Tank 11 is considered HM HHW[f]). Both HM low heat waste (LHW) and Purex HHW are even higher in Mn compared to Purex LHW and HM HHW.[37] Thus, SB4 was initially anticipated to be higher in Mn than SB1-SB3 depending on how much Tank 11 waste was added to SB4. Moreover, future sludge batches made with HM LHW and Purex HHW will continue to have a high Mn content. These differences in the Mn concentration come about from the following:

- The HM wastes were generated from higher activity uranium (U^{235})-aluminum alloy fuel than the Purex wastes which were generated with U^{238}.
- A manganese dioxide precipitation strike was used in the head end of both processes to remove fission products like Zr and Nb by sorption if the beta/gamma activity of the wastes were above certain limits.
- Even more Mn was used when the activity was higher and this coincided with processing of the HHW (Purex and HM).
- The HM fuel was also clad in aluminum and during waste generation the entire assembly was dissolved in nitric acid without a separate aluminum decladding step as done in Purex processing [38], therefore the HM HHW is diluted by large concentrations of Al in the sludge compared to the HM LHW and the Purex HHW.

Therefore, it is appropriate to continue to use the -5 EE factor (2006) instead of the -2 EE factor (2003) for manganese in the presence of elevated nitrate. The median value of manganese for SB5, 6, and 7 are all high and, indeed, the median value of manganese for SB6 was outside (higher) than the maximum tested to develop the model. When the DWPF model is revised to include the data from SB5, 6, and 7, the model maximum for manganese will be revised.

Figure 5e shows the model ranges for Xi (ξ) which is

$$\xi = \left(2[F] + 4[C] + 4[O_T] - 5[N] - 5[Mn]\right)\frac{45}{T}$$

Figure 5e demonstrates the range of this composite model term and demonstrates that all the sludge batches to date including all the DWPF campaigns were targeted within the model and model parameters, which is why the impacts of parameters not included in the model (antifoam and Ar bubbling) are being assessed in this study.

The last figure, Figure 5f, shows the range of REDOX ($Fe^{+2}/\Sigma Fe$) for all the crucible studies performed from 1997 to present and compares those ranges to those measured in the DWPF. Both the model maximum and minimum are shown in Figure 5f along with the DWPF operational window. Note that at values of $Fe^{+2}/\Sigma Fe > 0.33$ metallic and sulfide droplets and nodules have been observed in various crucible studies. Figure 6 shows a quantile plot for the SME/MFT wt% solids for various crucible studies and DWPF campaigns. The nominal wt% solids is shaded in Figure 6 but the actual value of any batch is used to adjust the molar concentrations to a 45 wt% solids basis during REDOX modeling.

[f] e-mail on 01/03/07 from Jeffrey Gillam to C.M. Jantzen

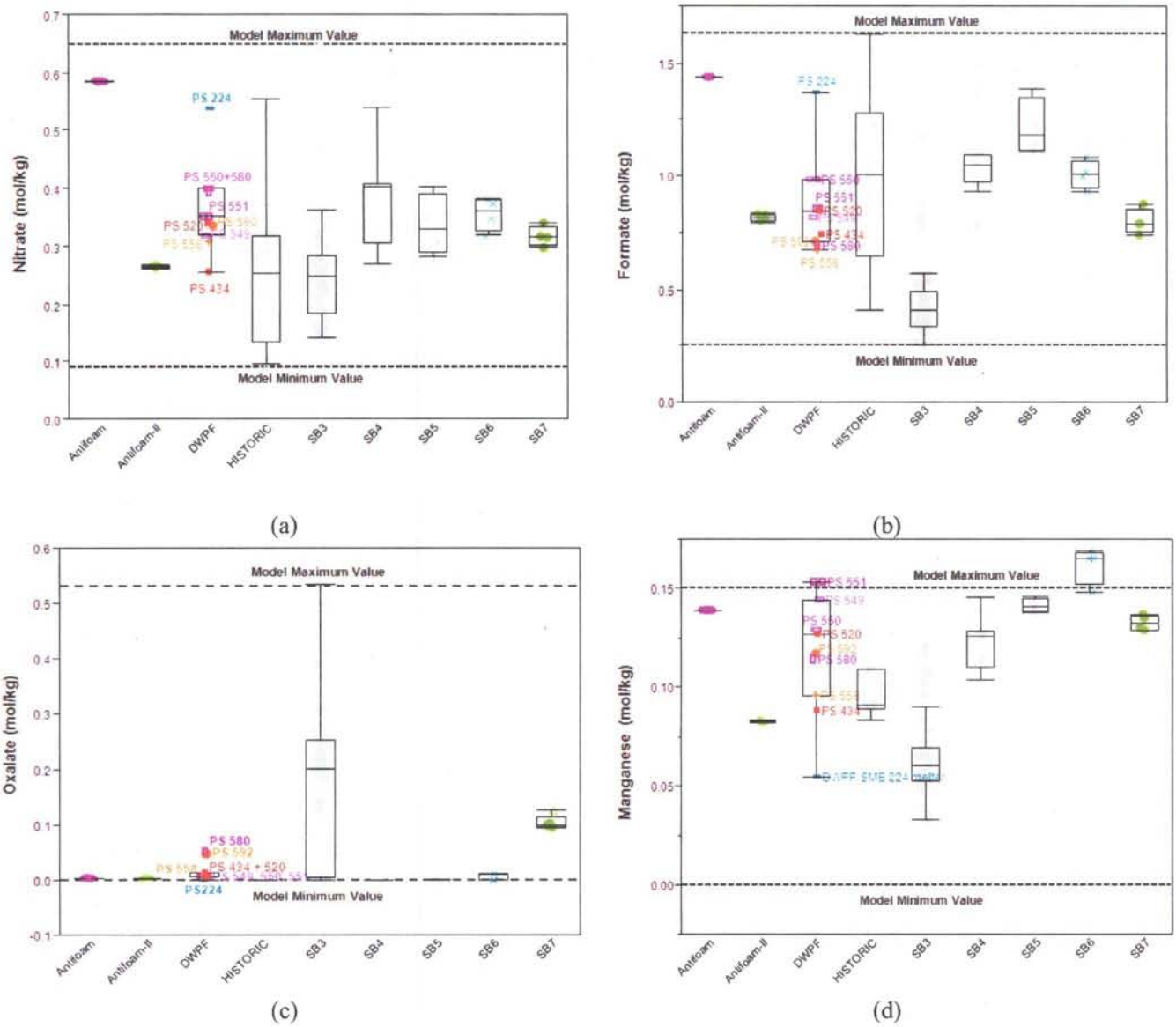

Figure 5. Quantile plots of different glass populations showing the feed and REDOX ranges for (a) nitrate+nitrite (mol/kg), (b) formate (mol/kg), (c) oxalate (mol/kg), (d) manganese, (e) Xi (ξ) mol/kg, and (f) REDOX ($Fe^{2+}/\Sigma Fe$). Crucible data and DWPF data are shown for comparison.

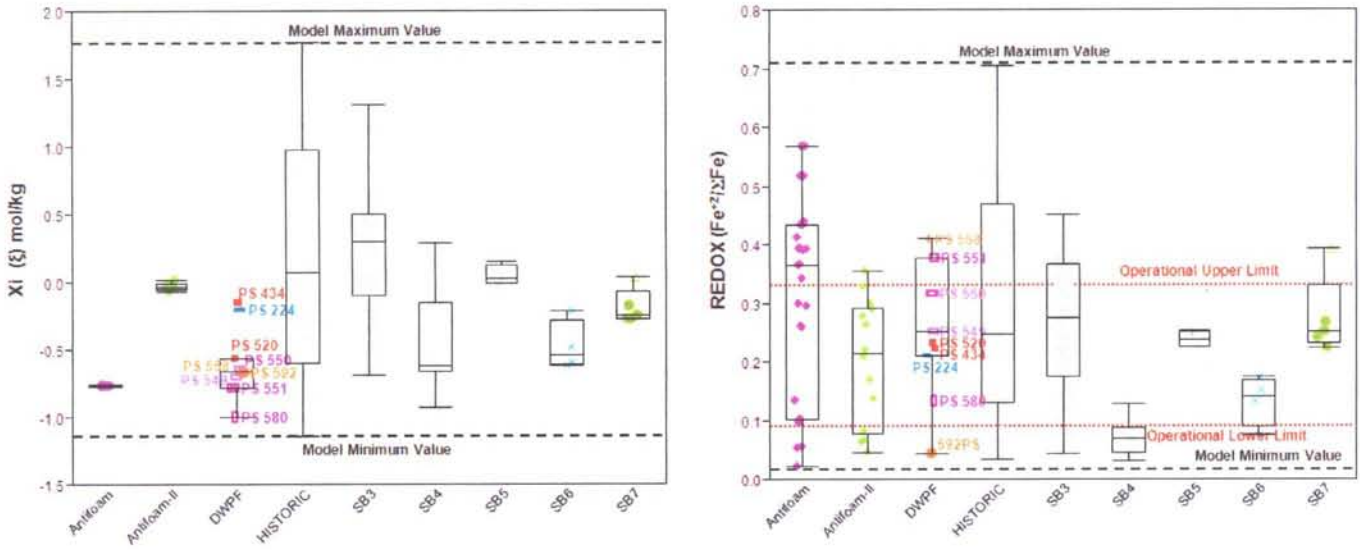

(e) (f)

Figure 5. (continued). Quantile plots of different glass populations showing the feed and REDOX ranges for (a) nitrate+nitrite (mol/kg), (b) formate (mol/kg), (c) oxalate (mol/kg), (d) manganese (mol/kg), (e) Xi (ξ) mol/kg, and (f) REDOX ($Fe^{2+}/\Sigma Fe$). Crucible data and DWPF data are shown for comparison.

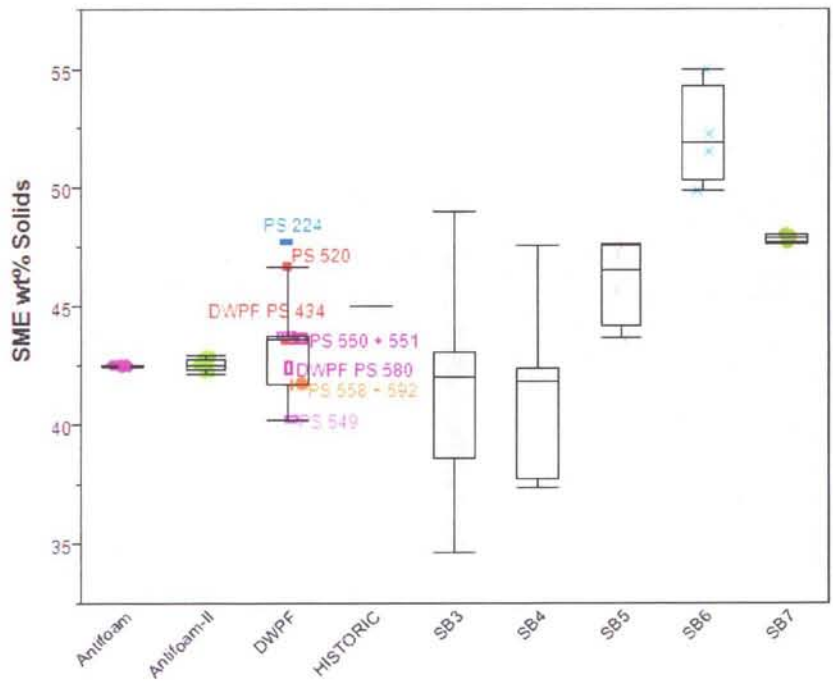

Figure 6. Quantile Plot of the different glass populations showing the variation in SME wt% solids. The model nominal range of 40-50 wt% solids is shaded in the figure. The actual wt% solids is not a concern for the REDOX model as all the SME wt% solids are normalized to a 45 wt% basis to correct all the concentrations as done with all the historic REDOX data. Crucible data and DWPF engineering scale data are shown for comparison.

2.2.5 VALIDATION OF THE EE MODEL (SB4-SB7 AND DWPF DATA)

The EE model (Equation 13) is shown in Figure 7 along with melter data from DWPF SME Batch 224 taken and analyzed during SB2 processing. It can be seen in Figure 7 that the SME 224 measured REDOX is superimposed directly on the predicted REDOX correlation. Additional glasses from the SRNL Slurry Melt Rate Furnace (SMRF) which processed SB2/SB3, and SB4 feeds are also superimposed (red circle and purple squares) and fall within the 95% confidence bands of the model. The SRNL Minimelter also processed SB2 feeds with frit 200 and frit 320 and the measured REDOX validation data is overlain on Figure 7. Data from crucible studies related to SB4 are also shown in Figure 7 (all star shaped symbols regardless of color are SB4 crucible data). All the SB2, SB3 and SB4 validation data fall within the 95% confidence bands of the model.

Sealed crucible data from SB5 [39] and SB6 [11] testing is overlain on the Equation 13 fit in Figure 8 to validate the EE REDOX equation for these sludge batches. The correlation of predicted REDOX vs. measured REDOX gives a slope of 1.0 and an intercept of zero and the data from SB5 and SB6 falls within the 95% confidence bands.

Sealed crucible data from SB7a [40] and SB7b [41] testing is overlain on the Equation 13 fit in Figure 9. Note that the one data point that does not fit within the model defined by Equation 13 and that is sample SB7-7. As noted by Newell [11] and Newell and Stone [12] SB7-10, which contained ARP components did not appear to have an impact on glass REDOX.

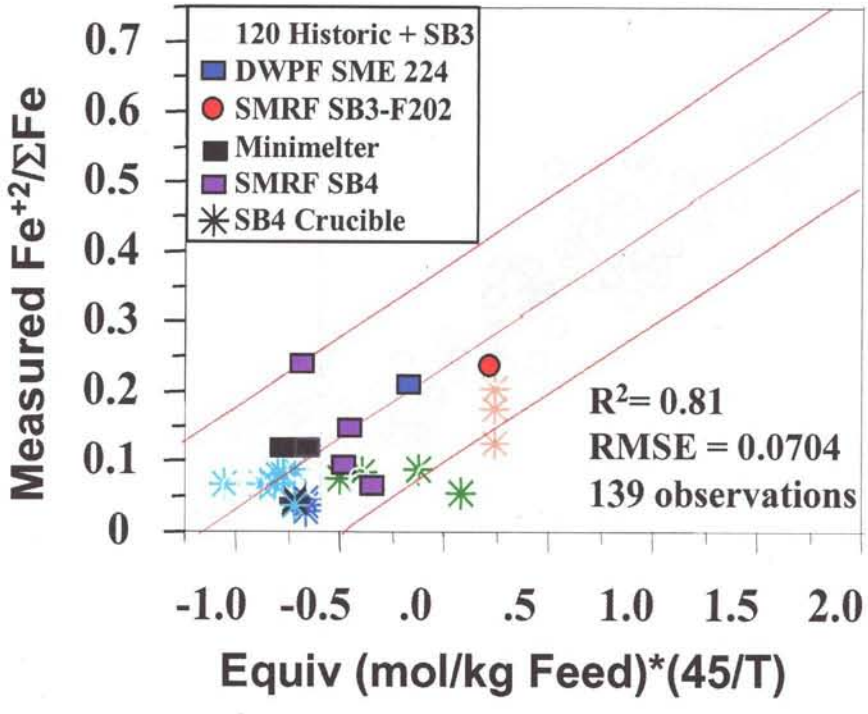

Figure 7. Fit of Xi(ξ) to the pooled historic, SB3, and SB4 2006 EE REDOX data [10] which generates the slope and intercept of Equation 13.

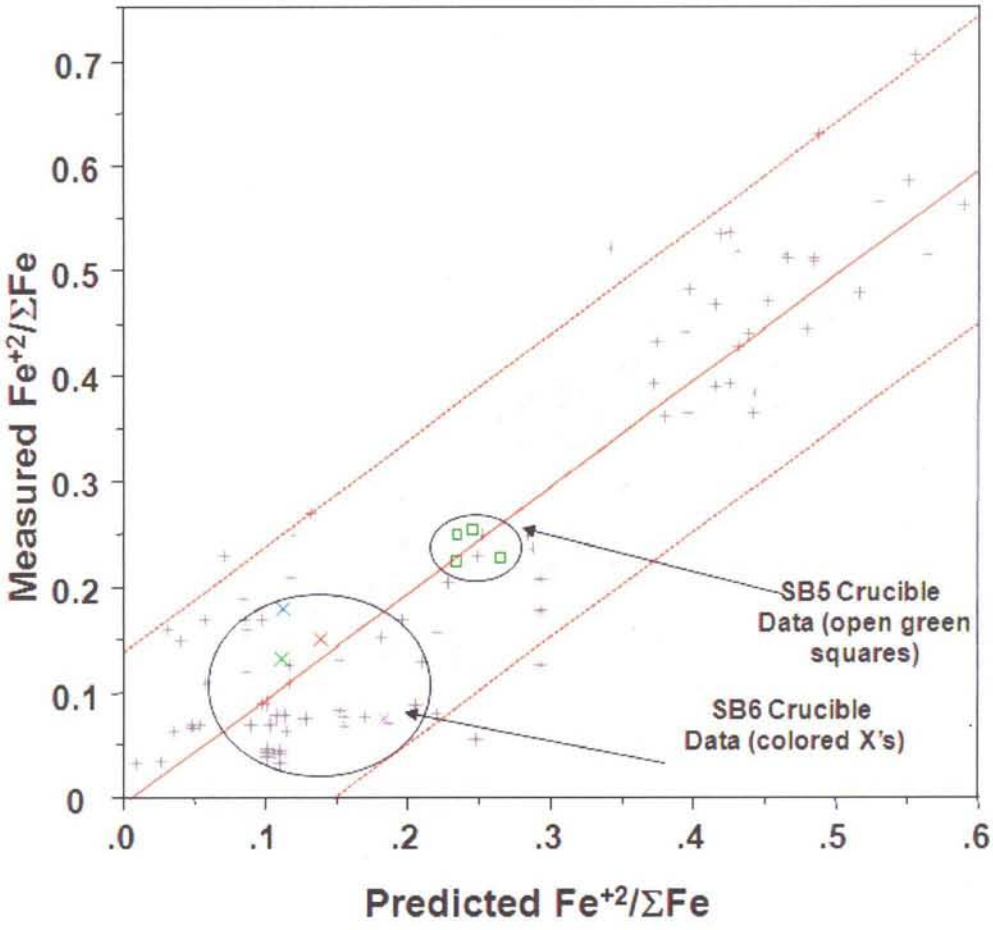

Figure 8. Fit of Equation 13 to the 2006 EE REDOX model data (pooled historic, SB3, and SB4 REDOX data) [10] with data from SB5 and SB6 crucible testing overlain from References 39 and 11, respectively. The correlation of predicted REDOX vs. measured REDOX gives a slope of 1.0 and an intercept of zero and the data from SB5and SB6 falls within the 95% confidence bands.

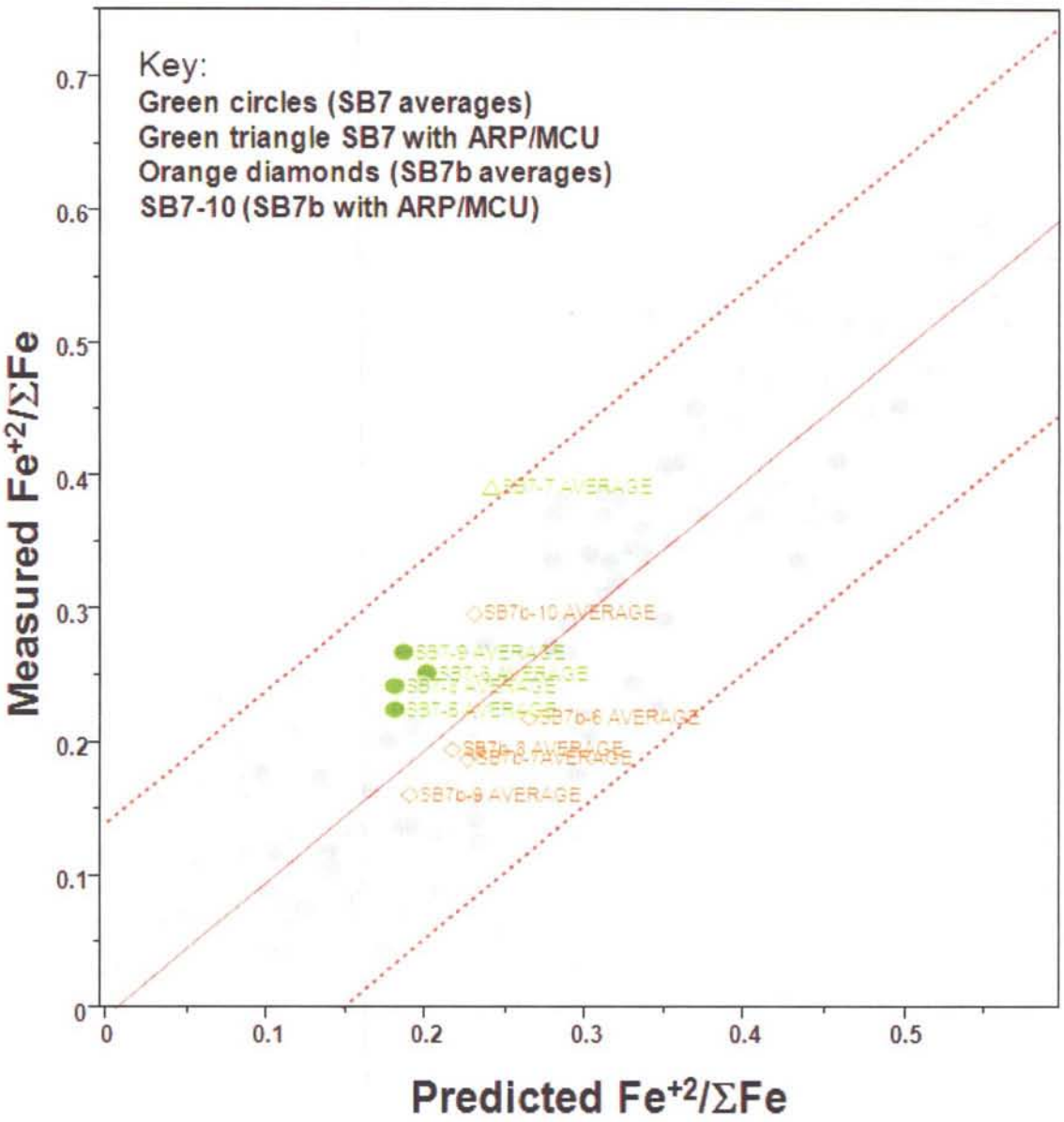

Figure 9. Fit of Equation 13 to the 2006 EE REDOX model data (pooled historic, SB3, and SB4 REDOX data) [10] with data from SB7a (green solid circles) and SB7b (open orange diamonds) crucible testing overlain from References 40 and 41. The correlation of predicted REDOX vs. measured REDOX gives a slope of 1.0 and an intercept of zero and the data from SB7and SB7b falls within the 95% confidence bands except for SB7-7.

3.0 THE THEORETICAL EE TERM FOR ANTIFOAM

The IIT-747 antifoam is a proprietary compound of the Illinois Institute of Technology (IIT) but a deBourg Corporation Material Safety Data Sheet (MSDS #31152, Rev. 1 dated February 2002) for antifoam 747 states that it is an organo-modified silioxane containing primarily polyether modified polymethylsiloxane copolymers like polyether modified heptmethyltrisiloxane (hepta-MTS) or octamethyltrisiloxane (octa-MTS). These compounds can be thought of as hydrides of both organic (ethers and methyl groups) and inorganic compounds like silica in the form of siloxane. The organic monomer chains confer hydrophobic properties while the -Si-O-Si-O- siloxane is purely inorganic.[42] The siloxane is R_2SiO where R is either a hydrogen atom or a hydrocarbon group.

Choi [14] notes that the IIT-747 is not a pure compound since it has a range of molecular weights: it is primarily a mixture of polyethyleneoxide (PEO) chains and methyltrisiloxane (MTS) groups. Koopman [43] states that the IIT-747 is made up of two major and two minor components. The primary component (90%) and the secondary component (9%) are chemically similar to each other, except for the length of the PEO chain, $-(OCH_2CH_2)_n-$ or C_2H_4O, where n can vary from 8-12. The PEO chains are considered likely sites for attack and cleavage by acids under sufficiently vigorous conditions such as those existing in the SRAT and SME.[43]

Stripping of the antifoam decomposition products was assumed to occur in the 2000 SRAT testing performed by Koopman [43] and attempts were recently made to quantify the amounts with little success [44]. Long chain siloxanes with boiling points above 400°C were the major decomposition products identified as being stripped.[44] Antifoam fragments were also seen during non-radioactive experimentation when hexa-MTS was found in the Slurry Mix Evaporator Condensate Tank (SMECT).[45] This was supported by findings of ~340 mg/L Si when the DWPF radioactive SMECT was sampled in 2004 to support the DWPF recycle evaporator project.[46]This suggests that the poly-MTS groups cleave off as they are found in the SMECT and likely do not participate in the melter reduction reactions. Choi [14] shows that any remaining MTS groups in the SRAT/SME likely decompose in the melter in a similar manner to polydimethysiloxane by a free radical mechanism for thermo-oxidative decomposition. Choi further states that if the poly-MTS survives to the melter that the oxidative decomposition in the presence of O_2 will begin around 350°C in the melter cold cap and that the siloxane will decompose to SiO_2 at ~600°C in the melter cold cap.

The main antifoam contributor to the melter, is therefore, the monomer polyether chains which Choi [14] proposes will decompose stoichiometrically to polyoxymethylene (POM) which is $(CH_2O)_n$.[j] In other words, in the PEO chains of the monomers ($-(OCH_2CH_2)_n- = C_2H_4O$ = PEO), the two CH_2 groups share one oxygen. If the PEO chains cleave during thermal decomposition and they form a neutral formaldehyde and a CH_2 radical, i.e. $(CH_2O) + (CH_2)$ [47] which for the simplicity of developing an electron transfer term is represented as $(CH_2O_{0.5})_n$ and then the electron transfers for POM can be multiplied by 2 times the *n* chain length for the decomposition of PEO, i.e. if there are 8 PEO chains it will decompose to 16 POM chains. The thermal decomposition is stepwise potentially forming aldehydes which decompose to CO, CH_4 and H_2, but the methane is not thermodynamically favored and further

[j] It should be noted that ethylene oxide has many reaction paths. It can be hydrolyzed by water, $C_2H_4O + H_2O \rightarrow HO–CH_2CH_2–OH$, and become ethylene glycol (wikipedia.org/wiki/Ethylene_glycol). This reaction can be catalyzed by acid or bases or at neutral pH at elevated temperatures. In the presence of HNO_3, the $(CH_2CH_2)O + HNO_3$ can form mono-nitroglycols or di-nitroglycols, i.e. $HO-CH_2CH_2-ONO_2$(mono) or $O_2NO-CH_2CH_2-ONO_2$ (di). Reaction with $NaNO_2$ can form 2 nitroethanols $HO–CH_2CH_2–NO_2$. If ethylene glycol is indeed formed, the antifoam may act similarly in terms of electron transfers to the use of ethylene glycol as a reductant. Further testing would have to be done to determine the stoichiometry of the electron transfers of a mole of ethylene glycol to a mole of antifoam.

reacts in the cold cap eventually decomposing to CO and H_2, according to Choi. [14] These conservative decomposition products are used to account for any potential sources of H_2 in the flammability calculations but for simplicity and consistency with previous REDOX modeling, it is assumed that sufficient O_2 is being generated by the decomposition of the nitrate salts and manganic species that the final gaseous products will be CO_2 and H_2O vapor. Based on DWPF SME 551-565 data Choi [14] estimated that ~80% of the antifoam carbon may reach the melter and react.

Because neither the MTS nor the PEO/POM species form alkali or alkaline earth or transition metal type salts, an EE term must be based on the number of carbons in each part of the organic group and their relative EE terms. This is the same strategy used to fit a carbon term for coal in the EE model (coal does not participate in salt formation). However, the antifoam molecule contains carbons of different oxidation states so it is more complex.

The MTS end groups of the antifoam molecule have 7-8 carbons of -4 charge and the 8 chain PEO groups have 16 carbons (16 POM's) of -1 charge while the 12 chain PEO groups have 24 carbons (24 POM's) of -1 charge. Since the ratio of the 8:12 polymer chains is 90%:10%, there are 16.8 (sum of 0.9*16 + 0.1*24) carbons of -1 charge in the weighted POM chains and 8 carbons in the MTS if the MTS groups are assumed to be octa-MTS instead of hepta-MTS for a total of 24.8 carbons in the antifoam organic molecule. Therefore, the following two EE values are derived:

- electron transfers for one carbon in an octa-MTS
- electron transfers of one carbon in a POM

The chemical formula for methyl groups is CH_3 so that an octa-MTS is approximately $(CH_3)_8Si_3O_2$. The carbons in the octa-MTS carry a -4 charge and the final decomposition products are considered to be primarily CO_2 and steam by Choi [14]. Since the carbon in CO_2 carries a +4 charge, then there is a +8 EE transfer per MTS group (see Equation 16) or an electron exchange of 64 for the octa-MTS. Sodium nitrate (or nitrite) and Fe^{+3} provide the reduction half reactions (also exchanging 64 electrons), and their decomposition products are N_2, Na_2O, Na^+ and Fe^{+2}. The latter three species (Fe^{+2}, Na^+, and Na_2O) may complex with the SiO_2 to form Na_2SiO_3 and/or $FeSiO_3$ medium range order structures in the glass.

Equation 16

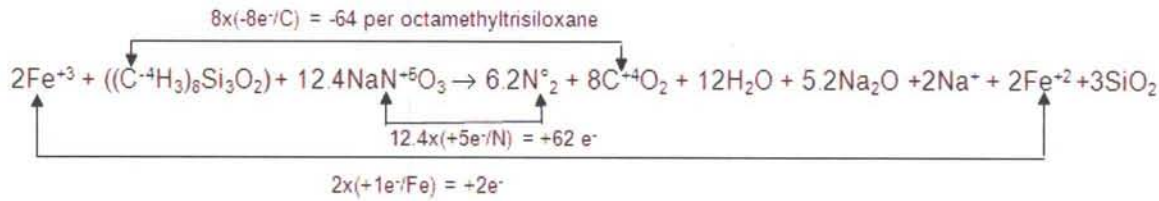

The chemical formula for the ethylene group base units is $CH_2O_{0.5}$ so that the carbon has a -1 charge and their final decomposition products are considered to be primarily CO_2 and steam by Choi[14]. Since the carbon in CO_2 carries a +4 charge, then there is a +5 EE transfer per POM group or per carbon (see Equation 17) or an electron exchange of 80 electrons for an 8 membered PEO polymer chain. Sodium nitrate (or nitrite) and Fe^{+3} provide the reduction half reaction (also exchanging 80 electrons), and their decomposition products are N_2, Na_2O, NaOH, steam, and Fe^{+2}. The latter two species (Fe^{+2} and Na_2O) may complex with the SiO_2 to form Na_2SiO_3 and/or $FeSiO_3$ medium range order structures in the glass.

Equation 17

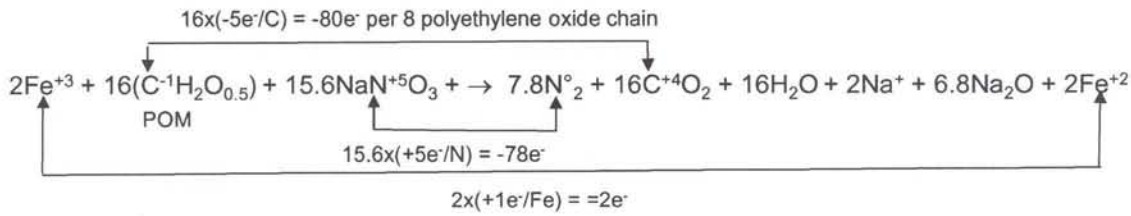

For a 12 PEO chains (24 POM's) the electron equivalents is 120 electrons (12 x 2 x 5 = 120). These varying electron transfers per mole/kg of antifoam added will be fitted against the DWPF and crucible data discussed in the next section.

Due to the differences in the oxidation states of the carbons in antifoam and the relationship derived by Choi [14] showing the equivalency of antifoam in mg/kg and TOC adjusted for the carbon from formic acid and oxalate/oxalic acid, the modeling will be performed on a mol/kg carbon basis. This requires that the +8 electrons per carbon for the octa-MTS (Equation 16) should be weighted by 8/24.8 carbons (~1/3 of the 49% carbon in antifoam) times 8 EE per carbon for an EE of 2.58. The +5 electrons per carbon for the POM (Equation 17) should be weighted by 16.8/24.8 carbons (~2/3 of the 49% carbon in antifoam). Since experimentation and modeling have shown that the octa-MTS likely cleave off the antifoam during processing in the SRAT and SME and do not participate as much in reduction of the melt pool, the +8 electron transfer (Equation 16) does not necessarily have to be considered at all. Therefore, the EE of the 16.8/24.8 POM carbons times 5 EE per carbon yields a total EE transfer term of +3.39 per mol/kg of carbon for the antifoam REDOX model term. This term will be designated as C_A for $Carbon_{(antifoam)}$ and further get multiplied by an "efficiency" factor ("eff") that is expected to be >80% according to Choi [14]. The eff will be fit empirically to the data discussed in Section 3.1.

Note that in the treatment above the split between the carbons from the octa-MTS and the POM's is 0 and 100%, respectively. However, experimentation has shown that small amounts of the octa-MTS do participate in reduction of the melt pool and an alternative way of deriving the C_A term for antifoam would be as follows:

Equation 18 $$eff * C_A(total) = eff_{MTS} * C_{A-MTS} + eff_{POM} * C_{A-POM}$$

So by assuming a different split between POM and octa-MTS carbons and a different "eff" term for each of the organic species in the antifoam, the same total antifoam impact term, "eff $*C_A$ (total)" can be derived as done for 0% octa-MTS and 100% POM carbons. Since the exact split between the POM and octa-MTS carbons is not known, the split of 100% POM carbon and 0% octa-MTS is used for the derivation of the "eff" term. An example of the impact of using Equation 18 will be given in Section 3.1.

3.1 Fitting The Theoretical Antifoam REDOX Term to Experimental Data

The available data for adding an antifoam term to the REDOX model was available in different units as follows:

- Data from sealed crucible studies on non-radioactive surrogates where the mg/kg (ppm) antifoam added to each crucible in increasing amounts was known
- Data from DWPF (radioactive sealed crucible studies and pour stream samples) was summarized as the total amount of antifoam added in gallons and then this was converted to mg/kg (ppm) antifoam adjusted per SME volume and density
- Data from DWPF was available as measured TOC in mg/kg (ppm) carbon which had to be adjusted for the carbon content contributed by formic acid and oxalates/oxalic acid and coal (if known)

For the historic data concentrations of antifoam were set at 800 ppm as a default value. The following conversions were made to put all of the data onto the basis of mol/kg carbon in antifoam:

- Crucible data was converted from mg/kg (ppm) antifoam → mg/kg carbon in antifoam (multiply by 0.49 wt% carbon in antifoam)→mol/kg of carbon in antifoam (divide by molecular weight of 12*1000)
- DWPF gallons of antifoam were converted → mg/kg of antifoam (adjusted for SME volume and density) → mg/kg of total carbon in antifoam (multiply by 0.49 which is the carbon percent in antifoam) →mol/kg of total carbon in antifoam (divide by molecular weight of 12*1000). The DWPF antifoam concentrations from gallons were also adjusted for the 20X dilution performed in the Additive Mix Feed Tank (AMFT).
- DWPF TOC data in mg/kg was adjusted for the carbon content coming from formates, oxalates and coal and then the mg/kg were converted to mol/kg

To prove the equivalency of mol/kg carbon coming from the gallons measured for the DWPF samples modeled to mol/kg carbon from TOC a plot of these two parameters is shown in Figure 10a for the DWPF samples that will be modeled. A similar plot generated by Choi [14] for a larger DWPF database showing the equivalency in ppm or mg/kg is shown in Figure 10b. Both the mol/kg and the mg/kg data fit in Figure 10 have slopes close to one. The mol/kg has an intercept close to zero while the mg/kg has an intercept of ~482.

Note that in Figure 10 both datasets (mol/kg and mg/kg) for the DWPF SME/MFT/PS 549 and 550 samples are excluded as the gallons and the TOC are not equivalent for these two points. That means that during REDOX modeling the values shown in Table 2 for these points will have different calculated REDOX values when evaluated from gallons versus when evaluated from TOC.

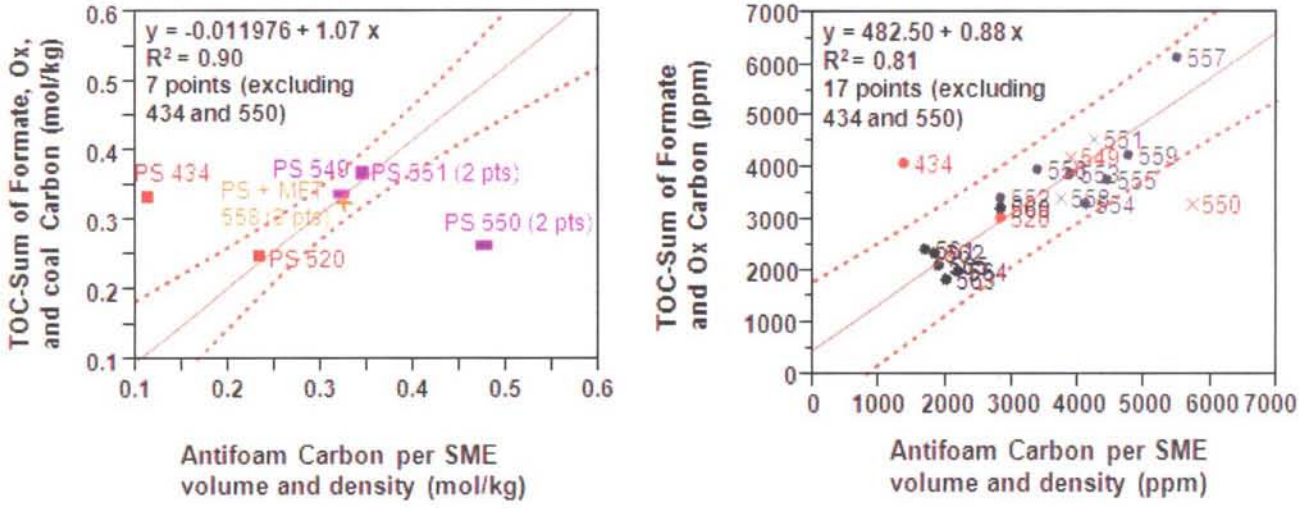

(a) (b)

Figure 10. Graphical representation of the equivalency of the carbon content of antifoam calculated from the gallons measured in DWPF processing to the carbon content measured by TOC when adjusted for the carbon content attributed to formates, oxalates, and coal. (a) For the REDOX model this equivalency must be shown in mol/kg for the DWPF samples that are modeled while (b) Choi [14] demonstrated this equivalency on a larger DWPF data set in mg/kg. Note that in both datasets (mol/kg and mg/kg) that SME/MFT/PS 549 and 550 are excluded from the fits provided.

A compilation of all of the data collected on the impact of antifoam on glass REDOX is given in Table 2 and Table 3 where the antifoam is expressed as mol/kg carbon in the total antifoam added and the TOC values have been adjusted for the carbon coming from the formic acid and the oxalate/oxalic acid as described above and in Figure 10. Feed compositions including the amount of antifoam carbon in mol/kg of slurry, analyzed values of Fe^{+2}, analyzed values for total Fe, and the computed values of the REDOX ratio determined using the procedure of Baumann [33,34] are given in Table 2.

The sealed crucible data using simulants in Table 3 will be used to verify whether the electron transfer of +3.39 from the (16.8/24.8)*5EEs given in Equation 17 for the 16.8 POM chains are valid. Then the DWPF radioactive MFT sealed crucible data and PS samples will be evaluated. Then an effective "eff" term will be defined empirically so that the model with and without an "antifoam term" overlap. If the antifoam term has been derived correctly and the "eff" term empirically fit correctly the two correlations should overlap as the antifoam term was derived in a similar manner to all the other terms in the REDOX model, i.e. by counting electron exchanges.

3.1.1 THE DWPF REDOX MODEL FITTED WITH AN ANTIFOAM TERM

The available data from DWPF facility tests are given in Table 2 while the majority of the data available from crucible studies with various simulated feeds doped with varying levels of antifoam from References 57 and 58 is given in Table 3. The majority of the data in Table 3 is from a study done by Johnson and Stone [57] which was supplemented with a study performed with mercury containing feeds by the same authors.[58] The simulated feed for the first antifoam study [57] was a high nitrate feed and so many of the initial doping levels gave REDOX values at or near the detection limit of the REDOX methodology

forming the plateau observed in Figure 11 before an antifoam impact could be observed. The data shaded in Table 3, much of which was at or near the detection limit of the REDOX method [4,7,8], was not used to develop the antifoam term for the REDOX model.

The data circled in Figure 11 are used in the model but it should be noted that in Table 3 the replicates for these samples are diverse while represented in Figure 11 as a pooled average. For the REDOX model, the individual replicates were used and, as shown, when the pooled averages are used there is a bias in these samples toward lower REDOX measurements than indicated by the amount of antifoam used in ppm (Figure 11).

It should be noted that the data shaded in Table 3 were not used in modeling. Those glasses whose measured REDOX values are proximate to the detection limit (i.e., $Fe^{2+}/\Sigma Fe \leq 0.05$ but ≥ 0.015) are not used. It is believed that measurement error near the detection limit is responsible for the "wobble" in the data circled in Figure 11 as several of the REDOX ratios measured in this region are not reproducible (see samples 13312 Table 3). Data for other replicates, such as sample 21166 in Table 3 are also poor but glasses above $Fe^{2+}/\Sigma Fe = 0.33$ may contain metallic globules that alter the local environment of the glass surrounding a metallic inclusion and/or alter the $Fe^{2+}/\Sigma Fe$ measurement response.

It should also be noted that the $Fe^{2+}/\Sigma Fe$ ratios given in Table 3 were computed by averaging the Fe^{2+} measurements and then averaging the ΣFe measurements and taking the ratio of these averaged values rather than taking the individually calculated $Fe^{2+}/\Sigma Fe$ ratios and averaging them. This gives slightly different $Fe^{2+}/\Sigma Fe$ values than those reported in the references cited and plotted in Figure 11 as the references cited took the average of the computed $Fe^{2+}/\Sigma Fe$ ratios. Taking the average of the individual measurements and then averaging them minimizes error as discussed in Section 2.2.3 and allows "fliers" not to be excluded from the modeling.

The data from Newell and Riley [48] is not used as the crucibles labeled as having excess antifoam had lower $Fe^{+2}/\Sigma Fe$ ratios than those deficient in antifoam. Therefore, the data is suspect as the sealed crucibles may have leaked during the feed to glass transition or the samples may have become mislabeled. Lastly, there are two data points from the work of Jantzen and Stone [10] where excess antifoam was added to simulate SB4 SME product followed by sealed crucible experiments and $Fe^{+2}/\Sigma Fe$ measurement and calculation performed. The data for the 1 gram sample and 2 gram antifoam sample both gave the same measured REDOX. Since it cannot be determined which of the two is in error, neither of these samples is included in the REDOX antifoam database. Thus, antifoam modeling relies solely on the work of Johnson and Stone [57,58] with two simulated feeds.

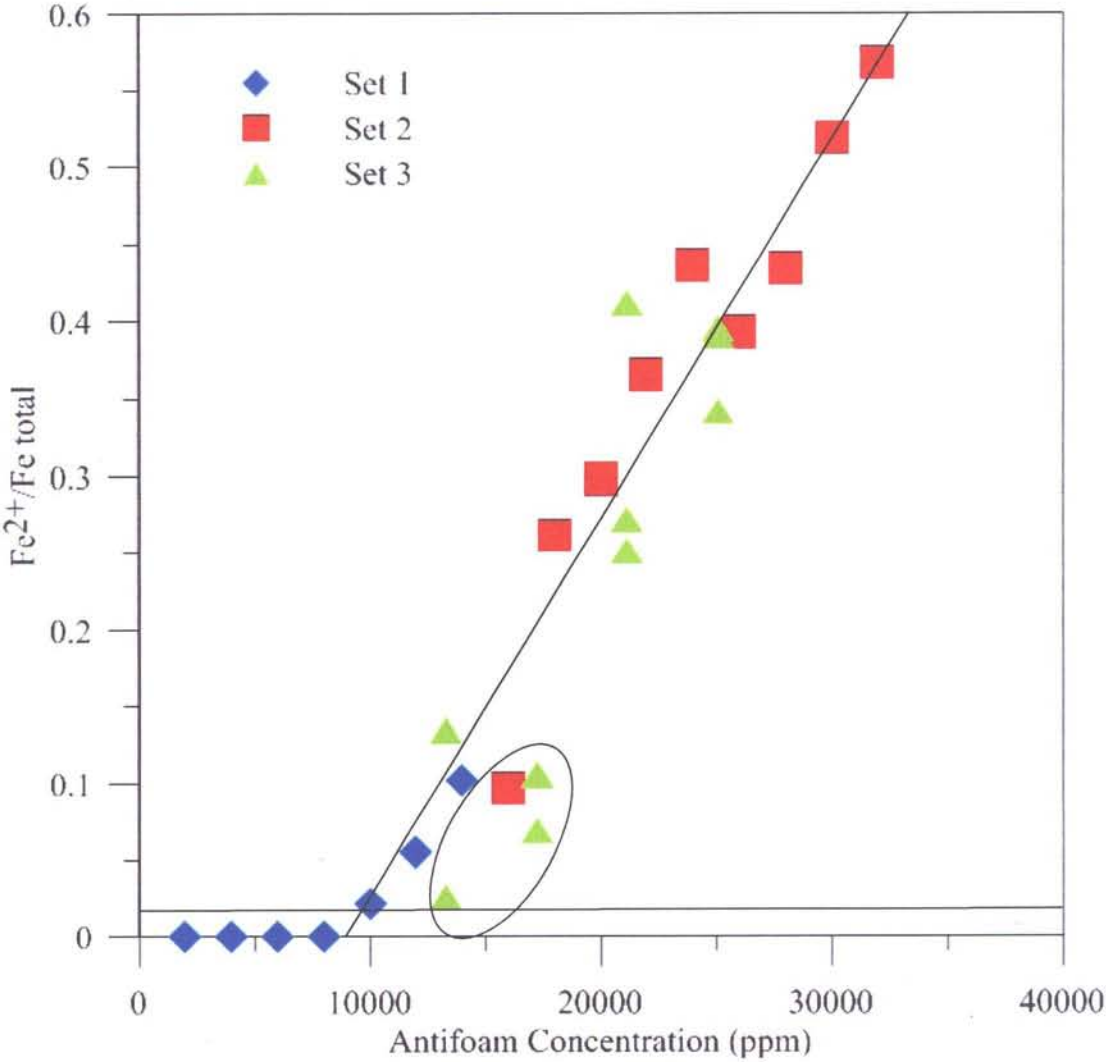

Figure 11. Average $Fe^{2+}/\Sigma Fe$ ratio as a function of antifoam concentration [from Reference 57]

In all of the data used from the crucible studies, the IIT-747 was added after SRAT processing. Therefore, fitting of the measured $Fe^{+2}/\Sigma Fe$ from the crucible to the calculated REDOX from the feed assumes that the antifoam POM's and MTS's degraded in the furnace as they do in the SRAT, SME, and melter.

Using the +3.39 EE transfer derived in the previous section for each mole of POM carbon in the antifoam would give the DWPF REDOX model the following form:

Equation 19

$$\frac{Fe^{2+}}{\Sigma Fe} = f\left[\left(2[F]+4[C]+4[O_T]+3.39*eff[C_A]-5[N]-5[Mn]\right)\frac{45}{T}\right] = f[\xi_A]$$

where f = indicates a function
[F] = formate (mol/kg feed)
[C] = coal (carbon) (mol/kg feed)
$[O_T]$ = $oxalate_{Total}$ (soluble and insoluble) (mol/kg feed)
[CA) = carbon from antifoam (mol/kg feed)
[N] = nitrate + nitrite (mol/kg feed)
[Mn] = manganese (mol/kg feed)
T = total solids (wt%)

And would give ξ_A, the {R-O} term including antifoam the following form:

$$\xi_A = \left[\left(2[F]+4[C]+4[O_T]+3.39*eff[C_A]-5[N]-5[Mn]\right)\frac{45}{T}\right]$$

where the "eff" term must be determined empirically from the Johnson and Stone [57,58] crucible studies and then applied to the DWPF pour stream (PS) samples. Therefore, a fit of ξ_A will make it simpler to fit the "eff" term since it gets weighted by the weight percent solids term, 45/T, like the remainder of the reductants and oxidizers. In addition a fit of ξ_A avoids confounding the fit of the "eff" term along with the slope and intercept of the model.

Fitting of the "eff" term for the effectiveness of antifoam carbon ranged from 80-100% for the weighted POM term of 16.8/24.8 carbons or an EE of +3.39. Figure 12a shows that an "eff" of ~85% or 0.85 allows the antifoam data to overlap the 2006 EE model data almost exactly while an "eff" of 1.00% biases the antifoam data lower than the 2006 EE model data. Therefore, the "eff" term is defined as 0.85 for this dataset. The 0.85 "eff" term is in agreement with the >80% projected by Choi.[14] Using Equation 18 an eff for octa-MTS of 11% and an eff for POM of 80% gives an equally suitable fit to the data. The overall EE of 0.85*3.39EE for POM REDOX only impact is 2.88 EE's while the overall EE of 0.8*3.39 + 0.11*2.88 is 2.99.

Note that the antifoam {R-O}*45/T data has smaller confidence bands than the 2006 EE model data. That is because the antifoam data from the AFA and the Antifoam-II studies has an R^2 of 0.94while the model data only has an R^2 of 0.80 for this term. The slopes of the two datasets when "eff" is 0.85 are 0.200 for the 2006 EE model data and 0.219 for the antifoam data from both studies.
When the REDOX data generated with the antifoam term were fit as a linear function of ξ_A they fell within the confidence bands of the 2006 EE model and so the slope and intercept were not refit. This gives the form of the DWPF REDOX model with an antifoam term as:

Equation 20

$$\frac{Fe^{2+}}{\Sigma Fe} = 0.2358 + 0.1999\xi_A \ .$$

Figure 13 shows the 2006 EE REDOX model data with the antifoam data overlain based on Equation 20. The antifoam data fits comfortably within the existing model slope and intercept.

3.1.2 APPLICATION OF THE ANTIFOAM TERM TO DWPF POUR STREAM AND MELTER FEED TANK DATA

During SB2, a DWPF sample was taken and the REDOX analyzed. This sample was designated SME 224 but was a pour stream sample (see Table 2). This sample was taken and analyzed before Ar bubbling, before ARP/MCU additions, and before the current foaming/antifoam issues. SME 224 is shown on Figure 14 for reference. The SME 224 sample fits the EE model which now includes a nominal 800 ppm for every historic batch in the database (see footnote to Table 2). Therefore the position of SME 224 is slightly different in Figure 14 than shown in Figure 7.

The data for the DWPF facility data, which includes both PS samples and MFT samples that have been vitrified in the SRNL SCF in sealed crucibles (all of the data in Table 2) is overlain on Figure 13 to see how well the DWPF data fits the Equation 19 model with an "eff" of 0.85. Two different overlays are shown in Figure 14. One overlay (Figure 14a) uses the carbons generated from the gallons added and the other overlay (Figure 14b) uses the carbons generated from the measured TOC values in Table 2 which have been adjusted for the carbon from other sources (formates, oxalates, and coal).

There are some subtle differences in the two DWPF data overlays, since some DWPF data was available in gallons and some data was only available as measured TOC (see Table 2). Note that the position of PS 550 and 434 are quite different in the two overlays. This is because the TOC and gallons do not track each other in either Figure 10a or Figure 10b.

Note also that in Figure 14a and b that PS 580 is biased higher than the crucible MFT 580 samples and in general all the PS samples that were bubbled with Ar in the melter (the MFT crucible studies were not bubbled with Ar) are all biased between the OLS fit of the 2006 EE REDOX model and the U95 percent confidence band. Therefore, there is an impact of Ar bubbling which will be discussed in Section 4.0 and an Ar impact term will be developed in Section 4.3.2.The Ar impact is due to a phenomena called Ar de-gassing since Ar bubbling was initiated during melting batch 538 and affected all subsequent melter campaigns.

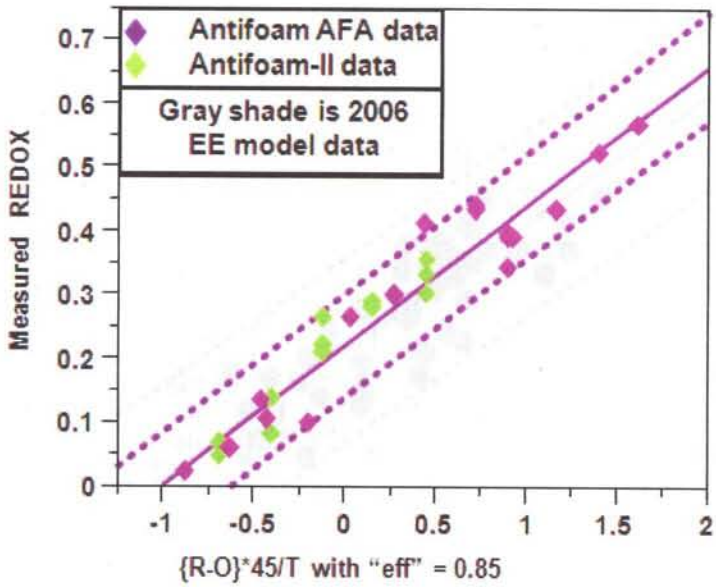

(a)

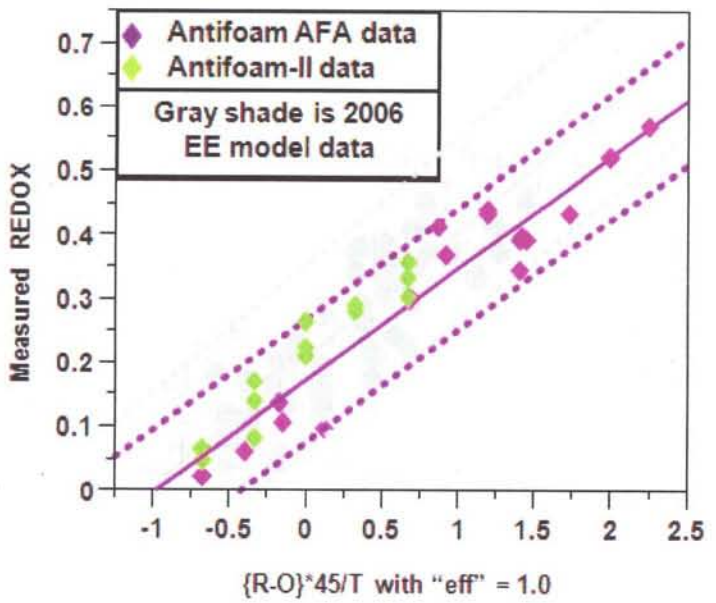

(b)

Figure 12. Fitting the Xi (ξ_A) term or {R-O}*45/T with an effective antifoam efficiency term. Top is with an "eff" of 85% and bottom is with an "eff" of 100%.

Table 2. Measured REDOX Data on DWPF Feeds and Glass Containing Varying Amounts of IIT-747 Antifoam

Sample ID	Frit	SRAT/SME/MFT or Pour Stream (PS)	Target Waste Loading	Measured REDOX	Fe^{+2}	# Fe Measurements	Total Fe	SME/MFT wt% Solids	Formate mol/kg	Nitrate mol/kg	Oxalate mol/kg	Coal mol/kg	Mn mol/kg	C_A mol/kg (from gallons or mg/kg)	C_A mol/kg (from TOC Adjusted for Formate and Oxalate or mg/kg)	Predicted REDOX Mn=5	Predicted REDOX with Antifoam from gallons or mg/kg @Mn=5	Predicted REDOX with Antifoam from Adjusted TOC @Mn=5	Reference(s)
DWPF MELTER DATA WITH ANTIFOAM*																			
DWPF PS 224	200	PS	---	**0.210**	**0.210**	**6**	**1.000**	**47.70**	**0.795**	**0.311**	**0**	**0**	**0.054**	**0.0326***	**0.00****	**0.206**	**0.212**	**0.195**	7,8
DWPF PS 434	510	PS	---	**0.222**	**0.197**	**2**	**0.885**	**43.59**	**0.741**	**0.255**	**0.014**	**0.007**	**0.088**	**0.1146**	**0.3305**	**0.122**	**0.2736**	**0.402**	
DWPF PS 520	418	PS	---	**0.232**	**0.160**	**2**	**0.693**	**46.65**	**0.843**	**0.338**	**0.005**	**0.007**	**0.127**	**0.2345**	**0.2436**	**0.094**	**0.2524**	**0.257**	
DWPF PS 549-Ar	418	PS	---	0.253	0.259	2	1.028	40.17	0.814	0.319	0.006	0.007	0.144	0.3219	0.3395	0.106	0.3011	0.312	
DWPF PS 550-Ar	418	PS	---	0.316	0.286	2	0.864	43.74	0.983	0.401	0.006	0.007	0.129	0.4765	0.2653	0.106	0.388	0.263	49
DWPF PS 550-Ar	418	PS	---	0.316	0.217	2	0.719	43.74	0.983	0.401	0.006	0.007	0.129	0.4765	0.2653	0.078	0.388	0.263	
DWPF PS 551-Ar	418	PS	---	0.375	0.275	2	0.740	43.62	0.855	0.352	0.006	0.007	0.153	0.3455	0.3705	0.078	0.2836	0.298	
DWPF PS 551 - Ar	418	PS	---	0.375	0.328	2	0.871	43.62	0.855	0.352	0.006	0.007	0.153	0.3455	0.3705	0.100	0.2836	0.298	
DWPF MFT 558	418	MFT	---	0.474	0.220	2	0.464	41.62	0.671	0.308	0.006	0.007	0.095	0.3271	0.3254	0.100	0.304	0.303	
DWPF MFT 558	418	MFT	---	0.410	0.212	2	0.517	41.62	0.671	0.308	0.006	0.007	0.095	0.3271	0.3254	0.100	0.304	0.303	50
DWPF PS 558-Ar	418	PS	---	0.407	0.354	3	0.869	41.62	0.671	0.308	0.006	0.007	0.095	0.3271	0.3254	0.040	0.304	0.303	
DWPF MFT 568	418	MFT	---	0.157	0.060	3	0.382	39.88	0.742	0.346	0.006	0.007	0.135	0.1381	**0.00****	0.040	0.1295	**0.040**	
DWPF MFT 568	418	MFT	---	0.057	0.0293	3	0.511	39.88	0.742	0.346	0.006	0.007	0.135	0.1381	**0.00****	0.040	0.1295	**0.040**	51
DWPF MFT 568	418	MFT	---	0.025	0.012	3	0.483	39.88	0.742	0.346	0.006	0.007	0.135	0.1381	**0.00****	0.035	0.1295	**0.040**	
DWPF MFT 580	418	MFT	---	0.029	0.012	3	0.414	42.37	0.689	0.396	0.050	0.007	0.114	0.0486	0.0710	0.035	0.065	0.079	
DWPF MFT 580	418	MFT	---	0.040	0.023	3	0.561	42.37	0.689	0.396	0.050	0.007	0.114	0.0486	0.0710	0.035	0.065	0.079	52
DWPF MFT 580	418	MFT	---	0.050	0.023	3	0.462	42.37	0.689	0.396	0.050	0.007	0.114	0.0486	0.0710	0.035	0.065	0.079	
DWPF PS 580-Ar	418	PS	---	0.132	0.056	3	0.425	42.37	0.689	0.396	0.050	0.007	0.114	0.0486	0.0710	0.100	0.065	0.079	53
DWPF MFT 592	418	MFT	---	0.021	0.021	3	0.969	41.71	0.707	0.335	0.046	0.007	0.116	0.0319	0.0380	0.100	0.1197	0.124	
DWPF MFT 592	418	MFT	---	0.022	0.022	3	0.990	41.71	0.707	0.335	0.046	0.007	0.116	0.0319	0.0380	0.100	0.1197	0.124	54
DWPF MFT 592	418	MFT	---	0.025	0.024	3	0.975	41.71	0.707	0.335	0.046	0.007	0.116	0.0319	0.0380	0.100	0.1197	0.124	
DWPF PS 592-Ar	418	PS	---	0.044	0.0424	3	0.975	41.71	0.707	0.335	0.046	0.007	0.116	0.0319	0.0380	0.206	0.1197	0.124	55

* note that a minimum of 800 mg/kg of antifoam was assumed for DWPF PS224 which is ~130 gallons of antifoam.

**TOC minus the carbon in formate and oxalate gave a negative number for C_A so C_A was set equal to zero.

Shaded data is Below the Detection Limit for the $Fe^{+2}/\Sigma Fe$ measurement

Table 3. Measured REDOX Data on Simulated Glasses* Containing Varying Amounts of IIT-747 Antifoam

Sample ID	Frit	SRAT/SME/MFT or Pour Stream (PS)	Target Waste Loading	Measured REDOX	Fe^{+2}	# Fe Measurements	Total Fe	SME wt% Solids	Formate mol/kg	Nitrate mol/kg	Oxalate mol/kg	Coal mol/kg	Mn mol/kg	C_A mol/kg (from mg/kg added)	Predicted REDOX Mn=5	Predicted REDOX with Antifoam from mg/kg added @Mn=5	Reference(s)
SB4 ANTIFOAM STUDY																	
SB4-41-418 full antifoam 747 (2g)	418	SME	35.0	0.57	0.353	4	0.615	41.66	0.975	0.404	0	0	0.119	0.038	0.403	0.6830	10
SB4-41-418 1/2 antifoam 747 (1g)	418	SME	35.0	0.53	0.299	4	0.564	41.66	0.975	0.404	0	0	0.119	0.019	0.253	0.3923	
ANTIFOAM STUDY (AFA SLUDGE)																	
Baseline AFA	418	SME	35.9	0.0006	0.001	1	1.62	41.69	1.438	0.586	0.004	0	0.1392	0.033	<0	<0	56, 57
Baseline AFA	418	SME	35.9	0.0006	0.001	1	1.62	41.69	1.438	0.586	0.004	0	0.1392	0.033	<0	<0	
AFA-2000A	418	SME	35.9	0.0007	0.001	1	1.49	42.45	1.438	0.585	0.004	0	0.1392	0.079	0.104	<0	
AFA-2000B	418	SME	35.9	0.0007	0.001	1	1.49	42.45	1.438	0.585	0.004	0	0.1392	0.079	0.104	<0	
AFA-4000A	418	SME	35.9	0.0007	0.001	1	1.51	42.48	1.438	0.586	0.004	0	0.1392	0.151	0.126	<0	
AFA-4000B	418	SME	35.9	0.0007	0.001	1	1.51	42.48	1.438	0.586	0.004	0	0.1392	0.151	0.126	<0	
AFA-6000A	418	SME	35.9	0.0007	0.001	1	1.51	42.45	1.438	0.586	0.004	0	0.1392	0.223	0.149	<0	
AFA-6000B	418	SME	35.9	0.0007	0.001	1	1.51	42.45	1.438	0.586	0.004	0	0.1392	0.223	0.149	<0	
AFA-8000A	418	SME	35.9	0.0007	0.001	1	1.38	42.45	1.439	0.586	0.004	0	0.1393	0.298	0.174	0.018	
AFA-8000B	418	SME	35.9	0.0007	0.001	1	1.38	42.45	1.439	0.586	0.004	0	0.1393	0.298	0.174	0.018	
AFA-10000A	418	SME	35.9	0.022	0.011	1	0.5	42.45	1.438	0.586	0.004	0	0.1392	0.369	0.196	0.062	
AFA-10000B	418	SME	35.9	0.022	0.011	1	0.501	42.45	1.438	0.586	0.004	0	0.1392	0.369	0.196	0.062	
AFA-12000A	418	SME	35.9	0.054	0.029	1	0.533	42.48	1.438	0.585	0.004	0	0.1392	0.446	0.222	0.11	
AFA-12000B	418	SME	35.9	0.056	0.03	1	0.532	42.48	1.438	0.585	0.004	0	0.1392	0.446	0.222	0.11	
AFA-14000A	418	SME	35.9	0.102	0.052	1	0.508	42.48	1.438	0.585	0.004	0	0.1392	0.515	0.244	0.152	
AFA-14000B	418	SME	35.9	0.102	0.052	1	0.51	42.48	1.438	0.585	0.004	0	0.1392	0.515	0.244	0.152	
AFA-16000A	418	SME	35.9	0.098	0.049	1	0.501	42.47	1.438	0.586	0.004	0	0.1392	0.592	0.268	0.198	
AFA-16000B	418	SME	35.9	0.096	0.048	1	0.500	42.47	1.438	0.586	0.004	0	0.1392	0.592	0.268	0.198	
AFA-18000A	418	SME	35.9	0.261	0.129	1	0.493	42.46	1.438	0.586	0.004	0	0.1392	0.666	0.292	0.243	
AFA-18000B	418	SME	35.9	0.260	0.128	1	0.492	42.46	1.438	0.586	0.004	0	0.1392	0.666	0.292	0.243	
AFA-20000A	418	SME	35.9	0.299	0.14	1	0.468	42.47	1.438	0.585	0.004	0	0.1392	0.745	0.319	0.292	

Sample ID	Frit	SRAT/SME/MFT or Pour Stream (PS)	Target Waste Loading	Measured REDOX	Fe^{+2}	# Fe Measurements	Total Fe	SME wt% Solids	Formate mol/kg	Nitrate mol/kg	Oxalate mol/kg	Coal mol/kg	Mn mol/kg	C_A mol/kg (from mg/kg added)	Predicted REDOX Mn=5	Predicted REDOX with Antifoam from mg/kg added @Mn=5	Reference(s)
AFA-20000B	418	SME	35.9	0.296	0.139	1	0.469	42.47	1.438	0.585	0.004	0	0.1392	0.745	0.319	0.292	56, 57
AFA-22000A	418	SME	35.9	0.365	0.185	1	0.507	42.47	1.438	0.586	0.004	0	0.1392	0.814	0.340	0.333	
AFA-22000B	418	SME	35.9	0.366	0.185	1	0.506	42.47	1.438	0.586	0.004	0	0.1392	0.814	0.340	0.333	
AFA-24000A	418	SME	35.9	0.440	0.216	1	0.492	42.47	1.438	0.585	0.004	0	0.1392	0.891	0.366	0.381	
AFA-24000B	418	SME	35.9	0.434	0.214	1	0.494	42.47	1.438	0.585	0.004	0	0.1392	0.891	0.366	0.381	
AFA-26000A	418	SME	35.9	0.393	0.189	1	0.482	42.47	1.438	0.586	0.004	0	0.1392	0.962	0.387	0.423	
AFA-26000B	418	SME	35.9	0.393	0.189	1	0.482	42.47	1.438	0.586	0.004	0	0.1392	0.962	0.387	0.423	
AFA-28000A‡	418	SME	35.9	0.434	0.208	1	0.479	42.47	1.438	0.585	0.004	0	0.1392	1.038	0.413	0.47	
AFA-28000B‡	418	SME	35.9	0.434	0.208	1	0.479	42.47	1.438	0.585	0.004	0	0.1392	1.038	0.413	0.47	
AFA-30000A	418	SME	35.9	0.519	0.261	1	0.503	42.48	1.438	0.585	0.004	0	0.1392	1.112	0.437	0.516	
AFA-30000B	418	SME	35.9	0.518	0.261	1	0.504	42.48	1.438	0.585	0.004	0	0.1392	1.112	0.437	0.516	
AFA-32000A	418	SME	35.9	0.568	0.278	1	0.489	42.47	1.438	0.585	0.004	0	0.1392	1.184	0.460	0.56	
AFA-32000B	418	SME	35.9	0.567	0.278	1	0.49	42.47	1.438	0.585	0.004	0	0.1392	1.184	0.460	0.56	
AFA-13312A	418	SME	35.9	0.134	0.056	1	0.417	42.49	1.437	0.585	0.004	0	0.1391	0.507	0.242	0.147	
AFA-13312B	418	SME	35.9	0.0026	0.001	1	0.384	42.50	1.437	0.585	0.004	0	0.1391	0.503	0.240	0.144	
AFA-13312C	418	SME	35.9	0.026	0.012	1	0.462	42.50	1.437	0.585	0.004	0	0.1391	0.503	0.240	0.144	
AFA-17239A	418	SME	35.9	0.0690	0.027	1	0.391	42.49	1.437	0.585	0.004	0	0.1391	0.648	0.287	0.233	
AFA-17239B	418	SME	35.9	0.105	0.04	1	0.3825	42.50	1.437	0.585	0.004	0	0.1391	0.645	0.286	0.231	
AFA-17239C	418	SME	35.9	0.106	0.041	1	0.3855	42.51	1.437	0.585	0.004	0	0.1391	0.646	0.286	0.231	
AFA-21166A	418	SME	35.9	0.411	0.169	1	0.411	42.47	1.438	0.586	0.004	0	0.1392	0.799	0.335	0.324	
AFA-21166B	418	SME	35.9	0.251	0.11	1	0.439	42.51	1.437	0.585	0.004	0	0.1391	0.798	0.336	0.324	
AFA-21166C	418	SME	35.9	0.272	0.0995	1	0.366	42.48	1.438	0.585	0.004	0	0.1392	0.796	0.335	0.323	
AFA-25093A	418	SME	35.9	0.391	0.149	1	0.3815	42.47	1.438	0.586	0.004	0	0.1392	0.949	0.383	0.415	
AFA-25093B	418	SME	35.9	0.342	0.1375	1	0.4025	42.48	1.438	0.585	0.004	0	0.1392	0.948	0.384	0.416	
AFA-25093C	418	SME	35.9	0.394	0.15	1	0.3805	42.48	1.438	0.585	0.004	0	0.1392	0.948	0.385	0.417	
ANTIFOAM-II STUDY (SLUDGES 11-HG3-5627 and 11-HG6-5760)																	
FCJ-HG-800A	418	SME	35.0	0.065	0.033	1	0.504	42.91	0.836	0.268	0.0016	0	0.0834	800	0.219	0.099	58
FCJ-HG-800B	418	SME	35.0	0.046	0.023	1	0.497	42.91	0.836	0.268	0.0016	0	0.0834	800	0.219	0.099	
FCJ-HG-800C	418	SME	35.0	0.063	0.031	1	0.49	42.91	0.836	0.268	0.0016	0	0.0834	800	0.219	0.099	

Sample ID	Frit	SRAT/SME/MFT or Pour Stream (PS)	Target Waste Loading	Measured REDOX	Fe^{+2}	# Fe Measurements	Total Fe	SME wt% Solids	Formate mol/kg	Nitrate mol/kg	Oxalate mol/kg	Coal mol/kg	Mn mol/kg	C_A mol/kg (from mg/kg added)	Predicted REDOX Mn=5	Predicted REDOX with Antifoam from mg/kg added @Mn=5	Reference(s)
FCJ-HG-3100A	418	SME	35.0	0.136	0.067	1	0.492	42.72	0.825	0.266	0.0019	0	0.0830	3100	0.217	0.155	58
FCJ-HG-3100B	418	SME	35.0	0.081	0.060	1	0.74	42.72	0.825	0.266	0.0019	0	0.0830	3100	0.217	0.155	
FCJ-HG-3100C	418	SME	35.0	0.168	0.078	1	0.463	42.72	0.825	0.266	0.0019	0	0.0830	3100	0.217	0.155	
FCJ-HG-5400A	418	SME	35.0	0.219	0.109	1	0.497	42.52	0.814	0.264	0.0022	0	0.0826	5400	0.215	0.212	
FCJ-HG-5400B	418	SME	35.0	0.264	0.131	1	0.496	42.53	0.814	0.264	0.0022	0	0.0826	5400	0.215	0.212	
FCJ-HG-5400C	418	SME	35.0	0.207	0.100	1	0.483	42.52	0.814	0.264	0.0022	0	0.0826	5400	0.215	0.212	
FCJ-HG-7700A	418	SME	35.0	0.278	0.131	1	0.472	42.33	0.803	0.263	0.0025	0	0.0822	7700	0.212	0.268	
FCJ-HG-7700B	418	SME	35.0	0.289	0.142	1	0.491	42.33	0.803	0.263	0.0025	0	0.0822	7700	0.212	0.268	
FCJ-HG-10000A	418	SME	35.0	0.300	0.138	1	0.46	42.15	0.793	0.261	0.0028	0	0.0819	10000	0.211	0.326	
FCJ-HG-10000B	418	SME	35.0	0.355	0.173	1	0.488	42.15	0.793	0.261	0.0028	0	0.0819	10000	0.211	0.326	
FCJ-HG-10000C	418	SME	35.0	0.328	0.154	1	0.469	42.15	0.793	0.261	0.0028	0	0.0819	10000	0.211	0.326	

‡ at 28,000 ppm antifoam nickel nodules were visibly observed.

*For the AFA glasses only 60% of the formate was considered active during modeling per M.E. Stone; a minimum of 800 mg/kg of antifoam was assumed for all the historical samples in the 2006 EE database.

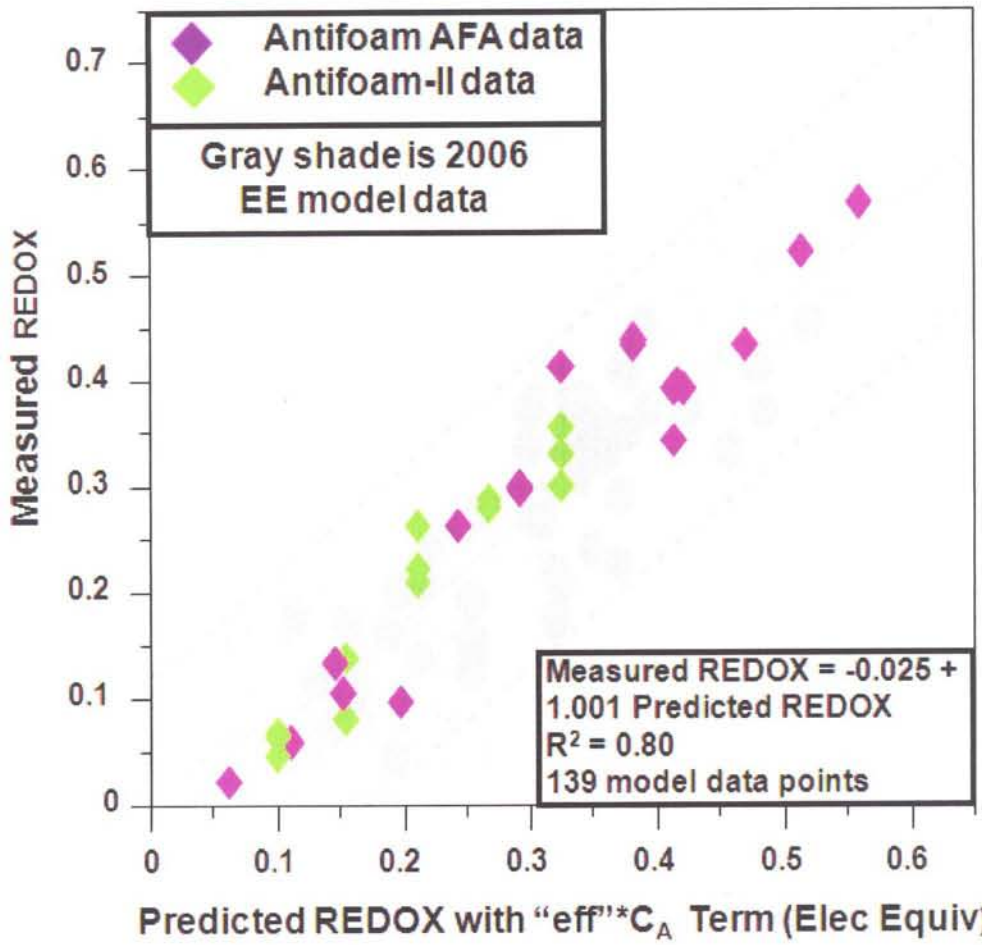

Figure 13. DWPF REDOX Model (gray shaded symbols from Reference 10) and Antifoam Crucible Data (AFA Study and Antifoam-II Study) Overlain from references 57 and 58. Equation 19 with an "eff" factor of 0.85 was used to generate this plot.

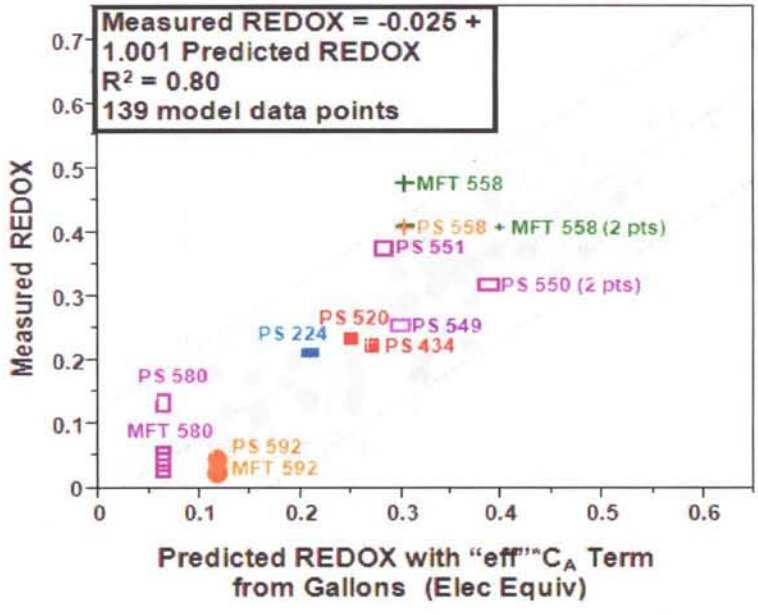

(a)

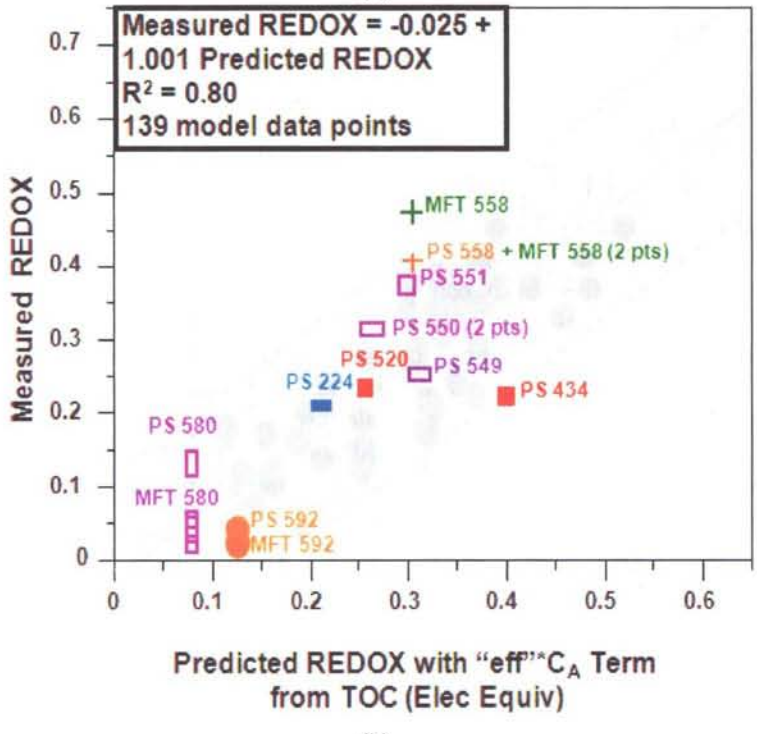

(b)

Figure 14. The Measured and Predicted REDOX for the Pour Stream and MFT Crucible Studies Using the New Antifoam Term: (a) antifoam carbon determined from gallons added and (b) antifoam carbon determined from adjusted TOC measurement.

4.0 ARGON GAS BUBBLING

4.1 Argon Degassing in Liquid Solutions and Molten Metals and Glass

Argon is an inert gas. Argon gas does not add electrons to form negative ions as in reducing ionic species in a solution or in molten metals or in glass as the electron affinity of argon is zero. [59] However, inert gasses can be used to "sparge" or "degas" or "deoxygenate" a solution including molten "solutions" or melts.

4.1.1 ARGON DEGASSING IN SOLUTIONS

If a deoxygenated solution is needed for a chemical experiment, the solution is bubbled with an inert gas. The inert gas can substitute in the solution for the unwanted dissolved species, i.e. dissolved reactive gases such as oxygen and carbon dioxide. Nitrogen, argon, helium, and other inert gases are commonly used for sparging or degassing. To complete the substitution, the solution should be stirred vigorously and bubbled for a long time. [60] This was the methodology used by Jantzen at SRNL to deoxygenate the Basalt Waste Isolation Project basaltic groundwater with argon and equilibrate the groundwater with rock in an Ar glove box to achieve low oxidation potential (low Eh) groundwater to perform leach tests on rock, metal, and glass coupons under low Eh conditions.[61]

4.1.2 ARGON DEGASSING IN MOLTEN METALS

Gas injection into molten metals (also considered a solution) is utilized in many high temperature processes [62] to degas hydrogen and/or oxygen species out of the molten metal. Argon has been used to degas molten aluminum containing hydrogen to minimize porosity in cast aluminum ingots [63,64], and to degas oxygen from molten silver by injecting argon through an immersed nozzle.[65] In the latter study, the deoxygenation efficiencies were very high and the atomic percent of oxygen in the metal decreased as a function of the bubbling time. The mechanism and rate of degassing/deoxygenation were studied and fit to several kinetic models. The rate data were found to be consistent with the model describing the liquid-phase mass transfer during bubble formation at the nozzle and bubble ascent through the melt. From a comparison between the measured and calculated times of bubble formation, it was shown that mass transfer during bubble formation makes a large contribution to the deoxidation process.

The largest single use for argon is inert-gas-shielded arc welding of metals and in inert-gas-shielded tungsten electrode arc cutting. Inert-gas-shielded welding and cutting are used for the nonferrous metals (aluminum and magnesium) and for stainless steel and other kinds of steel to protect the hot metal from the action of air or oxygen. [66]

4.1.3 ARGON DEGASSING IN MOLTEN GLASS

Much is known about the solubility of inert gases in molten glass and in molten magmas. [67] The presence of noble gasses in magmas is geochemical evidence of melt degassing in nature.[68]

The solubility of noble gases in glass and melts is negatively correlated with their atomic radius, thus Ar ($r = 0.341$ nm) is less soluble than He ($r = 0.256$ nm) or Ne ($r = 0.275$ nm). The solubility of any noble gas in a silicate melt increases with increasing SiO_2 content and near ambient pressure, the solubility of

the noble gas in glass depends only on the nominal Non-Bridging Oxygen (NBO) divided by Si ratio known as the NBO/Si. For DWPF this means that Ar solubility in the glass is related to the viscosity of the melt, i.e. the more network modifiers a glass has the more intrinsic vacancies and extrinsic interstitials exist in the glass. [69] Thus, more soluble gases can be incorporated into these interstitial sites of vacancies also known as "free volume" and the molar volume increases while the glass density decreases as shown in Figure 15 [70]

The solubility mechanisms of noble gases in silicate melts and glasses have been modeled on the assumption that the gas occupies holes known as "free volume" or "ionic porosity" in the structure.[67] This has been proven for Kr in SiO_2 glass by x-ray absorption data. The presence of the gas occupies a free volume in the glass which is expressed as a partial molar volume. For Ar in a pure SiO_2 glass the free volume has been measured as 16.4±1.4 cm^3/mol of SiO_2.[67]

An excellent synopsis of the impacts of melt degassing from Reference 68 is given below:

> "The dissolution of noble gases in silicate melts is thought not to involve chemical interactions between the inert gas atoms and the surrounding melt: due to their inert nature, noble gas develops van der Waals interactions with silicate melts and seems to display a "physical solubility" in which the size of the noble atom plays a key role [71,72]. Several experimental studies have indeed highlighted that the solubilities of noble gases decrease with increasing size of the gas atom [73,74,75] and are strongly dependent on melt composition [74,76,77,78]. SiO_2-rich compositions generally show higher noble gas solubilities than those depolymerized [73; 74,76,77,78,79]. These features have suggested that the noble gas atoms may be accommodated in holes and free spaces of the melt on the basis on their atomic sizes. Rings of interconnected silicon tetrahedra have been proposed to work as solubility sites [80]. All noble gases have higher solubilities in silica-rich melts than in more mafic [*Mg-Fe bearing*] ones, as, in general, silicon and other tetrahedrally coordinated cations (Al, Fe^{3+}, and Ti^{4+}) are network-formers, while Na+, K+, Mg^{2+}, Ca^{2+}, and Fe^{2+} break the silicate polymers. In alumina-free melts, Shibata et al. [77] found a direct relationship between noble gas solubility and degree of polymerization, the latter being expressed as NBO/T, namely the number of non-bridging oxygens per atom of tetrahedrally coordinated cations [81].[1] Noble gas solubility was also observed to be independent on the nature of network-modifier cations breaking the polymers [77]. In contrast, Marrocchi and Toplis [82] observed a lack of correlation between Ar solubility and polymerization in Al-bearing melts. According to these authors, the number of the solubility sites for the noble gases, as well as their distribution, both vary as a function of the Al content of the liquid, owing to the different role of cations which act either as network modifiers or as charge balancers for Al.
>
> In accordance with the idea of physical interstitial dissolution, noble gas solubility has been found to correlate with several melt properties related to the free space in the silicate network: density [70,74], molar volume [75] and ionic porosity [76]."

Examples of the effects of noble gas solubility on glass physical properties are given in Figure 15.

[1] The DWPF viscosity model is based on a modification of the 1975 Brawer and White reference.

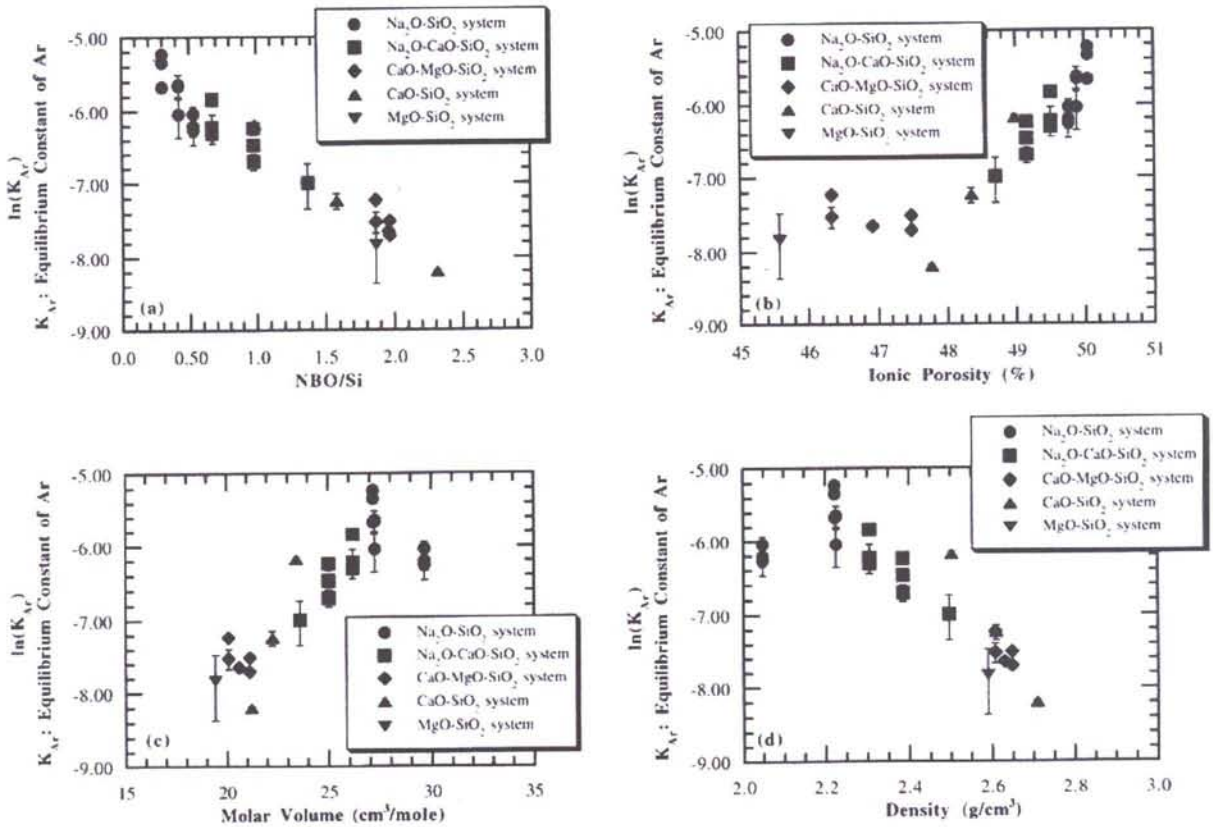

Figure 15. Comparisons of correlation between the natural logarithm of equilibrium constant of Ar and (a) NBO/Si, (b) ionic porosity, (c) molar volume, and (d) density, respectively, for simple silicate glasses. The same trends are observed for other noble gases (from Reference 77)

4.2 Effective Oxygen Fugacity (REDOX) of Argon

The chemical dissolution of inert gases[§] in the glass results in a fugacity of the physically dissolved gas. Oxygen fugacity, fO_2, which for all intents and purposes is numerically equal to the partial pressure of oxygen (pO_2) for ideal gases such as O_2, N_2 and Ar is normally expressed as 10^{-xx} atmospheres. While values of fO_2 such as 10^{-22} or 10^{-25} are so low that the equivalent partial pressures of oxygen are physically unrealistic, fO_2 remains a convenient expression of the relative "lack of oxygen" in a given system.

The REDOX equilibrium in a glass melt can be represented by

Equation 21 $$M^{(m+n)+}_{melt} + \frac{n}{2} O^{2-}_{melt} \leftrightarrow M^{m+}_{melt} + \frac{n}{4} O_{2\,melt}$$

where M = the polyvalent ion such as Fe
m^+ = the lower valency state such as Fe^{2+}
$(m+n)^+$ = the higher valency state such as Fe^{3+}
n = the number of electrons transferred
O^{2-} = the oxygen ion activity or basicity of the melt
O_2 is the physically dissolved oxygen in the holes of the network structure.[69]

Therefore, a plot of log Fe^{2+}/Fe^{3+} gives a slope of –n/4 when plotted against log oxygen fugacity. Thus for an EE exchange between ferric and ferrous iron of 1 the slope is -1/4 or -0.25.

Equation 21 is written as reversible as going from LHS to RHS is the reduction of ferric to ferrous iron and going from RHS to LHS is the oxidation of ferrous to ferric iron. Since the DWPF melt pool reductants shift the equilibrium to the RHS where dissolved oxygen exists in the glass, it is the dissolved oxygen on the RHS of Equation 21 that is being displaced by the Ar in the melt pool. This is because the dissolved oxygen on the RHS of Equation 21 is stripped off and the equilibrium between the RHS and the LHS no longer exists, so any Fe^{3+} that has been converted chemically to Fe^{2+} stays as Fe^{2+} since Equation 21 can no longer proceed to the LHS. In addition, more Fe^{3+} is converted to Fe^{2+} to restore equilibrium. Therefore, O_2 or air must be added or admixed to the argon being used in the DWPF bubblers or enough oxidants must be used to overwhelm the effect of the argon degassing. Both these cases for providing more oxygen to the melt pool will be modeled and discussed below.

Very pure argon such as Grade 6.0 argon (99.9999% or 6 nines pure) imparts a logarithm of the oxygen fugacity (log fO_2) of -6 to -7 atm according to Reference 83. However, Abbott Welding Supply maintains that Grade 6.0 has <0.2 ppm O_2 which calculates to log fO_2 equal to -6.6990 (Table 4). The negative logarithms can also be written as –log fO_2 = 6.6990 atm. (Table 4). The gas coming from cryogenic argon, such as that used for the bubblers in DWPF contains between <0.6 ppm O_2 to 1.6 ppm O_2 which calculates to a -log fO_2 range of = 5.7959 to 6.2218 atm. (Table 4). High purity argon (99.999%) contains 1-2 ppm O_2 (depending on vendor) which calculates to -log fO_2 = 6 or 5.69897 atm. (Table 4). And welding grade argon (99.995-99.997) contains between 5 ppm to 7 ppm O_2 which calculates to -log fO_2 = 5.3 to 5.15 atm. (Table 4).

§ Gaseous, H2O, CO2 and SO3 are controlled chemically by an acid-base relationship in the glass (Mysen and Richert – Reference 67).

Table 4 also gives the DWPF acceptable REDOX range in terms of oxygen fugacities (-log fO_2) derived from the Schreiber EMF plot for $Fe^{2+}/\Sigma Fe$ between 0.09 and 0.33. This range is provided since the DWPF target for $Fe^{2+}/\Sigma Fe$ had been $Fe^{2+}/\Sigma Fe \sim 0.2$ ($-\log fO_2 \sim 5.16$ atm) and recently moved to $Fe^{2+}/\Sigma Fe \sim 0.1$ (-log fO_2 ~3.89 atm) to accommodate the Ar sparging of O_2 from the melt [84]. However, the cryogenic argon source being used for DWPF has a calculated $-\log fO_2 \sim 6.22$ which is equivalent to a $Fe^{2+}/\Sigma Fe$ of ~0.28.

Note that all the values calculated in Table 4 assume that Ar is an ideal gas and that the partial pressure of oxygen (pO_2) is the same as the oxygen fugacity (fO_2). This is proven using ASPEN modeling in Appendix A.

Table 4. Relative Oxygen Fugacities of Ar and Air at Room Temperature and DWPF Oxygen Fugacity REDOX Targets

Species	Gas Purity	Oxygen Fugacity (atm)
Argon	Ar Grade 6.0 Purity (99.9999%) also known as Scientific or Research[f] Grade Argon (<0.2 ppm[f] O_2) *	-log fO_2 = 6 to 7 [ref 83] -log fO_2 = 6.6990 [0.2ppm]
	Cryogenic Liquid Ar (<0.6 ppm O_2)*	-log fO_2 = 6.2218 [0.6 ppm]
	High Purity 5.0 Ar[f] (99.999%; 1-2 ppm O_2) *	-log fO_2 = 6.0000 [1 ppm] -log fO_2 = 5.69897 [2 ppm]
	High Purity 4.8 Ar[f] (99.998%)*; 5 ppm Ar	-log fO_2 = 5.3010 [5 ppm]
	Welding Grade Ar (99.995-99.997; 5 to 7 ppm O_2) *	-log fO_2 = 5.3010 [5 ppm] -log fO_2 = 5.1549 [7 ppm]
Air‡	$0.78N_2$-$0.21O_2$	-log fO_2 = 0.68 [83,85]
DWPF Glass	**DWPF REDOX Targets and Associated Oxygen Fugacity from Schreiber's EMF Series for Total Iron in Glass Between 5-10 wt% [16]**	
	$Fe^{2+}/\Sigma Fe$ = 0.09	-log fO_2 = 3.76
	$Fe^{2+}/\Sigma Fe$ = 0.10	-log fO_2 = 3.89
	$Fe^{2+}/\Sigma Fe$ = 0.15	-log fO_2 = 4.52
	$Fe^{2+}/\Sigma Fe$ = 0.20	-log fO_2 = 5.16
	$Fe^{2+}/\Sigma Fe$ = 0.25	-log fO_2 = 5.79
	$Fe^{2+}/\Sigma Fe$ = 0.30	-log fO_2 = 6.42
	$Fe^{2+}/\Sigma Fe$ = 0.33	-log fO_2 = 6.80

* log fO_2 = log (ppm/1,000,000)

‡ fO_2 of air is 0.21, the volume percent in dry air, the logarithm of 0.21 is -0.68.

f grades from Abbott Welding Supply home web page; grade 6 is six nines pure, grade five is five nines pure, grade 4.8 is four nines and an eight pure.

4.3 Experimental Evidence: Ar Bubbling Impact on DWPF Melt REDOX

The DWPF currently balances the oxidants and reductants in the melter feed to achieve the desired REDOX ratio. Whether the feeds are chemically balanced such that the reductants > oxidants or oxidants>reductants, the impact of the Ar will be additive to the impact from the chemical balancing. Once an Ar impact term is determined the feed chemistries can be balanced such that oxidants > reductants so that the extra oxidants provide the needed oxygen to counteract the Ar degassing. In order to prove this concept, the recent data acquired from the DWPF pour stream samples and some Ar bubbled sealed crucible experiments that were performed at SRNL were examined.

4.3.1 CRUCIBLE STUDIES

Sealed crucible studies were performed on SB6-21 non-radioactive SME product which contained Hg° in a hood in 773-A. A special Ar bubbler made of Inconel pipe was fabricated by the SRNL glass shop and a hole drilled into the crucible so that Ar could be continuously bubbled through the crucible during the sludge to glass transition (Figure 16). The Ar supply in 773-A comes from cryogenic argon and so is the same purity as that being used by DWPF as the tanker truck delivers to both facilities on the same day. The Ar is passed through a drierite column behind the furnace to remove any moisture and then a glass splitter allows the Ar to be used to bubble the crucible and the furnace at the same time or to bubble Ar in the crucible without purging the furnace. Tests were performed at room temperature with molasses in a glass beaker to predetermine an effective bubbling rate for the small volume (Figure 17). A video is also available of the bubbling experiment with molasses.

(a) (b)

Figure 16. Experimental setup to bubble Ar through DWPF simulated feeds in a sealed crucible during the feed to glass conversion. Furnace chamber can be simultaneously purged with argon if desired.

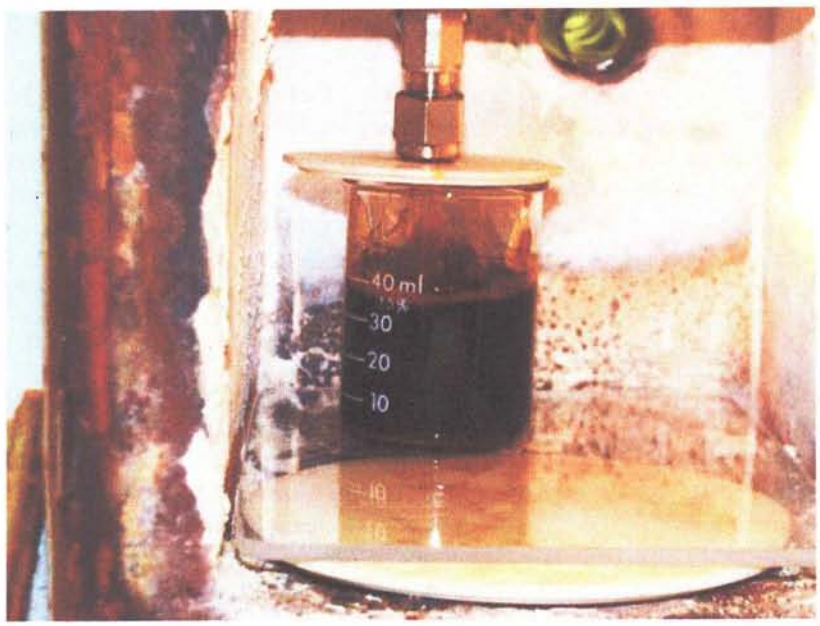

Figure 17. Bubbling Ar through molasses to determine an effective Ar bubbling rate.

Experiments were performed in the sealed crucibles under the following conditions:

- Ar bubbling in the crucible and in the furnace chamber-duplicate tests;
- Ar bubbling in only the crucible and not the furnace chamber; and
- the normal way that REDOX sealed crucibles are performed with no Ar bubbling and no Ar in the furnace chamber.

The measured $Fe^{2+}/\Sigma Fe$ ratios are given in Table 5, each crucible glass is sampled and dissolved once for the REDOX measurement and two reads are performed on each dissolution, i.e. A & B pairs. The REDOX ratios from the duplicate Ar bubbling experiments where Ar was bubbled in the crucible and in the feed were 0.266 and 0.267 for the two samples prepared in this manner. The SB6-21 feed in which there was no Ar purge and no bubbler in the crucible gave $Fe^{2+}/\Sigma Fe$ ratios of 0.147-0.149, the ratio reported for this feed which were tested in triplicate in Reference 11 was 0.147, 0.149, and 0.151, and the predicted REDOX with antifoam is 0.1466. The last set of crucible tests that were performed bubbled Ar into the crucible but did not purge the furnace with Ar and this gave an oxidized REDOX of 0.028-0.032 likely because of air inleakage around the bubbler entrance into the crucible as seen in Figure 16. It will be shown that in Section 4.4 that it does not take much O_2 (as air) to oxidize a melt that is being purged with Ar.

Table 5. Measured REDOX Ratios in SRNL Crucible Studies Targeted for $Fe^{+2}/\Sigma Fe$=0.15 with and without Ar Bubbling

Sample	Argon Bubble Crucible	Argon Purge Furnace	Lab ID	Fe^{2+}	Fe(total)	$\frac{Fe^{2+}}{Fe(total)}$
EA Glass REDOX Standard	N/A	N/A	N/A	0.132	0.733	0.180
SB6-21 SME Prod (slow increase to 1100°C, 4 hours) (A)	Yes	Yes	10-2777	0.180	0.676	0.266
SB6-21 SME Prod (slow increase to 1100°C, 4 hours) (B)	Yes	Yes	10-2777	0.180	0.675	0.267
SB6-21 SME Prod (direct increase to 1100°C, 4 hours) (A)	No	No	10-2778	0.099	0.666	0.149
SB6-21 SME Prod (direct increase to 1100°C, 4 hours) (B)	No	No	10-2778	0.098	0.668	0.147
SB6-21 SME Prod Center section (slow increase to 1100°C, 4 hours) (A)	Yes	Yes	10-2781	0.202	0.758	0.266
SB6-21 SME Prod Center section (slow increase to 1100°C, 4 hours) (B)	Yes	Yes	10-2781	0.203	0.760	0.267
SB6-21 SME Prod (A) (slow increase to 1100°C, 4 hours)	Yes	No	10-2788	0.022	0.679	0.032
SB6-21 SME Prod (B) (slow increase to 1100°C, 4 hours)	Yes	No	10-2788	0.019	0.679	0.028

4.3.2 TARGETING REDOX WITH AR BUBBLING

A large number of DWPF pour stream glasses have been analyzed for the $Fe^{2+}/\Sigma Fe$ ratio while the melt pool has been bubbled with argon. This data may be found in Table 2 and was shown in Figure 14b. However, Figure 14b included the data for glasses that had been made from DWPF MFT feeds in sealed crucibles and then had the REDOX determined. These MFT glasses had not been Ar bubbled. Therefore, only the data from DWPF pour stream samples given in Table 2 is plotted as Figure 18a, i.e. only the argon bubbled PS samples are overlain on the 2006 EE DWPF REDOX model. One additional set of data from Table 5 for the Ar bubbled crucible study is added to the plot (furnace chamber Ar purged as well). The PS data plotted will all be for SME/MFT batches corresponding to numbers above 538 when Ar bubbling commenced in the DWPF.

Figure 18a demonstrates that most of the PS samples are biased above the OLS for the 139 model points that were not bubbled (the no bubbling line in the figure) except for two points (PS 549 and PS 592 which are biased low). Therefore, those two points are considered outliers for the following reasons:

- PS 549 was taken just after Ar bubbling was initiated and the melt pool likely had not reached a steady state with the Ar bubbling
- PS 592 was almost at the detection level of the REDOX measurement in the SCF and the Ar bubbled PS sample was approximately the same REDOX as the MFT samples which were not bubbled.

Thus PS 549 and PS592 are excluded from further modeling. When the historic 139 model points and the 8 pour stream data points are fit with an OLS regression separately the pour stream data falls along a parallel line to the "no bubbling" OLS. The "Ar bubbling" OLS appears as a constant offset to the "no bubbling" OLS. This simplifies defining an Ar impact on REDOX.

In order not to include the slope and intercept effects the Ar impact is determined from {R-O}*45/T or ξ_A as the "eff" term was. The plots of Xi defined as {R-O}*45/T or ξ_A are shown in Figure 18b where the same offset is observed. The equations for the "no bubbling" and "Ar bubbling" OLS for {R-O}*45/T or ξ_A are given in Figure 18b. If these equations are solved at {R-O}*45/T or ξ_A equal to 1.0, then the difference between the two OLS is the Ar impact or 0.09906. This is rounded off to 0.1 for the Ar impact term. The impact of Ar sparging on REDOX can therefore be quantified as:

Equation 22

$$\frac{Fe^{2+}}{\Sigma Fe} = 0.2358 + 0.1999\xi_A + 0.1_{Ar}$$

Where ξ_A is defined by Equation 19 and the REDOX model using ξ_A is defined by Equation 20.

It is of interest to be able to reference Figure 18a and Figure 18b to the Technical Safety Requirements (TSR) recently defined by Choi. [14] Using the TSR limits of 2013 ppm of carbon from antifoam, assuming the remaining carbon is coming from formates and imposing the minimum NO_3 of 15,000 ppm and the maximum NO_3 of 30,000 and the TOC/NO_3 ratios defined by Equation 23,

Equation 23

$$MAX\ \frac{TOC}{[NO_3]} = 7.2791E^{-10}[NO_3]^2 - 5.0035E^{-05}[NO_3] + 1.5347$$

These ratios are broader than the DWPF REDOX range as shown in Table 6 for the chemical balancing of the melt pool independent of the additional $\frac{Fe^{2+}}{\Sigma Fe} = 0.1_{Ar}$ impact from Ar.

Table 6. $Fe^{2+}/\Sigma Fe$ Ratios Associated with SB7B Nitrate and TOC Limits from

Nitrate	TOC	$Fe^{2+}/\Sigma Fe$ from Equation 20 without Ar	$Fe^{2+}/\Sigma Fe$ from Equation 22 with Ar
MAX	MIN	-0.05	+0.05
MIN	MAX	+0.55	+0.65
MIN	MIN	+0.18	+0.28
MAX	MAX	+0.32	+0.42

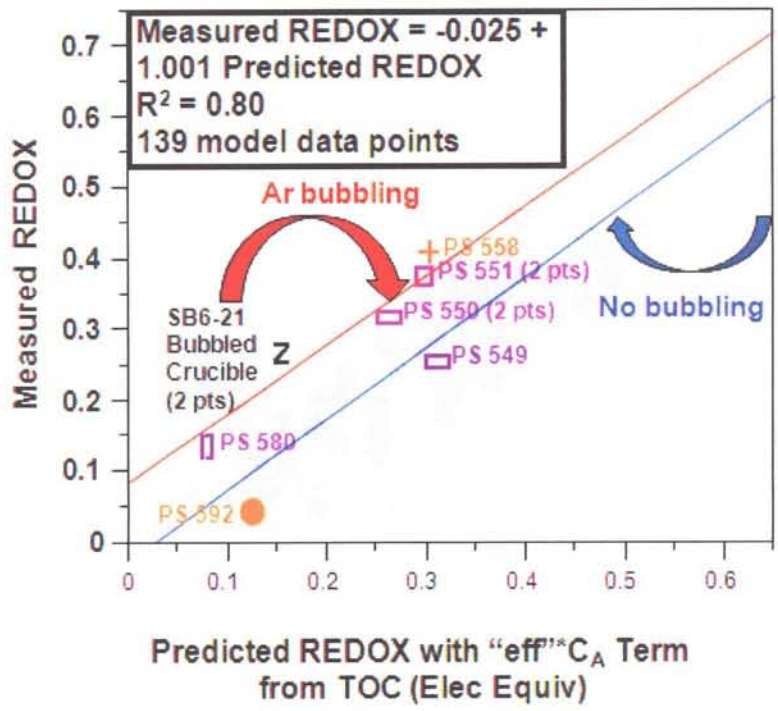

(a)

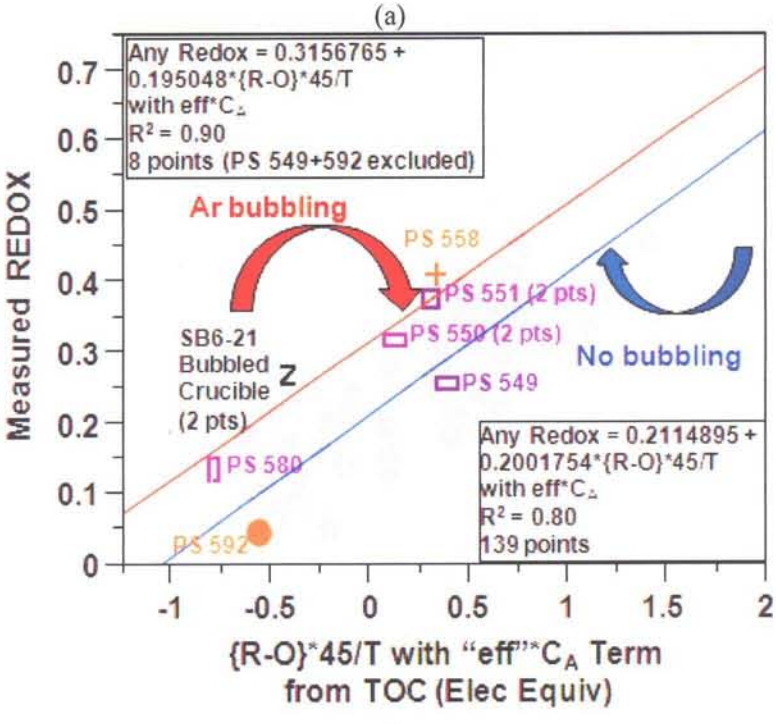

(b)

Figure 18. (a) Relationship between Predicted REDOX and measured Ar bubbled REDOX; (b) between measured REDOX and the Melter Feed Reductants and Oxidants {R-O}*45/T or ξ_A.

5.0 CONCLUSIONS

The impacts of antifoam on the DWPF melt pool REDOX has been de-convoluted from the impacts of melt pool bubbling with argon. Data from crucible studies with (1) varying antifoam concentrations without bubbling, and (2) with minimal antifoam and Ar bubbling were assessed. This allowed an antifoam term to be added to the REDOX model and suggested that (1) more oxidizing $Fe^{+2}/\Sigma Fe$ ratios could be targeted which would create more oxidizing species in the cold cap to offset the effects of Ar-sparging or (2) Ar-air gas mixtures could be blended with a mixing valve to control the melt pool REDOX at the same $Fe^{2+}/\Sigma Fe$ ratios (same –log fO_2) as chosen for the chemical REDOX balancing. Option 1 is preferred but the necessary Ar-air gas mixtures are given in Appendix B for Option 2.

The antifoam feed additive, is an organic chain structure composed of methyltrisiloxane (MTS) end groups and a center polymer chain of varying length (8 to 12 polyethyleneoxide or PEO groups), so an EE term for the REDOX model must be based on the number of carbons in each part of the organic group and their relative EE transfers.

The MTS end groups of the antifoam molecule have 7-8 carbons of -4 charge and the 8 chain PEO groups have 16 carbons of -1 charge while the 12 chain polymers have 24 carbons of -1 charge. Since the ratio of the 8:12 polymer chains is 90%:10%, there are 16.8 carbons of -1 charge in the weighted polymer chain and 8 carbons in the MTS if the MTS groups are assumed to be octa-MTS instead of hepta-MTS for a total of 24.8 carbons in the antifoam organic molecule (sum of 0.9*16 + 0.1*24). The -1 carbons of the PEO exchange 5EE's per carbon to oxidize to CO_2 in the melter while the octa-MTS exchange 8EE's per carbon. Experimentation and modeling have shown that the MTS cleave off the antifoam during processing and do not participate in reduction of the melt pool. Therefore, the EE of the PEO are 16.8/24.8 carbons * 5 EE per carbon for a total EE transfer term of +3.39 per mole/kg of antifoam carbon.

Experimentation and modeling has shown that the antifoam PEO's are 80-100% effective in melt pool reduction. The modeling performed for the REDOX model for antifoam suggests that the efficiency is 85%. Therefore, 85% of +3.39 EE yields an overall EE transfer of +2.88 per mol/kg of carbon from antifoam compared to +2 for formic acid and +4 for oxalate and coal.

The DWPF REDOX model then takes the form

$$\frac{Fe^{2+}}{\Sigma Fe} = f\left[\left(2[F] + 4[C] + 4[O_T] + 3.39 * eff[C_A] - 5[N] - 5[Mn]\right)\frac{45}{T}\right] = f[\xi_A]$$

where
- f = indicates a function
- [F] = formate (mol/kg feed)
- [C] = coal (carbon) (mol/kg feed)
- $[O_T]$ = $oxalate_{Total}$ (soluble and insoluble) (mol/kg feed)
- $[C_A]$ = carbon from antifoam (mol/kg feed)
- eff = effective antifoam impact = 0.85
- [N] = nitrate + nitrite (mol/kg feed)
- [Mn] = manganese (mol/kg feed)
- T = total solids (wt%)

$$\xi_A = \left[\left(2[F] + 4[C] + 4[O_T] + 3.39 * eff[C_A] - 5[N] - 5[Mn]\right)\frac{45}{T}\right]$$

When the REDOX data generated were fit as a linear function of ξ_A they fell within the confidence bands of the 2006 EE model and so the slope and intercept were not refit. This gives the form of the DWPF REDOX model with an antifoam term as:

$$\frac{Fe^{2+}}{\Sigma Fe} = 0.2358 + 0.1999\xi_A$$

There is an additive impact on the melt pool REDOX from the argon bubbling. Argon (Ar) degasses or sparges the oxygen from the melt. Thus, REDOX is a function of both the oxidants and reductants in the melt pool and the Ar sparging. While Ar is an inert gas, Ar replaces the free oxygen in a glass. This process also occurs when inert gasses are used to sparge the oxygen or other gasses out of solutions, molten metals, or glasses. The REDOX equilibrium in a glass melt can be represented by

$$Fe^{3+}_{melt} + \frac{n}{2} O^{2-}_{melt} \leftrightarrow Fe^{2+}_{melt} + \frac{n}{4} O_{2\ melt}$$

where n = the number of electrons transferred
O^{2-} = the oxygen ion activity or basicity of the melt
O_2 is the physically dissolved oxygen in the holes of the network structure.

The REDOX-oxygen balance equation is written as reversible as going from the right hand side (RHS) to the left hand side (LHS) is the reduction of ferric to ferrous iron and going from LHS to RHS is the oxidation of ferrous to ferric iron. Since the DWPF melt pool reductants shift the equilibrium to the RHS where dissolved oxygen exists in the glass, it is the dissolved oxygen on the RHS of this equation that is being displaced by the Ar in the melt pool. Because the free oxygen on the RHS of the equation is being sparged out, the equilibrium between the RHS and the LHS no longer exists, driving the equilibrium to the RHS.

Measurement of the REDOX of DWPF pour stream (PS) samples (with and without Ar bubbling) and measurement of a simulated SB6 feed that was Ar bubbled during the feed-to-glass transformation in a sealed crucible inside an Ar bubbled oven demonstrated that the argon bubbling impact is a linear constant of $Fe^{+2}/\Sigma Fe$ of ~0.1. Therefore, it is recommended that targeting a chemical REDOX of 0.1 should yield a realized $Fe^{+2}/\Sigma Fe$ of ~0.2. While there is no EE term that can be developed for Ar sparging, an "effective offset" term has been added to the REDOX model to account for Ar degassing. The impact of Ar sparging on REDOX was quantified and the Ar adjusted DWPF model takes on the form:

$$\frac{Fe^{2+}}{\Sigma Fe} = 0.2358 + 0.1999\xi_A + 0.1_{Ar}$$

6.0 PATH FORWARD

Many assumptions had to be made during the development of the antifoam term. A more definitive derivation could be made if the following were addressed:

- it would be helpful in developing the theoretical EE transfers if the long chain polymers discussed in Reference 44 (partitioning of antifoam during SRAT processing) were identified
  - it was noted in this study that a better extraction method was needed to get more definitive data

- it would be helpful in defining the "effective antifoam carryover to the melter" to repeat the partitioning study given in Reference 44 during SRAT processing and also perform similar experiments for SME processing

- while the Ar impact term is well defined as 0.1 it is based on 6 pour stream samples and 2 SRNL Ar bubbled crucible experiments. Two additional pour stream samples would be helpful along with the associated TOC measurements for additional confirmation.

Argon-air mixtures are given for argon sources varying between 0.6-1.66 ppm impurities of oxygen. Since SRNL (773-A) uses cryogenic argon from the same Air Liquide vendor as the DWPF, it is suggested that if sealed crucible studies with or without Ar are to be performed that it be done with the newly designed SRNL bubbled REDOX crucible methodology described in this report since the bubbled crucible data was used to quantify the Ar impact on the glass in this study.

7.0 ACKNOWLEDGEMENTS

The authors would like to gratefully acknowledge the assistance of Analytic Development personnel and the SCF personnel, specifically Damon Click, Phyllis Burkhalter, Rita Sullivan, and Dee Wheeler with the REDOX measurements of the radioactive DWPF samples. In addition, the assistance of specialist Holly Hall of SRNL was invaluable in helping simplify this difficult procedure so it could be performed remotely. In addition, the authors are indebted to the "non-radioactive crucible experiments and the REDOX measurement" team consisting of Whitney Riley, Pat Simmons, Beverly Wall, and Phyllis Workman.

The special talents of James G. Dobos of the SRNL glass shop and Ken J. Imrich of the Material Science & Technology Section of SRNL in developing the geometry of the bubbled crucible experiments in conjunction with the lead author are noted. Special thanks are also due to Sherry Vissage for her diligence in putting up with the design team and performing the bubbled crucible experiments.

Additional thanks are due to James M. Becnel of SRNL for performing the ASPEN calculations of the argon-air mixtures found in the appendices of this document and to James E. Laurinat of SRNL for suggesting that ASPEN be used.

The lead author would also like to acknowledge the support given by the reviewers in understanding the decomposition mechanisms of antifoam.

The data are recorded in WSRC-NB-2006-00137.

8.0 REFERENCES

1 B.A. Hamm, R.E. Eibling, M.A. Ebra, T. Motyka, and H.D. Martin, **"High-Level Insoluble Waste Preparation for Vitrification,"** Sci. Basis for Nuclear Waste Management, VIII, C. M. Jantzen, et al. (Eds.), Materials Research Society, Pittsburgh, PA 793-799 (1985).

2 W.G. Ramsey, C.M. Jantzen, and D.F. Bickford, **"Redox Analyses of SRS Melter Feed Slurry: Interactions Between Nitrate, Formate and Phenol Based Dopants,"** Nuclear Waste Management IV, Ceramic Transactions, V.23, G.G. Wicks, D.F. Bickford and L.R. Bunnell (Eds.), American Ceramic Society, Westerville, OH, 259-266 (1991).

3 T.B. Calloway, C.M. Jantzen, L.M. Medich, and N.R. Spennato, **"Analysis of the DWPF Glass Pouring System Using Neural Networks,"** Waste Management '98 (1998).

4 K.G. Brown, C.M. Jantzen, and J.B. Pickett, **"The Effects of Formate and Nitrate on Reduction/Oxidation (Redox) Process Control for the Defense Waste Processing Facility (DWPF),** U.S. DOE Report WSRC-RP-97-34, Rev. 1 (June 30, 1998).

5 M.J. Singleton, **"Comparison of Sludge Batches 1A, 1B, and 2,"** U.S. DOE Report HLW-PRE-200209950.

6 C.W. Hsu, **"Defense Waste Processing Facility Nitric Acid Requirement for Treating Sludge,"** U.S. DOE Report WSRC-RP-92-1056, Savannah River Technology Center, Westinghouse Savannah River Co., Aiken, SC (September, 1992).

7 C.M. Jantzen, J.R. Zamecnik, D.C. Koopman, C.C. Herman, and J.B. Pickett, **"Electron Equivalents Model for Controlling REDuction/OXidation (REDOX) Equilibrium During High Level Waste (HLW) Vitrification,"** U.S. DOE Report WSRC-TR-2003-00126, Rev.0 (May 9, 2003).

8 C.M. Jantzen, D.C. Koopman, C.C. Herman, J.B. Pickett, and J.R. Zamecnik, **"Electron Equivalents REDOX Model for High Level Waste Vitrification,"** Environmental Issues and Waste Management Technologies IX, J.D. Vienna and D.R. Spearing (Eds), Ceramic Transactions 155, 79-91 (2004).

9 M.E. Smith, T.M. Jones, D.H. Miller, and M.E. Stone, **"SB4 SMRF Runs with Frits 418 and 320"**, U.S. DOE Report WSRC-TR-2005-00569, Savannah River Site, Aiken, SC (2005).

10 C.M. Jantzen and M.E. Stone, **"Role of Manganese Reduction/Oxidation (REDOX) on Foaming and Melt Rate in High Level Waste (HLW) Melters,"** U.S. DOE Report WSRC-STI-2006-00066 (2007).

11 J.D. Newell, **"Defense Waste Processing Facility (DWPF) Sludge Batch 6 (SB6) REDOX Evaluation,"** SRNL-L3100-2010-00073 (June 2010).

12 J.D. Newell and M.E. Stone, **"Effect of CSSX/MCU Organic Waste on the REDOX of SB4,"** SRNL-PSE-2007-00263 (January 2008).

13 M.E. Smith and D.C. Iverson, **"Installation of Bubblers in the Savannah River Site Defense Waste Processing Facility Melter,"** U.S. DOE Report SRR-STI-2010-00784 and WM11 Paper # (2010-2011)

14 A.S. Choi, **"DWPF Melter Off-Gas Flammability Assessment,"** Calculation Sheet X-CLC-S-00164, Rev. 7 (September 2011).

15 C.M. Jantzen, J.B. Pickett, K.G. Brown, T.B. Edwards, and D.C. Beam, **"Process/Product Models for the Defense Waste Processing Facility (DWPF): Part I. Predicting Glass Durability from Composition Using a Thermodynamic Hydration Energy Reaction MOdel (THERMO),"** U.S. DOE Report WSRC-TR-93-0672, Westinghouse Savannah River Co., Aiken, SC, 464p. (Sept. 1995).

16 H.D. Schreiber, and A.L. Hockman, **"Redox Chemistry in Candidate Glasses for Nuclear Waste Immobilization,"** J. Am. Ceram. Soc., Vol. 70, No. 8, pp. 591-594 (1987).

17 C.M. Jantzen and M.J. Plodinec, **"Composition and Redox Control of Waste Glasses: Recommendation for Process Control Limit,"** U.S. DOE Report DPST-86-773, E.I. duPont deNemours & Co., Savannah River Laboratory, Aiken, SC (November, 1986).

18 M.J. Plodinec, **"Foaming During Vitrification of SRP Waste,"** U.S. DOE Report DPST-86-213, E.I. duPont deNemours & Co., Savannah River Laboratory, Aiken, SC (January, 1986).

19 H.D. Schreiber, C.W. Schreiber, M.W. Riethmiller and J.S. Downey, **"The Effect of Temperature on the Redox Constraints for the Processing of High-level Nuclear Waste into a Glass Waste Form,"** Scientific Basis for Nuclear Waste Management, XIII, V.M. Oversby and P.W. Brown (Eds.), Materials Research Society, Pittsburgh, PA, 419-426 (1990).

20 H.D. Schreiber, P.G. Leonhard, R.G. Nofsinger, M.W. Henning, C.W. Schreiber, and S.J. Kozak, **"Oxidation-Reduction Chemistry of Non-Metals in a Reference Borosilicate Melt,"** Advances in the Fusion of Glass, D.F. Bickford, W.E. Horsfall, F.E. Wooley, E.N. Boulos, J.N. Lingscheit, F. Harding, F. Olix, W.C. LaCourse, and L.D. Pye (Eds.), Am. Ceram. Soc., Westerville, OH, 29.1-29.14 (1988).

21 H.D. Schreiber, F.A. Settle, Jr., P.L. Jamison, J.P. Eckenrode, and G.W. Headley, **"Ruthenium in Glass Forming Borosilicate Melts,"** J. Less Common Metals, 115, 145-154 (1986).

22 D.S. Goldman and D.W. Brite, **"Redox Characterization of Simulated Nuclear Waste Glass,"** J. Am. Ceram. Soc., 69 [5], pp. 411-413, (1986).

23 P.K. Smith, **"Evaluation of the Chemical Reduction of Waste Constituents in the Glass Melter,"** U.S. DOE Report, DPST-81-467 (May 28, 1981).

24 M.E. Smith, D.H. Miller, and T.H. Lorier, **"The Impact of Feed Preparation Acid Stoichiometry and REDOX on Melt Rate for the SB3-418 Feed System,"** U.S. DOE Report WSRC-TR-2004-00350, Westinghouse Savannah River Company, Aiken, SC (2004).

25 C.G. Rasul and M. Cable, **"Spontaneous Bubble Formation in Silicate Melts at High Temperatures,"** J. Am. Ceram. Soc., 49[10], 568-571 (1966).

26 W.G. Ramsey, T.D. Taylor, K.M. Wiemers, C.M. Jantzen, N.D. Hutson, and D.F. Bickford, **"Effects**

of Formate and Nitrate Content on Savannah River and Hanford Waste Glass Redox" Proceed.of the Advances in the Fusion and Processing of Glass, III, New Orleans, LA, D.F. Bickford, et.al. (Eds.) Am. Ceramic Society, Westerville, OH, 535-543 (1993).

27 W.G. Ramsey, N.M. Askew, and R.F. Schumacher, **"Prediction of Copper Precipitation in the DWPF Melter from the Melter Feed Formate and Nitrate Content,"** U.S. DOE Report WSRC-TR-92-385, Westinghouse Savannah River Co., Aiken, SC (Nov.30, 1994).

28 W.G. Ramsey and R.F. Schumacher, **"Effects of Formate and Nitrate Concentration on Waste Glass Redox at High Copper Concentration."** U.S. DOE Report, WSRC-TR-92-484, Westinghouse Savannah River Co., Aiken, SC (October 23, 1992).

29 J.M. Gillam, **"Aluminum in Waste Tank Sludge: History and Status,"** U.S. DOE Memorandum CBU-PIT-2006-00068, Rev. 0, Savannah River Site, Aiken, SC (July 11, 2006).

30 A.S. Choi, **"Validation of DWPF Melter Off-Gas Combustion Model,"** U.S. DOE Report WSRC-TR-2000-00100, Westinghouse Savannah River Co., Aiken, SC (June 23, 2000).

31 A.S. Choi, **"Prediction of Melter Off-Gas Explosiveness,"** U.S. DOE Report WSRC-TR-90-00346, Westinghouse Savannah River Co., Aiken, SC (January 22, 1992).

32 D.C. Koopman, C.C. Herman, and N.E. Bibler, **"Sludge Batch 3 Preliminary Acid Requirements Studies with Tank 8 Simulant,"** U.S. DOE Report WSRC-TR-2003-00041, Westinghouse Savannah River Co., Aiken, SC (January 31, 2003).

33 E.W. Baumann, **"Colorimetric Determination of Iron(II) and Iron(III) in Glass,"** Analyst, 117, 913-916 (1992).

34 D.R. Best, **"Determining Fe^{+2}/Fe^{+3} and Fe^{+2}/Fe_{total} Using the HP8452A Diode Array Spectrometer,"** Procedure Manual L28, Procedure 1.8 Rev. 2 (March 14, 2001).

35 C.M. Jantzen, **"Verification and Standardization of Redox Measurement for DWPF,"** DPST-89-222, (January 1989).

36 C.M. Jantzen, N.E. Bibler, D.C. Beam, and M.A. Pickett, **"Characterization of the Defense Waste Processing Facility (DWPF) Environmental Assessment (EA) Glass Standard Reference Material,"** U.S. DOE Report WSRC-TR-92-346, Rev.1, 92p (February, 1993).

37 J.M. Gillam, **"Aluminum in Waste Tank Sludge: History and Status,"** U.S. DOE Memorandum CBU-PIT-2006-00068, Rev. 0, Savannah River Site, Aiken, SC (July 11, 2006).

38 National Technical Information Service, **"Final Environmental Impact Statement Waste Management Operations,"** Savannah River, Plan, Aiken, SC, ERDA-1537 (September, 1977).

39 C.M. Jantzen and J.D. Newell, **"Defense Waste Processing Facility (DWPF) Sludge Batch 5 (SB5) REDOX Evaluation,"** SRNL-PSE-2008-00184 (September 2008).

40 J.D. Newell, **"Defense Waste Processing Facility (DWPF) Sludge Batch 7 (SB7) REDOX Evaluation,"** SRNL-L3100-2011-00062 (April 2011).

41 J.D. Newell, **"Defense Waste Processing Facility (DWPF) Sludge Batch 7b (SB7b) REDOX Evaluation,"** SRNL-L3100-2011-00178 (August 2011).

42 www.wikipedia.org/wiki/Siloxane

43 D.C. Koopman, **"Comparison of Dow Corning 544 Antifoam to IIT-747 Antifoam in the 1/240th SRAT,"** U.S. DOE Report, WSRC-TR-99-00377, Rev. 0 (December 1999).

44 J.D. Newell, **"Antifoam Partitioning During SRAT Testing,"** SRNL-L3100-2011-00171 (August 2011).

45 D.P. Lambert, B.R. Pickenheim, M.E. Stone, J.D. Newell, and D.R. Best, **"Glycolic-Formic Acid Flowsheet Final Report for Downselection Decision,"** SRNL-STI-2010-00523, Rev. 1 (March 2011).

46 N.E. Bibler and T.L. Fellinger, "**Results for the DWPF Slurry Mix Evaporator Condensate Tank, Off-Gas Condensate Tank, and Recycle Collection Tank Samples**," U.S. DOE Report WSRC-TR-2004-00577, Rev. 0 (December 2004).

47 www.wikipedia.org/wiki/Ethylene Oxide

48 J.D. Newell and W.T. Riley, **"Summary of Glass REDOX Values Using Alternative Reductants,"** SRNL-L3100-2009-0063 (March 2009).

49 A.L. Billings, M.M. Reigel, and D.R. Click, **"REDOX Analysis of SB4, SB5, and SB6 Pour Stream Samples,"** SRNL-L3100-2011-00007, Rev.0 (January 2011).

50 F.C. Johnson and D.R. Click, **"REDOX Analysis of a SB6 Pour Stream Sample and Melter Feed Tank Batch 558 Sample,"** SRNL-L3100-2011-00092, Rev.0 (April 2011).

51 F.C. Johnson, **"REDOX Analysis of a Melter Feed Tank Batch 568A Sample,"** SRNL-L3100-2011-00140, Rev.0 (July 2011).

52 F.C. Johnson, **"REDOX Analysis of a Vitrified from MFT Batch 580,"** SRNL-L3100-2011-00182, Rev.0 (October 2011).

53 F.C. Johnson, **"REDOX Analysis of a SB7a Pour Stream Sample from MFT Batch 580,"** SRNL-L3100-2011-00181, Rev.0 (September 2011).

54 F.C. Johnson, **"REDOX Analysis of a Vitrified from MFT Batch 592,"** SRNL-L3100-2011-00224, Rev.0 (December 2011).

55 F.C. Johnson, **"REDOX Analysis of a SB7a Pour Stream Sample from MFT Batch 592,"** SRNL-L3100-2011-00233, Rev.0 (December 2011).

56 F.C. Johnson and D.R. Click, **"Chemical Composition Analysis of the Melter Feed Tank Batch 558 Sample,"** SRNL-L3100-2011-00113, Rev.0 (June 2011).

57 F.C. Johnson and M.E. Stone, "**Impact of Antifoam Additions on REDOX,"** SRNL-L3100-2011-00131, Rev.0 (July 2011).

58 F.C. Johnson and M.E. Stone, **"Impact of Antifoam Additions on REDOX in the Range of 800-10,000 ppm,"** SRNL-L3100-2012-00036, Rev.0 (April 2012).

59 A.C. Jenkins and G.A. Cook, **"Gas-Phase Properties,"** Chapter VII in **"Argon, Helium and the Rare Gases,"** Vol. I, G.A. Cook (Ed.), John Wiley & Sons, New York, p.173- 250 (1961).

60 www.wikipedia.org/wiki/Degasification

61 C.M. Jantzen and N.E. Bibler, **"The Role of Groundwater Oxidation Potential and Radiolysis on Waste Glass Performance in Crystalline Repository Environments,"** Sci. Basis for Nuclear Waste Management,IX, L.O. Werme (ed.), Materials Research Society, Pittsburgh, PA 219-229 (1986).

62 E.C. Nelson, **"Inert Atmospheres in Metallurgy,"** Chapter XVI in **"Argon, Helium and the Rare Gases,"** Vol. II., G.A. Cook (Ed.). John Wiley & Sons, New York, p.609-634 (1961).

63 R.D. Pehlke and A.L. Bement, Jr., **"Mass Transfer of Hydrogen Between Liquid Aluminum and Bubbles of Argon Gas,"** Trans. Met. Soc. AIME, 224 [6], 1237-1242 (1962).

64 R.A. Rapp, **"The Closed-Circuit Degassing of Liquid Aluminum by Argon,"** Journal of the Minerals, Metals, and Materials Society, v. 49 16-19 (1997).

65 M. Sano and K. Mori, **"Rate Determining Mechanism of Degassing by Inert Gas Flushing in Molten Metal,"** Transactions of the Japan Institute of Metals, V. 23 [8], 440-450 (1982).

66 T.P. Schoonmaker, **"Inert-Gas-Shielded Arc Welding and Cutting,"** Chapter XVII in **"Argon, Helium and the Rare Gases,"** Vol. II, G.A. Cook (Ed.). John Wiley & Sons, New York, p.635-684 (1961).

67 B.O. Mysen and P. Richet, **"Volatiles II. Noble Gases and Halogens,"** Chapter 16 in **"Silicate Glasses and Melts,"** Vol. 10 in the book series **"Developments in Geochemistry,"** pp.483-502 (2005).

68 G.I. Marziano, A. Paonita, A. Rizzo, B. Scaillet, and F. Gaillard, **"Noble Gas Solubilities in Silicate Melts: New Experimental Results and a Comprehensive Model of the Effects of Liquid Composition, Temperature and Pressure,"** Chemical Geology, 279,145-157 (2010).

69 F.W. Kramer, **"Solubility of Gases in Glass Melts,"** Chapter 13 in "Properties of Glass-Forming Melts," L.D. Pye, A. Montenero, and I. Joseph (Eds.) CRC Press, Boca Raton FL, pp. 405-482 (2005).

70 B.S. White, M. Brearley, and A. Montana, **"Solubility of Argon in Silicate Liquids at High Pressures,"** American Mineralogist, 74, 513-529 (1989).

71 R.H. Doremus, **"Physical Solubility of Gases in Fused Silica,"** J. Am. Ceram. Soc. 49, 461–462 (1966).

72 J.E. Shelby, **"Pressure Dependence of Helium and Neon in Vitreous Silica,"** J. Appl.Phys. 47, 135–139 (1976).

73 A. Jambon, H. Weber, and O. Braun, **"Solubility of He, Ne, Ar, Kr and Xe in a Basalt Melt in the Range 1250–1600 °C: Geochemical Implications,"** Geochim. Cosmochim. Acta, 50, 401–408 (1986).

74 G. Lux, **"The Behavior of Noble Gases in Silicate Liquids: Solution, Diffusion, Bubbles and Surface Effects, with Applications to Natural Samples,"** Geochim. Cosmochim.Acta 51, 1549–1560 (1987).

75 C.L. Broadhurst, M.J. Drake, B.E. Hagee, and T.J. Bernatowicz, **"Solubility and Partitioning of Ne, Ar, Kr and Xe in Minerals and Synthetic Basalts Liquids,"** Geochim.Cosmochim. Acta 56, 709–723 (1992).

76 M.R. Carroll and E.M. Stolper, **"Noble Gas Solubilities in Silicates and Glasses: New Experimental Results for Argon and the Relationship Between Solubility and Ionic Porosity,"** Geochim. Cosmochim. Acta 57, 5039–5051(1993)

77 T. Shibata, E. Takahashi, and J. Matsuda, **"Solubility of Neon, Argon, Krypton and Xenon in Binary and Ternary Silicates Systems: A New View on Noble Gas Solubility,"** Geochim. Cosmochim. Acta 62, 1241–1253 (1998).

78 B. Schmidt and H. Keppler, **"Experimental Evidence for High Noble Gas Solubilities in Silicate Melts Under Mantle Pressures,"** Earth Planet. Sci. Lett. 195, 277–290 (2002).

79 M.R. Carroll and E.M. Stolper, **"Argon Solubility and Diffusion in Silica Glass: Implications for the Solution Behavior of Molecular Gases,"** Geochim. Cosmochim. Acta 211–225 (1991).

80 J.F. Shackelford, P.L. Studt, P.L. and R.M. Fulrath, **"Solubility of Gases in Glasses: II. He, Ne, and H_2 in Fused Silica,"** J. Appl. Phys. 43, 1619–1626 (1972)

81 S.W. Brawer and W.B. White, **"Raman Spectroscopic Investigation of the Structure of Silicate Glasses, I. The Binary Silicate Glasses,"** J. Chem. Phys. 63, 2421–2432 (1975).

82 Y. Marrocchi and M.J. Toplis, **"Experimental Determination of Argon Solubility in Silicate Melts: an Assessment of the Effects of Liquid Composition and Temperature,"** Geochim. Cosmochim. Acta 69, 5765–5776 (2005).

83 G. Ventura, **"Kinematics and Dynamics of Lava Flows,"** Geological Society of America Special Paper #396, Geological Society of America, Boulder, CO, 80pp. (2005).

84 J.M. Bricker, D.C. Iverson, A.V. Staub, J.F. Iaukea, and J.E. Occhipinti, **"ENGINEERING POSITION: Response to Potential Reducing Effect of Argon During Melter Bubbler Operation,"** SRR-WSE-2010-00195 (September 7, 2010).

85 D.H. Lindsley, **"Experimental Studies of Oxide Minerals,"** Chapter 2 in Oxide Minerals, Mineralogical Society of America Short Course Notes, V. 3, L61-L88 (1976).

Appendix A

Calculation of the Fugacity Coefficients for Ar, Air, O_2 and N_2

The fugacity coefficient for component i, φ_i, is related to the gas fugacity of the component, f_i, through:

$$f_i = \varphi_i y_i P$$

where y_i is the component mole fraction and P is the total pressure. Thus, $\varphi_i = 1$ for ideal gas behavior.

Fugacity coefficients are calculated using Aspen Properties with the Benedict-Webb-Rubin-Lee-Starling (BWR-LS) equation of state (EOS). This is a virial EOS, which is most appropriate for gas phases exhibiting small deviations from ideal gas behavior, which is consistent with light gasses at 1150 °C and 1 atm.

Fugacity coefficients were calculated at 1150 °C and 1 atm for three systems of interest: 1) Ar – air, with air as a "mixture" component of 21 mol% O_2 and 79 mol% N_2; 2) Ar – O_2; and 3) Ar – N_2.

Air fugacity coefficients were calculated over the range from 1 parts per million (ppm, by mole) to 20 ppm air in Ar. Correspondingly, fugacity coefficients were calculated from 0.21 to 4.2 ppm O_2 in Ar and 0.79 to 15.8 ppm N_2 in Ar for the other two systems.

Over all conditions calculated, the fugacity of each component was constant to more than 8 significant figures. Results are presented in Table A1 show the system is very close to ideal gas behavior. Additionally, the fugacities of O_2 and N_2 were not affected by the presence or absence of the other.

Table A1. Calculated fugacity coefficients

Component	ϕ
Ar	1.0002110
Air	1.0002710
O_2	1.0002080
N_2	1.0002740

These values show the system differs from ideal gas behavior by only 0.0274%. So, assuming the fugacity of O_2 is equal to its partial pressure introduces no more than 0.0274% error.

This conclusion agrees with the provided O_2 fugacity as a function of purity in Ar. Given the O_2 concentration and the resulting O_2 fugacity (provided as the negative log of O_2 fugacity in atm), the fugacity coefficient can be calculated assuming a total pressure of 1 atm; values are provided in Table A2.

Table A2. O_2 fugacities (in atm) and fugacity coefficients from composition data

	Data		Calculated	
Ar Spec	y O_2	-log fO_2	f O_2	φ O_2
Cryogenic	6E-07	6.221800	6.0007E-07	1.000112
High Purity	2E-06	5.698970	2.0000E-06	1.000000
Welding	5E-06	5.3	5.0119E-06	1.002374
	7E-06	5.15	7.0795E-06	1.011351

Table A2 shows the calculated fugacity coefficient is close to 1 for all cases. The larger values calculated for the welding grade are likely due to the inherent product variability resulting in the limited number of significant figures provided. The fugacity value provided for the high purity grade may have been calculated assuming ideal gas behavior as this would result in a fugacity coefficient of exactly one.
The target fugacity of oxygen is given to be 1.69×10^{-5} atm (-log fO_2 = 4.771). Using the assumption that the O_2 fugacity is equal to its partial pressure, this becomes the target partial pressure of O_2 over the melt. The small correction from ideal behavior calculated using Aspen Properties would only be seen at the sixth significant figure.

Note that the target mole fraction of O_2, 1.69×10^{-5}, is larger than even the upper-end of the welding grade concentration of O_2 (see Table A2). To reach the target O_2 concentration, most of the required O_2 will have to come from another source and be mixed with whatever source of Ar is used.

Appendix B

Calculation of Ar-Air Mixtures for REDOX Control

The alternate methodology for control of the DWPF melt pool REDOX at the desired target of $Fe^{2+}/\Sigma Fe=0.2$ is to target the REDOX chemically by use of Equation 13 using the ξ_A value defined in Equation 19 in conjunction with Equation 20 and then using a mixing valve to bleed air into the Ar being used for bubbling such that the Ar-Air (N_2-O_2) mixture fixes the fO_2 of the melt pool at the same fO_2 that corresponds to $Fe^{2+}/\Sigma Fe=0.2$. From Table 4, this would be a $-\log fO_2 = 5.16$ atm. Then the melt pool is balanced chemically and gas equilibrated at the same $-\log fO_2$.

In order to determine the required Ar-air mixtures should this methodology be considered, the amount of O_2 impurity in the Ar being used at DWPF must be known. For the example of cryogenic Ar given in Table 4, the O_2 impurity level is <0.6 ppm. For the cryogenic Ar delivered to SRNL, the O_2 impurity level is 1.6 ppm and can vary slightly from delivery batch to delivery batch. Therefore, calculations were performed for Ar-O_2 and then Ar-air mixtures at O_2 impurities varying from 0.6 -1.6 ppm at intervals of 0.2 ppm. The data is given in Table B1 and shows that anywhere from 253-301 ppm air needs to be bled into the Ar used for bubbling the DWPF in order to control the melt pool $-\log fO_2$ at 5.16 atm. which corresponds to a REDOX target of $Fe^{2+}/\Sigma Fe=0.2$. This data is also shown graphically in Figure 19.

Table B1. Amount of Air Admixed with Various Levels of Pure Ar to Control the Gas Fugacity of the DWPF Melt Pool at $-\log fO_2 = 5.16$ atm. or $Fe^{2+}/\Sigma Fe = 0.2$

Desired Glass REDOX $Fe^{2+}/\Sigma Fe$	Desired Melt Pool $-\log fO_2$ (atm)	Desired Melt Pool O_2 (ppm)	Ar with 0.6 ppm O_2 impurity	Ar with 0.8 ppm O_2 impurity	Ar with 1.0 ppm O_2 impurity	Ar with 1.2 ppm O_2 impurity	Ar with 1.4 ppm O_2 impurity	Ar with 1.6 ppm O_2 impurity
			Additional Air (ppm) Needed					
0.09	3.76	174	8245	8236	8226	8217	8207	8198
0.10	3.89	129	6105	6095	6086	6076	6067	6058
0.15	4.52	30	1409	1400	1390	1381	1371	1362
0.20	5.16	6.9	301	291	282	272	263	253
0.25	5.79	1.6	49	39	30	20	11	1
0.30	6.42	0.38	---	---	---	---	---	---
0.33	6.80	0.16	---	---	---	---	---	---

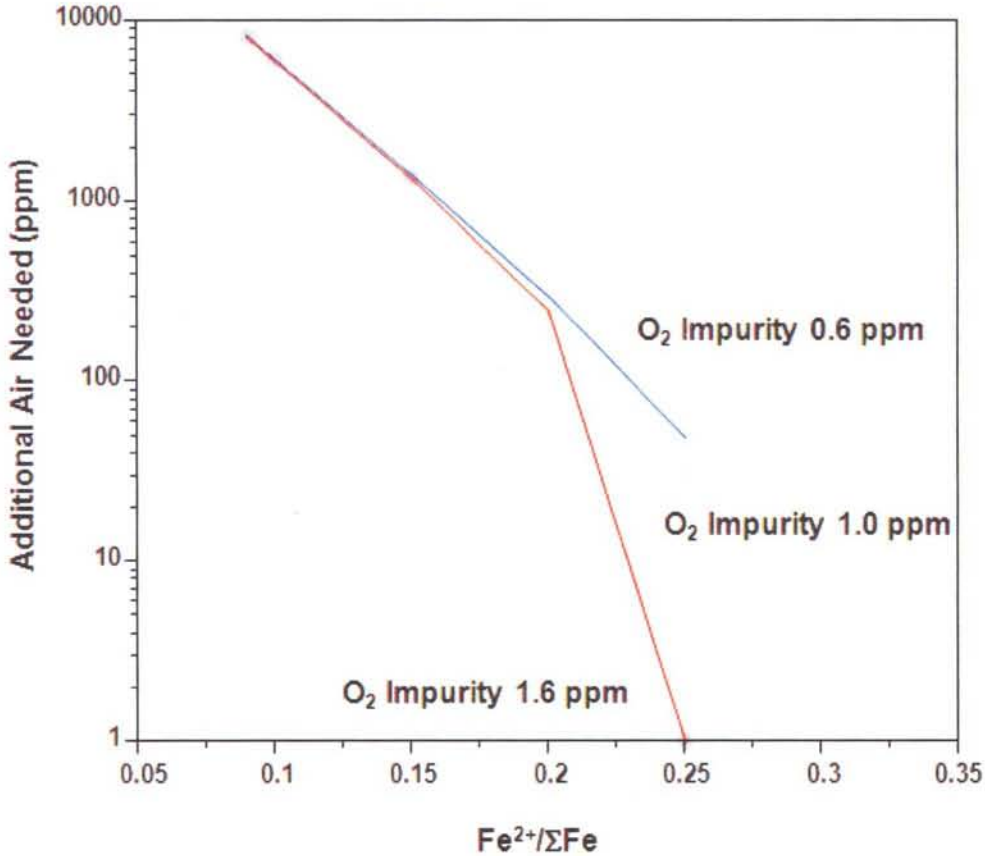

Figure Error! Main Document Only.. Target Air Concentrations in Cryogenic Argon Depending on Oxygen Impurity Level in Argon. Impurity levels of 0.6, 1.0 and 1.6 ppm O_2 in Ar are shown.

Distribution:

A. P. Fellinger, 773-41A
S. D. Fink, 773-A
K. M. Fox, 999-W
B. J. Giddings, 786-5A
C. C. Herman, 999-W
S. L. Marra, 773-A
F. M. Pennebaker, 773-42A
W. R. Wilmarth, 773-A
Records Administration (EDWS)

J. W. Amoroso, 999-W
C. J. Bannochie, 773-42A
J. M. Bricker, 704-27S
C. L. Crawford, 773-42A
T. L. Fellinger, 704-26S
J. M. Gillam, 766-H
B. A. Hamm, 766-H
E. W. Holtzscheiter, 704-15S
J. F. Iaukea, 704-30S
V. Jain, 704-30S
C. M. Jantzen, 773-A
M. T. Keefer, 241-156-H
D. C. Koopman, 999-W
D. P. Lambert, 999-W
D. W. McIlmoyle, 766-H
J. D. Newell, 999-W
J. E. Occhipinti, 704-S
J. M. Pareizs, 773-A
D. K. Peeler, 999-W
J. W. Ray, 704-S
S. H. Reboul, 773-A
A. Samadi-Dezfoul, 704-27S
H. B. Shah, 766-H
D. C. Sherburne, 704-S
M. E. Smith, 704-30S
A. V. Staub, 704-27S
M. E. Stone, 999-W
J. R. Zamecnik, 999-W
P. R. Jackson, DOE-SR, 703-46A
K. H. Subramanian, 766-H